UNIVERSITY OF KWAZULU-NATAL

Multiple Oxidation Events Increase Signal Specificity in the Tpx1-Pap1 Pathway for Hydrogen Peroxide

Selloane Limpho Wandile Parkies

216075087

A dissertation submitted in fulfilment of the requirements for the degree of Master of Science in the Discipline of Genetics, School of Life Sciences, College of Agriculture, Engineering and Science, University of KwaZulu-Natal, Pietermaritzburg, South Africa

Supervisor: Dr CS Pillay

2024

PREFACE

As the candidate's supervisor, I have approved this dissertation for submission.

Supervisor: Dr C. S. Pillay

Signature: [redacted]

Date: 11 June 2024

The research contained in this dissertation was completed by the candidate while based in the discipline of Genetics, School of Life Sciences of the College of Agriculture, Engineering and Science, University of KwaZulu-Natal, Pietermaritzburg, South Africa, under the supervision of Dr C. S. Pillay.

These studies represent original work by the candidate and have not otherwise been submitted in any form to another University. Where other authors have used the work, it has been duly acknowledged in the text.

DECLARATION

I declare that

(i) The research reported in this dissertation/thesis, except where otherwise indicated, is my original research.

(ii) This dissertation/thesis has not been submitted for any degree or examination at any other university.

(iii) This dissertation/thesis does not contain other persons' data, pictures, graphs or other information unless specifically acknowledged as being sourced from other persons.

(iv) This dissertation/thesis does not contain other persons' writing unless specifically acknowledged as being sourced from other researchers. Where other written sources have been quoted, then:

a) their words have been re-written, but the general information attributed to them has been referenced;

b) where their exact words have been used, their writing has been placed inside quotation marks, and referenced.

(v) Where I have reproduced a publication of which I am the author, co-author or editor, I have indicated in detail which part of the publication was actually written by myself alone and have fully referenced such publications.

(vi) This dissertation/thesis does not contain text, graphics or tables copied and pasted from the Internet unless specifically acknowledged, and the source is detailed in the dissertation/thesis and the References sections.

Signed: 

ABSTRACT

Oxidative stress can be split into two states: eustress is associated with beneficial physiological states and cell proliferation, and distress correlates with deleterious states, neurological disease, diabetes and disease. Many redox pathways in these physiological states across cellular life require multiple oxidation events for full activation. OxyR in *E. coli* needs four events, Nrf2-Keap1 in mammals requires three, Yap1 in baker's yeast needs three to four and Pap1 in *S. pombe* requires two oxidation events. This study investigated the purpose of the multiple oxidation events in hydrogen peroxide signal transduction in redox pathways. To achieve this, we developed and analysed a single and double oxidation computational Pap1-Tpx1-Trr1 model to compare how they respond to different hydrogen peroxide concentrations. We also utilised *in vitro* recombinant proteins, Tpx1 and Pap1, to assemble the Tpx1-Pap1 system and assessed the signal output at different hydrogen peroxide concentrations. The computational analysis showed that adding an oxidative step increases the system's capability to attenuate the signal at low hydrogen peroxide concentrations and amplify it at high concentrations. The *in vitro* system showed that a simplified Tpx1-Pap1 system can differentiate between different hydrogen peroxide concentrations. Multiple oxidation steps impart high pass filtering properties on the system, allowing systems to better differentiate between low and high signal inputs.

ACKNOWLEDGEMENTS

I want to express my gratitude to those who contributed to my degree.

Firstly, I would like to thank my supervisor, Dr C. S. Pillay, for the guidance, testing, discussions, and criticisms that have made me a better scientist. Your compassion, patience and mentoring have made me a better person. Thank you for always challenging me and creating an open and sincere environment in the lab.

I am indebted to the National Research Foundation for funding my academic career, thus allowing me to pursue my MSc degree and dream.

I am also thankful to the technical staff, Megan and Jess, who have eased the process of lab work and the assistance with lab equipment. To my colleagues, Tejal, Kelli, Nolyn and Erin, I am grateful for all the advice, assistance, ideas and good laughs they provided throughout our time together.

I would not have been able to get through this degree without my closest friends:

My science guys: Timothy and Diane. I am thankful for all the life we have done together on campus and off. With all the hikes, the coffees, teas, and wines we imbibed, and memories made, I can never thank you enough for being my friends. I am grateful to Ndzeli, Lolly and Zinzi for standing by me even when you did not understand what I was doing. Thank you for all the video calls, their deep faith in me, and for reminding me that I can do this so that you know I did.

I thank my family, Mpolokeng, Gaga and Palesa, for their complete support, love and prayers. They have always believed in me, have never stopped encouraging me, and have given me a reason to finish the race.

Finally, to God, who has provided abundantly. To the God who has seen me and looks after me, he has been my refuge and joy.

To all of them, I dedicate this dissertation.

ACRONYMS

ABESF	4-benzenesulfonyl fluoride hydrochloride
AEBSF	4-(2-aminoethyl) benzenesulfonyl fluoride hydrochloride
AP-1	Activator protein 1
ARE	Antioxidant response element
ATP	Adenosine triphosphate
BCA	Bicinchoninic acid
BSA	Bovine serum albumin
bZip	Basic Leucine Zipper Domain
Cap1	Candida AP-1-like transcription factor 1
COVID-19	Coronavirus disease 2019
CRD	Cysteine-rich domain
Crm1	Chromosomal Maintenance 1
Cu(I)	Copper ion (+1)
Cul3	Cullin 3
DNA	Deoxyribonucleic acid
DTT	Dithiothreitol
ECL	Enhanced chemiluminescence
EDTA	Ethylenediaminetetraacetic acid
ETC	Electron transport chain
Fe(II)	Iron ion (+2)
Fos	Fos proto-oncogene
FOXO	Forkhead box O
GAPDH	Glyceraldehyde 3-phosphate dehydrogenase
GOE	Great Oxygenation Event
GPx	Glutathione peroxidase
GR	Glutathione reductase
Grx	Glutaredoxin
GSH	Glutathione
H_2O	Water
H_2O_2	hydrogen peroxide
HCl	Hydrochloric acid
HOG	High-osmolarity glycerol
HSV-1	Herpes simplex virus 1
IAM	Iodoacetamide
IPTG	Isopropyl β- d-1-thiogalactopyranoside
JAK	Tyrosine-protein kinase
JNK	c-Jun N-terminal kinases
Jun	Jun proto-oncogene
KEAP1	Kelch-like ECH-associated protein 1
LB	Luria-Bertani
Maf	V-maf musculoaponeurotic fibrosarcoma oncogene homolog
MAPK	Mitogen-activated protein kinase

MKP	Dual specificity protein phosphatase
NADPH	Nicotinamide adenine dinucleotide phosphate
NEB	New England Biolabs
NEM	N-ethylmaleimide
NES	Nuclear export signal region
NF-κB	Nuclear factor kappa B
Ni-NTA	Nickel-nitrilotriacetic acid
NOX	NADPH oxidase
Nrf2	Nuclear factor erythroid 2-related factor 2
NsrR	Nitric oxide-sensitive repressor
O_2	Molecular oxygen
OH	Hydroxyl radical
OxyR	Hydrogen peroxide-inducible genes activator
p53	Cellular tumor antigen
PAGE	Polyacrylamide gel electrophoresis
Pap1	Pombe AP-1-like transcription factor 1
PBS	Phosphate buffered saline
PMSF	Phenylmethylsulfonyl fluoride
Prx	Peroxiredoxin
PySCeS	Python Simulator for Cellular Systems
RING	Really Interesting New Gene
ROS	Reactive oxygen species
RSV	Respiratory syncytial virus
SAPK	Stress-activated protein kinases
SciTE	SCIntilla Text Editor
SDS	Sodium dodecyl-sulfate
SOD	Superoxide dismutase
SoxR	Superoxide-sensitive repressor
Srx	Sulfiredoxin
STAT	Signal transducer and activator of transcription
Sty1	Suppressor of tyrosine phosphatase
TBST	Tris-buffered saline with Tween 20
TEMED	N,N,N’,N’-Tetramethylethylenediamine
TF	Transcription factor
Tpx	Thioredoxin peroxidase
Trr	Thioredoxin reductase
Trx	Thioredoxin
Txl	Thioredoxin-like protein
Yap1	Yeast AP-1-like transcription factor 1

List of Tables

List of Figure

Table of Contents

Chapter 1: Literature Review

1.1. Reactive oxygen species and aerobic metabolism

Oxygen metabolism and life on Earth

Life is nothing but electrons looking for a place to rest. - Albert Szent-Györgyi

Earth is now an aerobic world due to the Great Oxidation Event (GOE), which resulted from the activity of cyanobacteria (Aiyer, 2022). The GOE shifted the Earth's atmosphere and environment from a weakly reducing (Kasting, 2014; Pavlov & Kasting, 2002) to an oxidising one, with the atmosphere now made primarily of nitrogen and oxygen (Lyons et al., 2014). Coinciding with the accumulation of oxygen on Earth was the appearance of eukaryotes, the increased complexity of life observed in the Cambrian and Devonian eras, and the large body sizes of animals observed later (Figure 1.1) (Baudouin-Cornu & Thomas, 2007; Falkowski et al., 2005). The benefit of oxygen for cells was the expansion of the protein structural space, an increased variety of metabolic reactions and greater thermodynamic efficacy (Raymond & Segrè, 2006; Wang et al., 2011). However, oxygen also led to the mass extinction of anaerobic microbes previously dominating the planet because of oxygen's susceptibility to transform into reactive oxygen species (ROS) (Hodgskiss et al., 2019).

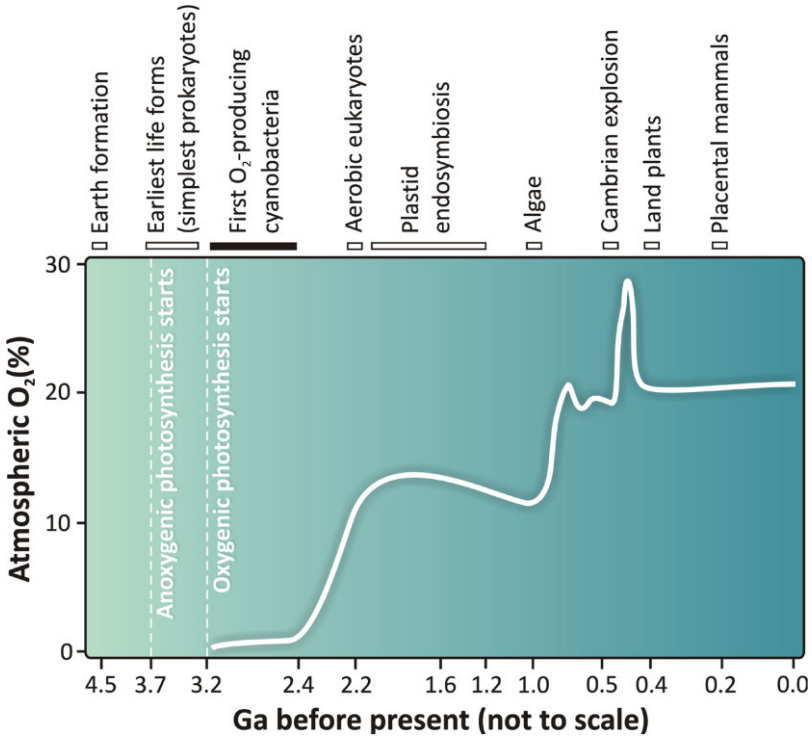

Figure 1.1: The concentration of atmospheric oxygen over Earth's history. The oxygen levels in Earth's atmosphere coincide with significant developments in life complexity—*image obtained from "Figure 1" in Govindjee and Shevela (2011) published in Frontiers (2011). The original work is an open-access article subject to a non-exclusive license between the authors and Frontiers Media SA*.

Reactive oxygen species and cell function

Aerobic metabolism has challenges due to its inherent oxygen-associated toxicity and mutagenic properties. Molecular oxygen has a dual nature stemming from the distribution of its valence electrons. It makes oxygen relatively unreactive with most non-radicals (Gilbert, 2012; Halliwell, 2006b; Halliwell & Gutteridge, 2015a), but it also serves as a precursor for many unstable and highly reactive molecules known as ROS (Rigoulet et al., 2011). While sometimes mislabelled as radicals, these ROS have diverse chemical properties, but they all share the common characteristic of being more reactive than molecular oxygen (Halliwell & Gutteridge, 2015a). Studying ROS and their impact on cellular processes has been crucial in elucidating the challenges and opportunities associated with aerobic metabolism and subsequent redox-related physiological functions.

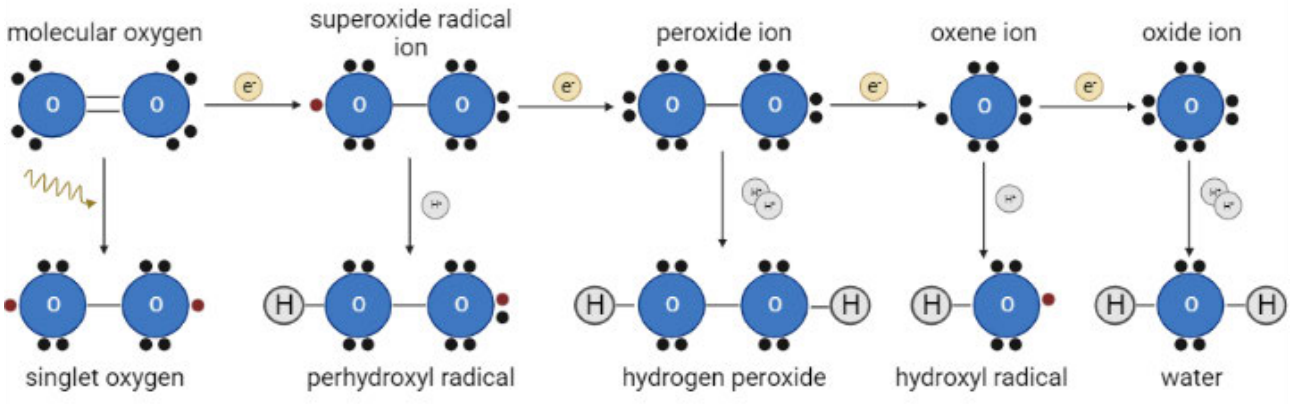

Figure 1.2: The generation of the different ROS from molecular oxygen. The various ROS are generated from molecular oxygen through sequential reduction reactions (superoxide radical, peroxide ion, oxene ion and oxide ion) and a photochemical reaction (singlet oxygen). Further reduction by hydrogen ions results in additional ROS, including the perhydroxyl radical, hydrogen peroxide, hydroxyl radical, and water—*created with BioRender.com adopted from Apel and Hirt (2004)*.

The transfer of either energy or electrons changes the stability of molecular oxygen. The transfer of energy in the form of light leads to the formation of the singlet oxygen radical. A single electron addition (reduction) forms the superoxide radical, and a double electron addition results in the peroxide ion. The triple electron addition to molecular oxygen forms the oxene ion, and adding hydrogen forms the hydroxyl radical. Water formation is the product of a quadruple reduction of oxygen and the addition of two hydrogen molecules (Figure 1.2). Each of these transformations can be generated by inter- and intra-cellular redox reactions and, in some cases, is catalysed by enzymes (Apel & Hirt, 2004).

In aerobes, there are numerous ROS sources, with the two primary sources being the enzymatic generation via NADPH oxidases (NOXs) and ROS being the by-product of aerobic metabolism and photosynthesis (Goncalves et al., 2015; Reczek & Chandel, 2017). The generation of ROS as a by-product of metabolism primarily occurs within the mitochondria

and chloroplasts. The mitochondria's electron transport chain (ETC) tends to leak electrons, partially reducing molecular oxygen and producing superoxide (Cadenas & Davies, 2000). This leakage of electrons primarily occurs through Complex I and III in the ETC, but under certain conditions, Complex II and glycerol-3-phosphate dehydrogenase can also generate superoxide; thus, most of the superoxide is localised within the mitochondrial matrix (Halliwell & Gutteridge, 2015a).

The superoxide radical is also a physiological by-product of NOXs and xanthine oxidases. In an aqueous environment such as the cytoplasm, the superoxide radical will act as an electron acceptor undergoing a reduction reaction to form hydrogen peroxide, which is a spontaneous reaction but is also catalysed by superoxide dismutase (SOD) (Kimura et al., 2005). The superoxide radical is not the most abundant form of ROS and rarely interacts with biomolecules. However, in the presence of nitric oxide, the superoxide radical produces the highly toxic peroxynitrite anion (Beckman et al., 1990).

Singlet oxygen is a volatile ROS. Its instability makes it highly reactive towards biomolecules, such as DNA, where it can induce mutations by forming 8-oxo-(d)G moieties, significantly impacting gene and genome function and stability (Ravanat & Cadet, 1995). It has also been linked to the oxidation of lipids via polyunsaturated fatty acids (Kimura et al., 2005). Select amino acids in proteins, such as histidine, methionine and cysteine, tryptophan and tyrosine, are prone to singlet oxygen oxidation (Klotz et al., 2003). The single oxidation of these residues can lead to mitochondrial damage, affecting the ion channels and inhibiting cellular caspases (Levine et al., 2001; Otsu et al., 2005). Fortunately, it is unlikely to be generated *in vivo* (Kimura et al., 2005).

Hypochlorous acid is a potent oxidant that can oxidise all biomolecules: lipids, proteins, and DNA (Kimura et al., 2005). Neutrophils use the potency of this ROS in the innate immune system to destroy pathogens by producing hypochlorous acid in the phagosome via NADPH oxidases (Gray et al., 2013; Varatnitskaya et al., 2021). The hydroxyl radical is considered the most detrimental ROS due to its indiscriminate reactivity with biomolecules (Park & Imlay, 2003). It has been shown to cause significant oxidative damage to lipids and proteins and can induce DNA strand breaks, base modifications and cross-linking. The hydroxyl radical can lead to necrosis and apoptosis at the cellular level (Lloyd et al., 1997) and premature ageing at the organismal level (Auten & Davis, 2009), and its production typically occurs through the Fenton reaction with Cu(I) and Fe(II) cofactors (Fenton, 1894; Pignatello et al., 2006).

Hydrogen peroxide is a ROS that plays a crucial role in redox biology (Winterbourn, 2008). It is primarily produced via the SOD-dependent reduction of the superoxide radical, making it a metabolic by-product (Kimura et al., 2005). Due to its chemical similarity to water and its stability, hydrogen peroxide can effectively diffuse across biological membranes and translocate away from its generation site (Battin & Brumaghim, 2009). Additionally, the polarisability of hydrogen peroxide allows it to act as an electrophile. Proteins that increase the polarisability of hydrogen peroxide can increase its reactivity by several orders of magnitude (Winterbourn, 2013). Thus, hydrogen peroxide predominantly oxidises a subset of cysteine-containing proteins but can only oxidise DNA or lipids slowly (Halliwell & Gutteridge, 2015a). However, it can undergo homolysis under certain conditions, generating more reactive ROS, such as the hydroxyl radical (Winterbourn, 2013). The Fenton reaction generates the hydroxyl radical via hydrogen peroxide reduction by Fe(II) (Thomas et al., 2009). Therefore, to maintain cellular homeostasis and protect against oxidative damage, cells need to develop mechanisms and enzymes to neutralise, remove and control ROS.

1.2. Redox eustress and distress in cellular function

The concept of stress, as understood in the biological setting, was formulated in 1985, but its origins can be traced back to Hans Selye's groundbreaking work in 1936 (Selye, 1936). Selye introduced the term "stress" from physics into the biological lexicon and defined it as the body's non-specific response to any demand. It can also be seen as a threat to homeostasis (Munck et al., 1984). He likened it to the interplay between damage and defence, much like tension or pressure represents the interaction between a force and the resistance it encounters (Selye, 1950). Selye observed consistent symptoms in his experiments on rats exposed to various chemical, physical, and environmental stressors, and this general stress response became known as Selye syndrome, later called the stress response (Selye, 1936).

Theories of oxidative stress and their limitations

Several theories linked oxidative stress within mammalian cells to pathophysiology: the oxidative stress theory of ageing (Harman, 1956; Lin & Flint Beal, 2003), the oxidative stress theory of disease (Aruoma, 1998; Ghezzi et al., 2017), and oxidative distress and eustress theory (Sies, 2019b, 2021). All these theories provided frameworks to investigate and understand the purpose and function of ROS within biological systems.

The oxidative stress theory of ageing was first postulated by Denham Harman in 1956, who posited that ageing was the accumulation of deleterious cell and tissue damage from ROS (Harman, 1956). The linking of oxidative stress and ageing led to the investigation of

mitochondria, giving rise to the mitochondrial theory of ageing (Balaban et al., 2005; Shigenaga et al., 1994). The mitochondrial theory of ageing hypothesised that progressive damage to mitochondrial DNA led to mitochondrial dysfunction, which affected the entire cell, thus leading to ageing (Srivastava, 2017). It is known that the functioning of the mitochondria decreases with age, which can increase the electron transport chain's leakiness and release more superoxide radicals (Pulliam et al., 2013). The oxidative stress theory of ageing and the mitochondrial theory of ageing could explain how caloric restriction increases lifespan by decreasing levels of oxidative damage and inhibiting the decline of repair systems and GSH. It also explains the link between low oxygen consumption and increased lifespan (Halliwell & Gutteridge, 2015a). In the lab, this theory has shown promising results; but clinical trials with antioxidants have not shown benefits for health or longevity (Howes, 2006; Lapointe & Hekimi, 2010).

The involvement of ROS in disease is widespread and has been implicated in over 200 disorders and tissue injuries, including diabetes, cancer, and neurodegenerative diseases (Mani, 2015). For example, oxidative stress contributes to Type 1 and Type 2 diabetes by causing inflammatory damage and loss of β-cell function, respectively (Sivitz & Yorek, 2010). Nonetheless, the role of ROS is unclear, as they are pro-proliferative and suppress apoptosis, which is helpful for cancer. On the other hand, ROS also induce senescence, increases the activity of the p53 and activates the class O subgroup of the Forkhead transcription factor family (FOXO), which would be detrimental to cancer (Carter & Brunet, 2007; Halliwell, 2006a). Additionally, studies have shown that knocking out glutathione peroxidase (GPx), an antioxidant enzyme, leads to intestinal cancer in mice, and the knocking out of peroxiredoxin peroxidases also leads to the development of lymphomas, sarcomas and adenomas (Chu et al., 2004). Neurodegenerative diseases exhibit impaired mitochondrial function, increased oxidative damage (Xu et al., 2021), misfolded aggregated proteins and inflammation (Fischer & Maier, 2015). These symptoms can be a function of accumulated oxidative damage, or they could lead to the generation of ROS and increased oxidative damage in the cell. Therefore, the precise relationship between oxidative stress and disease remains elusive—whether oxidative stress precedes the disease state or emerges simultaneously (Halliwell & Gutteridge, 2015a).

Alongside these two theories is a third framework with the concept of oxidative stress being split into two distinct states: oxidative eustress and oxidative distress (Figure 1.3). While oxidative stress generally refers to an imbalance between oxidants and antioxidants (Sies & Jones, 2007), this framework allows for a more precise classification of the stress. In the eustress and distress theory, cells utilise the oxidant for redox signalling and metabolism, but

under high loads, damage to proteins and biomolecules occurs (Sies, 2018, 2020). Notably, the oxidative theory of ageing, the oxidative theory of disease, and the theory of eustress and distress are not mutually exclusive and can all work simultaneously within mammalian cells.

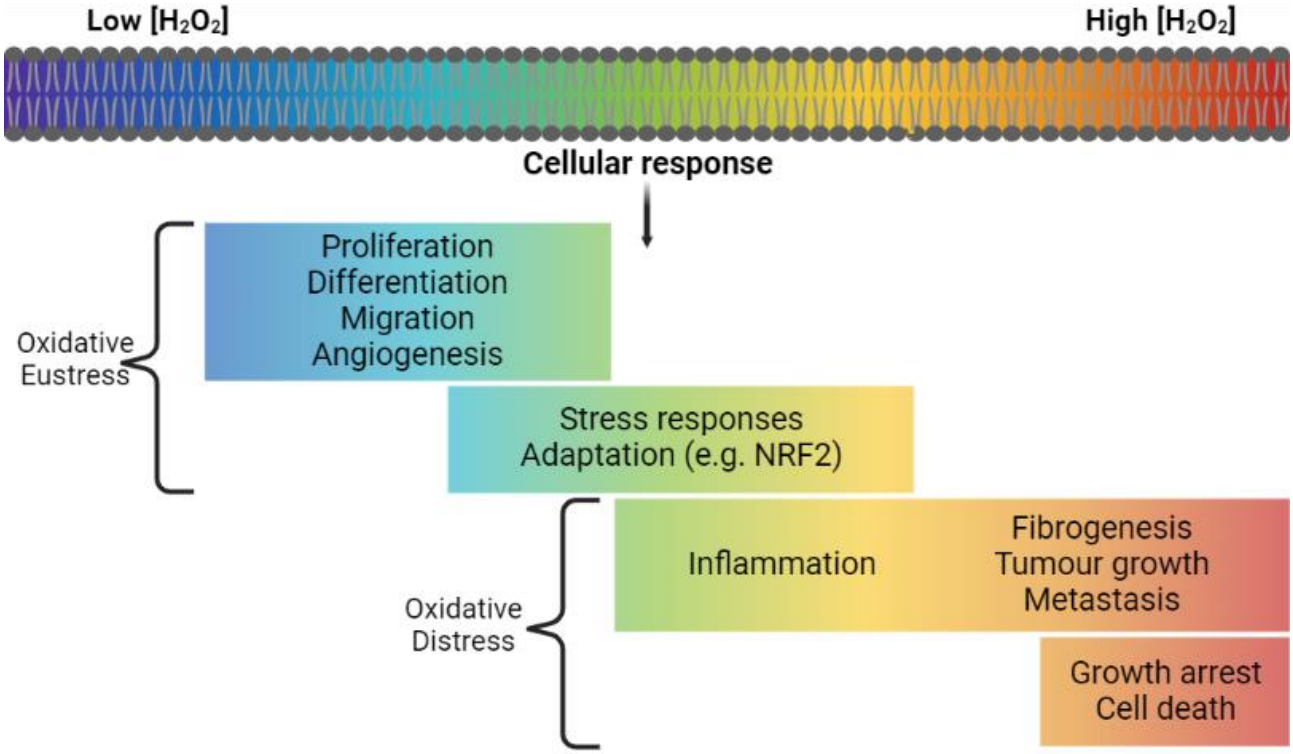

Figure 1.3: Eustress and distress are different cellular states. Oxidative stress and eustress are concentration-dependent states of cellular function with different cell fates—*created with BioRender.com and adapted from Sies (2020)*.

Oxidative distress and eustress are distinct cellular physiological states.

Oxidative distress results following a supraphysiological oxidant challenge on a cell, system or organism (Sies et al., 2017). Oxidative distress conditions damage receptors, enzymes and nucleic acids (Sies, 2019b) (Halliwell & Gutteridge, 2015a). These effects can alter cell signalling and mitochondrial function, causing ROS-induced inflammation and cytokine production in mammalian cells (Nitti et al., 2022). However, cell death via apoptosis or necrosis occurs if the ROS levels rise; these cells can release and spread inflammatory molecules (Halliwell & Gutteridge, 2015b). The downstream pathologies associated with oxidative distress, e.g. cancer, diabetes and neurodegenerative disorders (Hegde et al., 2012) are the same diseases discussed in the oxidative theory of disease, thus associating these two theories.

Oxidative eustress refers to the beneficial response of cells and organisms to oxidative stress. (Okegbe et al., 2012). Achieving oxidative eustress involves the intricate process of monitoring redox activity, managing the influx and efflux of ROS, and maintaining redox balance through various cellular mechanisms and pathways involved in redox regulation (Sies, 2021). Hydrogen peroxide exposure in neural cells can change the transcriptome to

increase neurogenesis and differentiation (Estrada et al., 2014). The effect differs across different regions of the neural system and uses different pathways, additionally influencing proliferation and modulating and maintaining self-renewal capacity (Terzi & Suter, 2020). In vertebrate embryos, eustress has been linked to proliferation, left-right symmetry and apoptosis (Timme-Laragy et al., 2018).

Oxidative eustress is driven by the oxidation of redox-sensitive proteins by hydrogen peroxide. Hydrogen peroxide's importance is due to its chemical properties that make it react specifically with these proteins, unlike other ROS. This will be discussed in greater detail in the next section. Fundamentally, the oxidation of these redox-sensitive proteins can alter gene expression, metabolism, growth, and defence to benefit and protect cell homeostasis (Sies, 2019a). An example is the direct oxidation and inactivation of glyceraldehyde 3-phosphate dehydrogenase (GAPDH), which reroutes the metabolic flux from the glycolytic to the pentose phosphate pathway (Talwar et al., 2023). As NADPH provides reducing power for cellular antioxidants, this modification increases the oxidative stress tolerance of the cell (Ralser et al., 2007). Additionally, ROS can influence the cell by oxidising redox-sensitive proteins upstream from transcription factors, like peroxiredoxins (Brigelius-Flohé & Flohé, 2011; Young et al., 2019), which propagate signalling downstream to redox-sensitive transcription factors such as the signal transducer and activator of transcription 3 (STAT3) (Simon et al., 1998). STAT3 is involved in hydrogen peroxide production, cell division, immunity and cell death (Carballo et al., 1999; Li et al., 2010). Furthermore, at the organismal level, oxidative eustress is associated with synaptic plasticity and pruning (Cobley, 2018; Sies, 2021). These outcomes are mediated by the activation of transcription factors, which upregulate hundreds of target genes involved in diverse cytoprotective processes (Paek et al., 2023).

Hydrogen peroxide as a signalling molecule and secondary messenger

As described above, a ROS commonly utilised as a signalling molecule is hydrogen peroxide, which has a relatively prolonged half-life and migration distance (Table 1.1)(Marinho et al., 2014; Mignolet-Spruyt et al., 2016). Hydrogen peroxide is also an excellent cell-to-cell signalling molecule, as it can travel 100 μM^{-1} extracellularly in mammalian tissue (Fichman et al., 2024). ROS waves, which are auto-propagating waves of ROS generation from cell to cell, allow hydrogen peroxide signals to travel even further, travelling distances of centimetres from the source site (Fichman et al., 2023).

Table 1.1: The chemical characteristics of ROS that affect it as a signalling molecule. –*Adapted from D'Autréaux and Toledano (2007) and Mittler (2017)*.

ROS	$t_{1/2}$	Migration distance from the source
Superoxide ($O_2^{\bullet-}$)	1-4 µs	30 nm
Hydroxyl radical (OH•)	1 ns	1 nm
Hydrogen peroxide (H_2O_2)	>1 ms	>1 µm
Singlet oxygen ($^1O_2$)	1-4 µs	30 nm

Despite hydrogen peroxide having the chemical characteristics to be a promising signalling molecule, the explanation of its efficacy and specificity is more complex. Redox-regulated proteins, which include biomolecules like transcription factors, kinases, and phosphatases, do not inherently possess a primary redox function, are not kinetically favoured for direct oxidation by hydrogen peroxide, and are lowly expressed within the cell (Ströher & Dietz, 2006). This is contrasted with the abundance of thiol-peroxidases. These proteins, such as peroxiredoxins that make up approximately 1% of the total soluble cellular protein content (Stöcker et al., 2018), react with hydrogen peroxide up to seven orders of magnitude faster than redox-regulated proteins (Winterbourn & Metodiewa, 1999). These ROS sinks could, therefore, hinder the effectiveness of hydrogen peroxide as a signalling molecule, intracellularly, particularly in interactions with the redox-regulated proteins (Stöcker et al., 2018). Two models have been proposed to address this intriguing paradox to elucidate how redox signalling can occur within a complex cellular environment: the redox relay and floodgate models.

The redox relay theory posits that antioxidants, like peroxiredoxin and thioredoxin (Trx), can serve as signal transducers in redox signalling pathways. As antioxidants exhibit high sensitivity to hydrogen peroxide, they are excellent redox targets for undergoing oxidation and transferring this oxidative signal to a target protein (Reczek & Chandel, 2015). As a result, this enables the signal to be transmitted to other proteins via a redox relay (Figure 1.4A) (Domènech et al., 2018). The floodgate model, on the other hand, proposes that signal transduction occurs once the peroxiredoxin has been inactivated by hyperoxidation, allowing for hydrogen peroxide to accumulate and act as a signalling molecule (Figure 1.4B) (Forman et al., 2010; Wang et al., 2018). Under these conditions, the competition between antioxidants and target proteins is no longer a limiting factor. As a result, this model allows for more localised and site-specific redox signalling (Winterbourn, 2013). Rather than being mutually

exclusive, cells could employ both the redox relay and floodgate models in specific compartments, for different pathways, or under certain oxidative conditions.

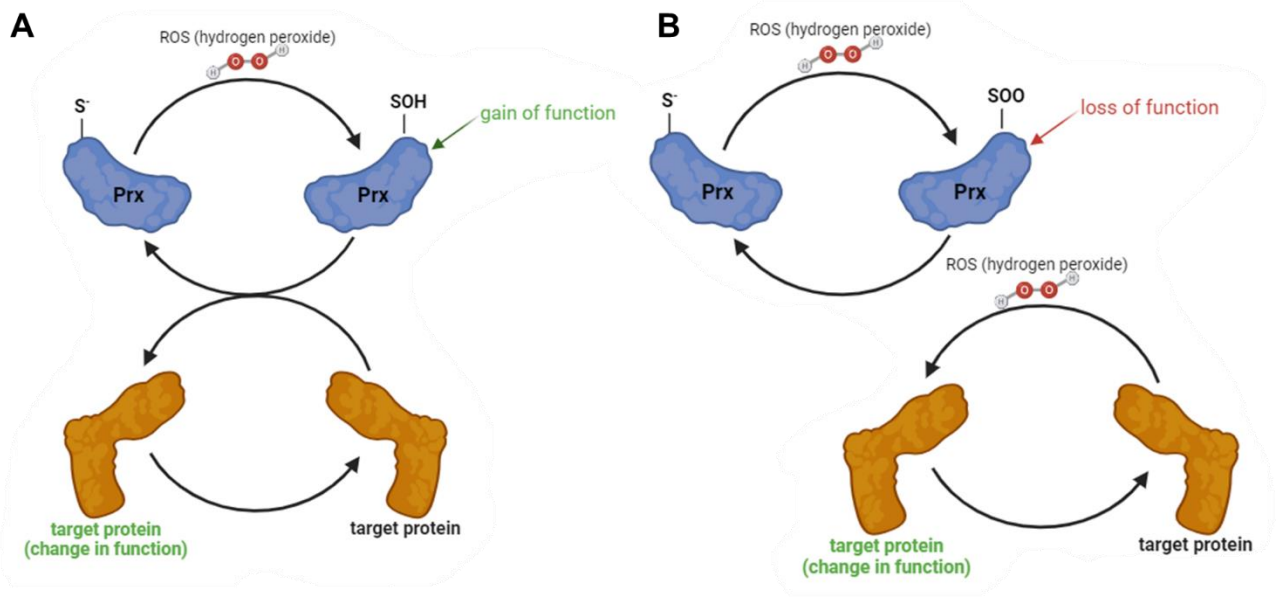

Figure 1.4: The mechanism of redox signalling. Redox signalling has multiple mechanisms through which it can occur, and the most pertinent ones are **(A)** the redox relay model (Reczek & Chandel, 2015) and **(B)** the floodgate model (Forman et al., 2010)—*created with BioRender.com*.

1.3. Thiol-based redox systems mediate redox homeostasis within cells.

Thiols are sulfur-containing compounds that play a critical role in redox biology in cells and proteins (Winterbourn & Hampton, 2008). Thiols constitute the large sulfur atom as the backbone, bonded to hydrogen to form the S-H bond. The low energy bond between sulfur and hydrogen makes it easy for hydrogen to dissociate, giving thiols nucleophilic and redox-active properties (Winterbourn & Metodiewa, 1999). Additionally, sulfur's chemical properties allow it to attain a range of oxidative states (-2 to +6) (Gupta & Carroll, 2014).

Cysteines are susceptible to redox reactions as their functional group is a thiol. However, its susceptibility to redox reactions depends on its p*Ka* value, which is influenced by its local environment. Therefore, different proteins will have different kinetic and thermodynamic properties for cysteine residues (Roos et al., 2012). Additionally, thiols can facilitate a variety of redox modifications, such as S-glutathionylation (-SSG), S-sulfhydration (-SSH), S-nitrosylation (-SNO), S-sulfenylation (-SOH), S-succinylation (-SO_2H), and S-sulfonylation (-SO_3H) (Figure 1.5). These modifications can change the structure and function of the protein; therefore, cells must closely regulate and control this interaction to avoid adverse impacts on protein function (Yang et al., 2016).

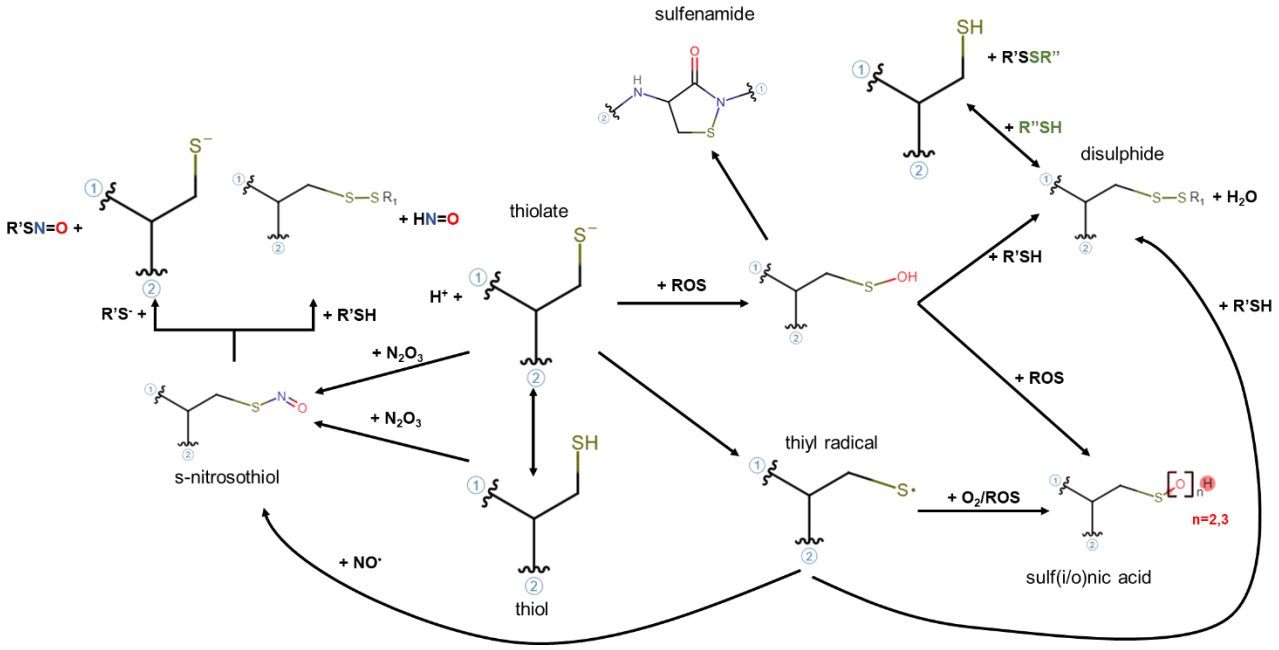

Figure 1.5: The diversity of thiol reactions in redox biochemistry. Cysteine, with its sulphur molecule, can exist in multiple oxidation states (-2 to +6), enabling it to undergo various oxidation processes and produce various oxidation isoforms based on the oxidant. These different isoforms exhibit distinct biological functions and occurrences. ① and ② indicate the rest of the protein chain—*adapted from Gupta and Carroll (2014)*.

Thioredoxin system

The thioredoxin system is a crucial disulphide reductase system, consisting of NADPH, thioredoxin and thioredoxin reductase (Trr). Thioredoxin is a small (12 kDa) well-conserved protein found in all living cells, yeasts, bacteria, plants, and animals (Holmgren, 1985). The thioredoxin motif has the redox-active centre Cys-Gly-Pro-Cys, which imparts to thioredoxin its critical ability to reduce proteins and form disulphide bonds (Lu & Holmgren, 2014). The N-terminal cysteine interacts with the disulphide bond of the target protein to form an intermediary complex with it. Then, it forms a disulphide bond with the C-terminal Cys to reduce the target protein (Figure 1.6). This oxidised thioredoxin isoform is then reduced by thioredoxin reductase and NADPH (Nagarajan et al., 2017). In this manner, this system can cleave the disulphide bonds of oxidised proteins and assist in maintaining the reducing environment observed in the cell (Gromer et al., 2004).

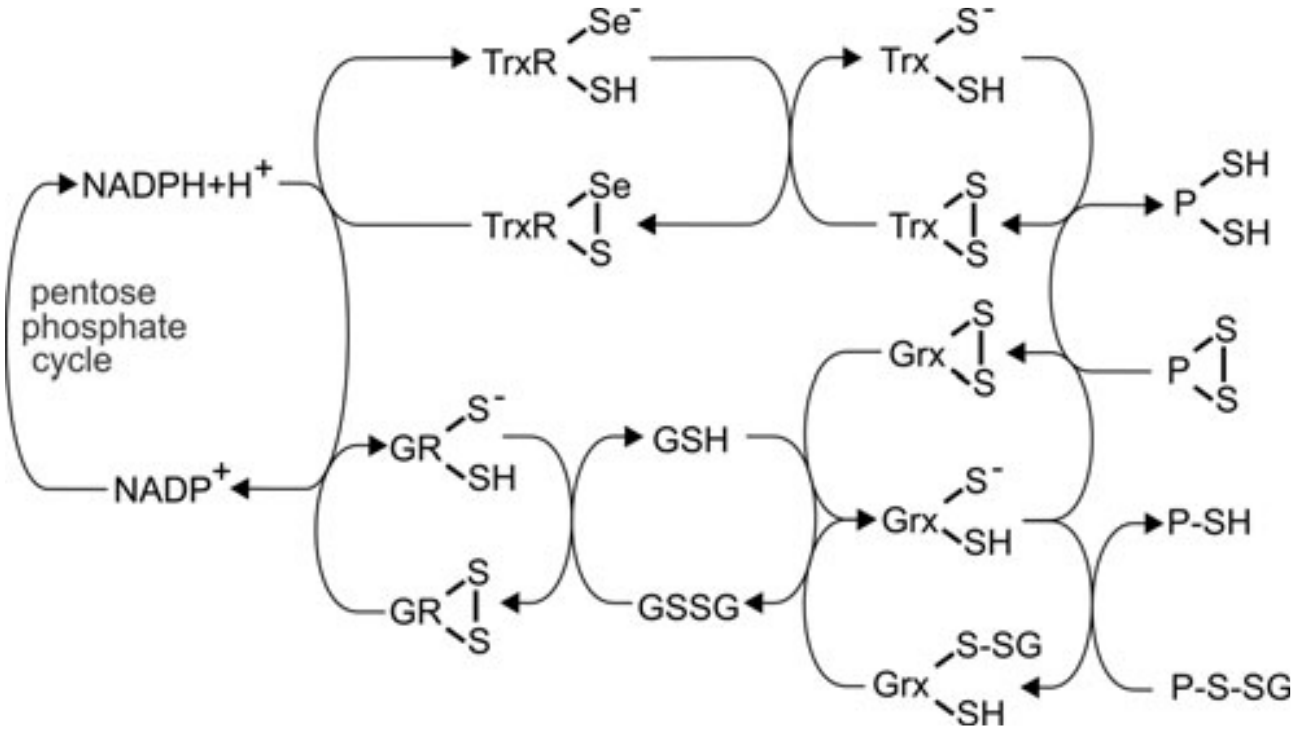

Figure 1.6: The reaction mechanism of the thioredoxin and glutaredoxin system in mammalian cells. Trx and Grx are part of the thioredoxin family and are major reductase systems that assist in maintaining the cell's reducing environment. The thioredoxin system has Trx, which reduces the target protein. Trx is reduced by TrxR with NADPH, providing the reducing power as an electron donor. The glutaredoxin system reduces the disulphide bonds of target proteins via Grx using a monothiol or dithiol mechanism. Oxidised Grx is reduced by GSH, which in turn is reduced by GR and NADPH (Mashamaite et al., 2015)—*image obtained from "Figure 3" in Hanschmann et al. (2013), licensed by Mary Ann Liebert, Inc. publishers under License Number 5730770138670*.

Glutaredoxin system

Similarly to the thioredoxin system, the glutaredoxin system is a vital disulphide bridge reductase which constitutes glutaredoxin (Grx), glutathione (GSH), glutathione reductase (GR) and NADPH. Glutaredoxin is a small protein structurally belonging to the same family of proteins as thioredoxin and has a similar function as thioredoxin but utilises GSH as a cofactor. It has an active site motif similar to that found in thioredoxin (Cys-X-X-Cys or Cys-X-X-Ser) (Fernandes & Holmgren, 2004). The mechanism of glutaredoxin reduction is similar to that of thioredoxin: the N-terminal cysteine attacks the target proteins' disulphide bond to form the intermediary mixed disulphide bond (Figure 1.6). The mixed disulphide bond forms an intermolecular disulphide bond, which GSH then reduces by forming another mixed disulphide bond between glutaredoxin and GSH. A second GSH molecule then reduces this mixed disulphide bond to form GSSG, which is reduced by glutathione reductase and NADPH (Lillig et al., 2008).

GSH is a tripeptide that plays a role in buffering the cellular redox state and the antioxidant response. Though it has millimolar concentrations, its reaction rates with protein disulfides are too slow to be of physiological significance. GSH can be found in its reduced isoform,

GSH, or its oxidised isoform glutathione disulphide, GSSG, which constitutes 2 GSH molecules bound via a disulphide bond (Meister & Anderson, 1983). Much like thioredoxin reductase, glutathione reductase is a flavoprotein that catalyses the NADPH-dependent reduction of GSSG to GSH, which helps maintain glutathione levels (Figure 1.6) (Carlberg & Mannervik, 1985).

Peroxiredoxin system

Peroxiredoxins are a large, highly conserved family of peroxidases that can reduce peroxides using their conserved peroxide-reducing cysteine, the peroxidatic cysteine (C_P) (Hall et al., 2009; Poole et al., 2011). The C_P has a high affinity for hydrogen peroxide, lipid peroxides and peroxynitrites, with the formation of the C_P-SOH having a 5 to 7 orders of magnitude higher than the rate constants for small thiols (Winterbourn, 2013), giving peroxiredoxins their antioxidant activity (Knoops et al., 2011). Peroxiredoxins can be grouped into 6 subfamilies (Poole & Nelson, 2016); however, an older convention separated them into 3 classes determined by the location and the presence of an additional cysteine residue called the resolving cysteine (C_R) (Chae et al., 1994; Rhee et al., 2001). The 2-Cys typical and 2-Cys atypical subfamilies are homodimeric and have both the C_P and the C_R residues, while the 1-Cys peroxiredoxins are monomeric.

In the 2-Cys typical subfamily, the C_P is oxidised to C_P-SOH, which then reacts with the C_R on the other subunit to form an intermolecular disulphide bond. By contrast, the C_P of the 2-Cys atypical subfamily reacts with the C_R on the same subunit to form an intramolecular disulphide bond. The 1-Cys subfamily does not have the C_R residue, so it forms a disulphide bond with cysteines on other proteins or small thiols (Fisher, 2011). The CP-SOH residue can be further oxidised in typically eukaryotic peroxiredoxins before forming the disulphide bond to form a sulfinic acid isoform (C_P-SO_2H). This isoform is catalytically inert and cannot react with peroxides or be reduced by thioredoxin or the glutathione/glutaredoxin system (Yang et al., 2002). Another enzyme, sulfiredoxin, which is ATP-dependent, is necessary to reduce the sulfinic acid isoform, but this process is relatively slow (Biteau et al., 2003; Woo et al., 2003). Nevertheless, as discussed in the floodgate model, this redox state is beneficial as it allows for localised hydrogen peroxide accumulation (Veal et al., 2018). Hyperoxidation is essential in coupling the circadian rhythm to cellular oxidation as the peroxiredoxin redox state shows an entrainable circadian rhythm independently of the transcription-translation feedback loops (O'Neill & Reddy, 2011).

The hyperoxidation of peroxiredoxin also increases its non-peroxidase activity, such as chaperone functions and peroxidase-independent signalling, inhibiting thioredoxin reduction (Rhee, 2016; Veal et al., 2018). Hyperoxidation transforms peroxiredoxins into dodecamers,

acting as chaperones that protect the cell against protein aggregation and assist heat shock proteins in removing and refolding damaged proteins (Veal et al., 2018). In humans, peroxidase-independent signalling is evidenced by the increased formation of the Prx1:MKP-5 and dissociation of the Prx1:MPK-1 complexes under high hydrogen peroxide concentrations and Prx1 hyperoxidation. These processes decrease p38 activity in favour of JNK-mediated signalling (Turner-Ivey et al., 2013). The hyperoxidation of Tpx1 allows for the oxidoreductase activity of thioredoxin to target other proteins, enabling the oxidative stress recovery of the cell (Day et al., 2012). The diverse functions of peroxiredoxins show their role in redox regulation by contributing to the cell's antioxidant defence and signalling networks that maintain the homeostasis of the cell.

1.4. Thiol-based redox signalling systems

Across the spectrum of life, thiol based redox signalling systems can be found. These systems induce oxidative stress responses in their respective organisms. In some key model organisms such as *E. coli*, *S. cerevisiae* and humans, these critical systems are coordinated by the transcription factors OxyR, Yap1 and Nrf2 respectively.

Regulation of prokaryotic redox signalling and adaptive stress response by OxyR

Prokaryotes such as *Escherichia coli* need to be able to sense and respond to hydrogen peroxide perturbations intracellularly and extracellularly (Stone & Yang, 2006). An excellent example is the OxyR transcription factor, which regulates a large hydrogen peroxide-inducible regulon within 10 minutes of oxidative stress (Storz & Tartaglia, 1992). This includes gene encoding catalase, an enzyme breaking down hydrogen peroxide into water. Another example is alkyl hydroperoxide flavoprotein, which can reduce biological hydroperoxides to their corresponding alcohol, glutaredoxin, and glutathione reductase (Figure 1.7) (Antelmann & Helmann, 2011). The induction of these proteins at lower levels of hydrogen peroxide (nM-µM) enables the cell to mount an adaptive response that enhances the bacterium's resistance to subsequent higher levels (1-5 mM) as the induced proteins have protective functions (Demple & Halbrook, 1983). In this regard, it has been shown that deleting OxyR increases the frequency of mutations observed within the bacterium genome, which is exacerbated under aerobic conditions (Sies, 1993). Furthermore, an overlap between the oxidative and other stress responses allows the bacterium to resist various stressors, such as heat shock, thereby enhancing its survival capabilities (Christman et al., 1985).

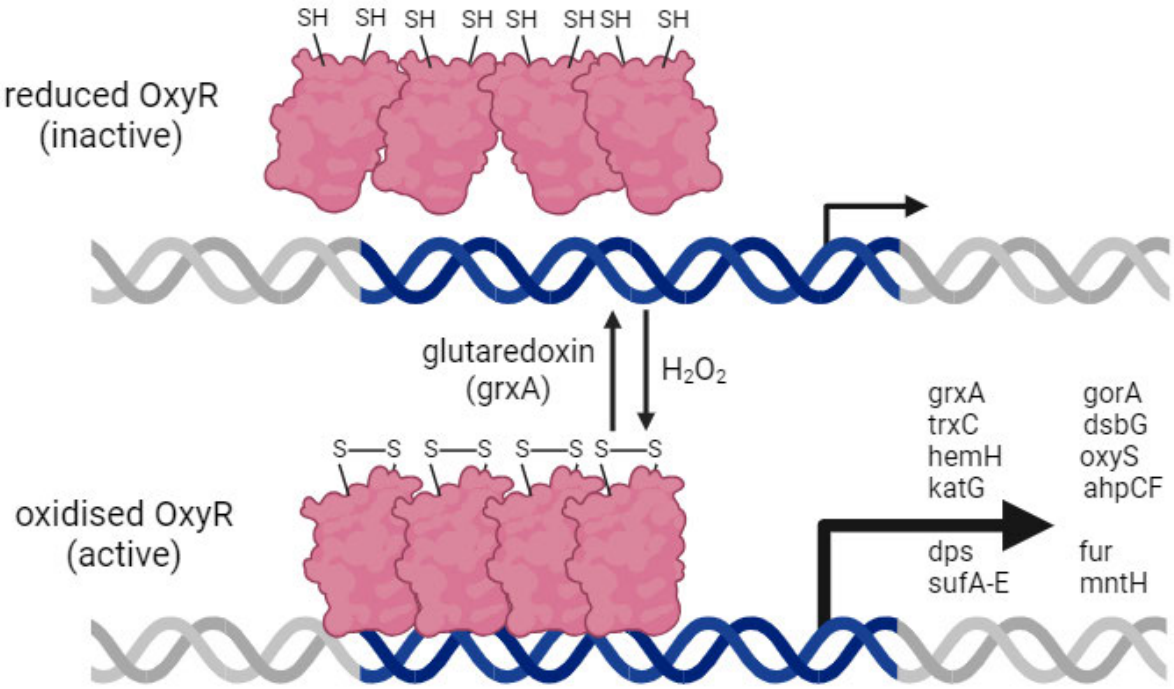

Figure 1.7: The activation and inactivation of OxyR. The tetramer transcription factor, OxyR, regulates a peroxide-inducible regulon. It is activated via peroxide thiol oxidation and the formation of disulfide bonds within each monomer and inactivated by OxyR-induced glutaredoxin (GrxA) (Antelmann & Helmann, 2011; Pomposiello & Demple, 2001)—*created with BioRender.com*.

OxyR forms a homotetramer, and its activity is regulated by thiol oxidation and reduction. The activation of OxyR by hydrogen peroxide can occur at concentrations that are just above the physiological concentrations (20 nM) (Åslund et al., 1999) and results in the oxidation of a cysteine residue (Cys-199) on each monomer to form an intramolecular disulphide (Figure 1.7). The importance of these cysteines is demonstrated by the fact that these are the only two cysteine residues conserved in OxyR homologs (Zheng, 1998). The formation of the disulphide bond within each monomer causes a conformational change within the regulatory domain of OxyR, influencing how OxyR interacts with the DNA sites and increasing its productive interactions with RNA polymerase for enhanced gene expression (Zheng, 1998).

Regulation of mammalian redox signalling and oxidative stress response by Nrf2-Keap1

The Nrf2-Keap1 pathway is integral to sensing stress and activating antioxidant stress responses in the mammalian cell. Nuclear factor erythroid 2-related factor 2 (Nrf2) is a transcription factor that binds to antioxidant response elements (AREs). As many antioxidant genes are downstream from AREs, Nrf2 acts as the master regulator of the antioxidant stress response within the cell (Enomoto, 2001; Higgins et al., 2009). Nrf2 has been linked to preventing and protecting many pathologies such as Parkinson's (Yang et al., 2022), multiple sclerosis (Suzen et al., 2022), Alzheimer's (Bahn et al., 2019), arthritis, airway diseases (Carlson et al., 2020) and some viral infections. In the case of airway diseases, the activation

of Nrf2 correlates with increased defence against bacteria by macrophages in the lungs, thus increasing the protection against opportunistic bacterial infections (Harvey et al., 2011). In some viral infections such as RSV, rotavirus, and HSV-1, Nrf2 activation correlates with decreased viral replication and cytotoxicity (Bender & Hildt, 2019).

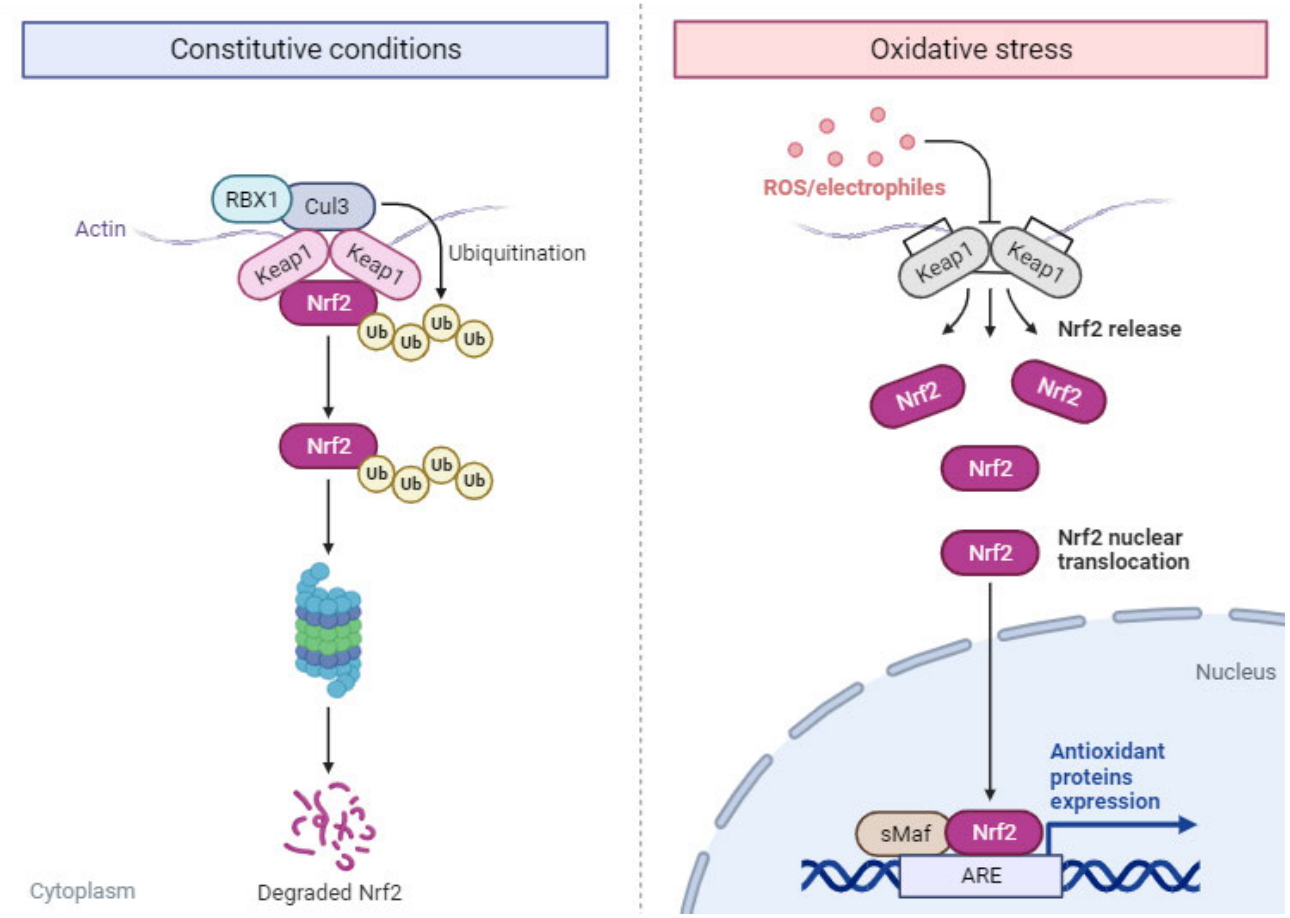

Figure 1.8: The regulation of Nrf2 via the Keap1 ROS oxidation. The inhibitory mechanism of Nrf2 is disrupted by the oxidation and formation of 3 disulphide bonds within the Keap1 protein (Dinkova-Kostova et al., 2002; Taguchi et al., 2011)—*created with BioRender.com*.

Keap1 is the primary inhibitor of Nrf2 activity because Nrf2 bound to Keap1 is tagged for ubiquitination (Figure 1.9). In the cytoplasm of an unstressed cell, Nrf2 is found in the Nrf2-Keap1 complex: this complex consists of one Nrf2 protein bound to a Keap1 homodimer. Keap1 connects Nrf2 to the Cul3/RING-box complex, tagging Nrf2 for ubiquitination (Dinkova-Kostova & Abramov, 2015). Therefore, Nrf2 does not translocate to the nucleus under normal physiological conditions.

The presence of oxidants and electrophiles induces the dissociation of the Nrf2-Keap1 complex. Nrf2 then localises to the nucleus and heterodimerises with Maf to induce target genes (Figure 1.8). Due to the thiol-rich nature of Keap1, it is a clear target for thiol oxidation (Zhang & Hannink, 2003), with Cys-151, Cys-273 and Cys-288 being the critical cysteines (Taguchi et al., 2011). Oxidation of Cys-151 on each monomer forms an intermolecular bond between the Keap1 monomers, and the oxidation of Cys-273 and Cys-288 increases the

reactivity of the surrounding cysteines. This enables the surrounding cysteines (Cys-236 and Cys-613) to form an intramolecular disulphide bond. The formation of these disulphide bonds results in conformational changes, causing this oxidised isoform of Keap1 to dissociate from Nrf2 (Baird et al., 2013; Baird et al., 2014; Fourquet et al., 2010). In this way, Keap1 acts as the ROS sensor in the Nrf2-Keap1 pathway.

Regulation of yeast redox signalling and response by Yap1

The Yap1 transcription factor is the *Saccharomyces cerevisiae* (baker's yeast) member of the subfamily of AP-1-like transcription factors found in mammals and humans (Moye-Rowley et al., 1989). This is the same family in which we find Cap1 in *Candida albicans*, Pap1 in *Schizosaccharomyces pombe*, and the AP-1 transcription factor in humans (Åslund et al., 1999). These factors are implicated in many cellular processes, such as apoptosis (Shaulian & Karin, 2001) and the transcriptional response to cytotoxins and oxidants (Ameyar et al., 2003). The activation of Yap1 has been demonstrated to enhance resistance to drugs, oxidative stress, and heat shock and benefits the cell by strengthening many of the vital pathways involved in essential cellular maintenance (Lee et al., 1999). It does this by inducing the expression of genes that are associated with carbon metabolism pathways, protein biosynthesis, heat shock and chaperoning, antioxidants, respiration and cell cycle and growth regulation (Jun et al., 2012).

Yap1 being an AP-like transcription factor means it consists of 3 central regions: (1) The basic leucine zipper domain (bZip) is the DNA binding dimerisation domain (Wang et al., 2023); (2) The nuclear exportin signalling region enables the interaction with the chromosomal maintenance 1 protein (Crm1), thus facilitating the exportation of protein out of the nucleus (Kırlı et al., 2015); and (3) the cysteine-rich domain (CRD) is split into 2 regions: one closer to the n-terminal, the n-CRD and one closer to the c-terminal, c-CRD. These regions contain the cysteine residues that make the protein redox-sensitive (Toone et al., 2001).

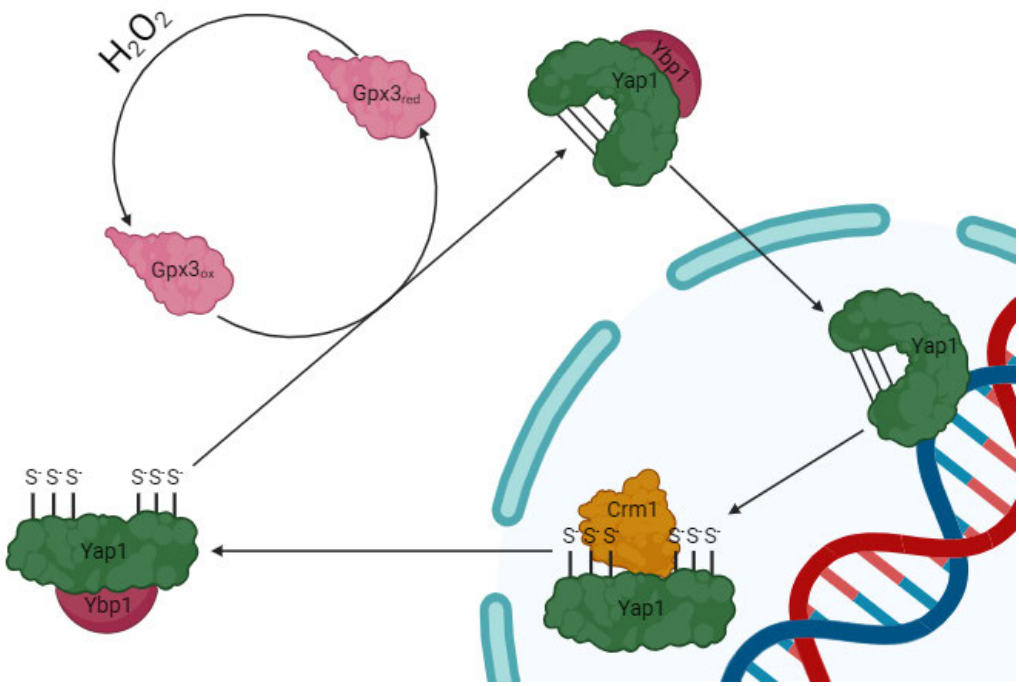

Figure 1.9:The mechanism of Yap1 activation in *S. cerevisiae*. Forming three disulphide bonds within Yap1 from GPx3-mediated hydrogen peroxide oxidation masks the nuclear export for the translocation of Yap1 to the nucleus (Boronat et al., 2014; Veal et al., 2003)—*created with BioRender.com.*

The mechanism of Yap1 activation closely parallels that of Pap1's: both are not directly oxidised by hydrogen peroxide but use an antioxidant to transduce that signal. However, in the case of Yap1, the antioxidant used is GPx3, and for hydrogen peroxide oxidation, another protein is called upon in the process, Yap1-binding protein (Ybp1) (Veal et al., 2003) (Figure 1.9). Hydrogen peroxide oxidises the catalytic cysteine on GPx3 to form GPx3-SOH. This then condenses with the cysteine residue on Yap1 to form an intermolecular disulfide bond between GPx3 and Yap1. This hydrogen peroxide-dependent reaction is chaperoned by Ybp1, which brings Yap1 and GPx1 together to favour this reaction. Forming an intramolecular disulfide bond within Yap1 resolves the Yap1-GPx3 intermediary (Bersweiler et al., 2017; Delaunay et al., 2000). Three disulfide bonds are formed in the full activation of Yap1 (Okazaki et al., 2007). The formation of these disulfide bonds causes structural change, which masks the exportin region of Yap1, disrupting the Yap1-Crm1 interaction. This causes the nuclear localisation of Yap1 as Crm1 can no longer interact with it to export it out of the nucleus (Kuge, 1997; Yan, 1998), enabling Yap1 to induce the genes associated with it.

The Tpx1-Pap1-Trr1 pathway in Schizosaccharomyces pombe

S. pombe has emerged as a model organism for investigating oxidative stress due to its conserved processes, which are more closely related to those of higher eukaryotic organisms and mammals compared to *S. cerevisiae* (Hoffman et al., 2015; Papadakis & Workman, 2015). This makes it ideal for exploring oxidative stress response processes with potential applications for human systems (Hayles & Nurse, 2018).

A critical pathway in *S. pombe*'s response to oxidative, multidrug, and nutritional stress is the Tpx1-Pap1-Trr1 pathway (Madrid et al., 2004; Vivancos et al., 2006). Central to this pathway is the Pap1 transcription factor, which has similarities with the previously discussed Yap1 (Toone et al., 2001). The Pap1 pathway enables the cell to mount a response to non-toxic hydrogen peroxide levels (70 – 200 µM) by triggering the induction of a slew of genes (Chen et al., 2008). The induced genes' induce the translation of proteins that detoxify the cell of hydrogen peroxide cell and undo oxidative damage (Song & Roe, 2008).

The redox activity of Pap1 is dependent upon a 2-Cys typical peroxiredoxin Tpx1 (Wood, Poole, et al., 2003; Wood, Schröder, et al., 2003), which serves as the redox sensor of the pathway (Vivancos et al., 2005) The exact mechanism of Pap1 oxidation by Tpx1 remains a subject of debate. However, one of the hypotheses is that Tpx1's C_P is oxidised by hydrogen peroxide to form the C_P-SOH. The C_P-SOH forms a transient disulphide complex with Pap1 at Cys-501 or Cys-532 in the c-CRD. A disulfide exchange reaction allows for forming a disulphide bond with one of the cysteines in the n-CRD, Cys-278 and Cys-285 (Bozonet et al., 2005). For the complete activation of Pap1, two disulfide bonds must be formed across the n-CRD and c-CRD (Cys-278–Cys-532 and Cys-285–Cys-501), which would require a second oxidised Tpx1 to oxidise the other Cys residue.

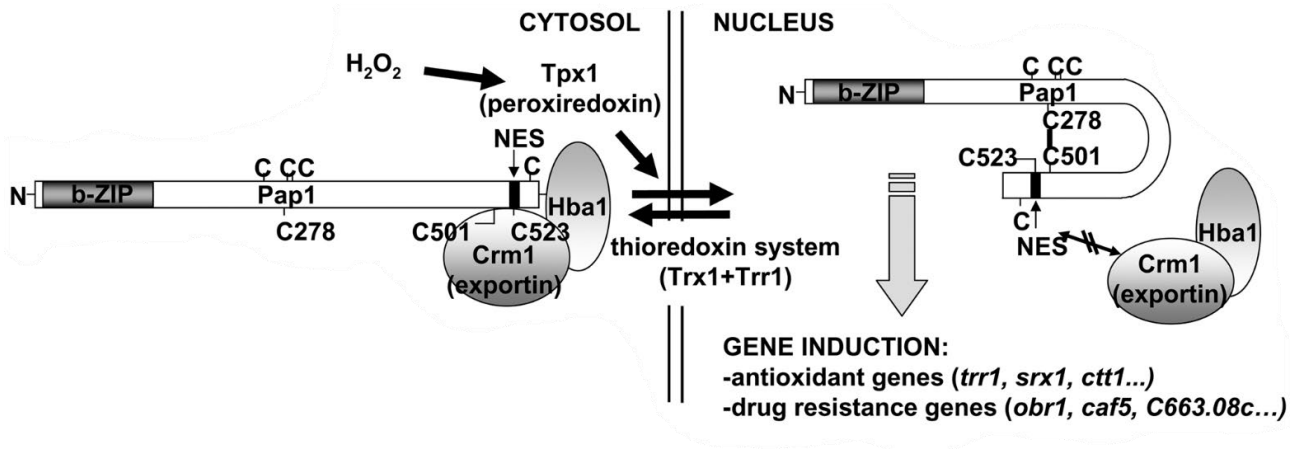

Figure 1.10: The activation of Pap1 via oxidised Tpx1 and its translocation in and out of the nucleus. Tpx1 oxidises Pap1, leading to the formation of disulphide bonds, thus disrupting Crm1's ability to bind to Pap1's NES, allowing for nuclear translocation of Pap1 and Pap1-dependent gene induction. The thioredoxin system reduces the disulphide bonds, allowing Crm1 to export Pap1 out of the nucleus—*adapted from "Figure 1. A" in Calvo et al. (2012) and the original work is an open-access article distributed under the terms of the Creative Commons Attribution Non-Commercial License*.

The formation of these bonds causes a conformational change in Pap1, disrupting the Crm1's ability to bind with Pap1 (Vivancos et al., 2004), inhibiting Pap1's export out of the nucleus, allowing Pap1 to activate its target genes (Pemberton & Paschal, 2005; Yan, 1998) (Figure 1.10). The thioredoxin system can reduce Pap1, similar to Tpx1 (Day et al., 2012). The reduction of Pap1 breaks the disulphide bonds, allowing for the reconstitution of the Pap1:Crm1 complex and Pap1's export from the nucleus (Figure 1.10).

The Tpx1-Pap1-Trr1 pathway's activation decreases as hydrogen peroxide (>500 µM) increases. This is due to Tpx1's propensity to become hyperoxidised at high hydrogen peroxide levels, forming a sulfinic acid (Day et al., 2012). Interestingly, the thioredoxin system cannot reduce the hyperoxidised peroxiredoxin isoform, but it is instead reduced by the sulfiredoxin (Srx1) (Bozonet et al., 2005; Halliwell & Gutteridge, 2015a), whose gene is induced by Pap1. However, hyperoxidised Tpx1 plays a role in activating Sty1, as it needs dual phosphorylation and Tpx1-mediated oxidation to translocate to the nucleus (Tomalin et al., 2016). Sty1 is a protein in the stress-activated protein kinase (SAPK) pathway in *S. pombe* (Papadakis & Workman, 2015).

A commonality observed across all these pathways is that they all require multiple oxidation events to activate the transcription factor fully. Curiously, unlike, say, an electronic alarm system, these pathways need multiple switches to activate cellular 'alarm' for oxidative stress. This raises the question of why such apparent redundancy exists within these cellular defence pathways.

1.5. Design principles of analogous signalling systems.

Achieving specific responses through kinetic insulation

The cell can process a large influx of external information despite its size, orchestrating appropriate responses to various stimuli. Though resource constraints seem challenging, the cell's strategy of reusing components across many signalling pathways efficiently mitigates wastage. However, this would make the cell susceptible to crosstalk, a symptom in many pathologies and disease states (Komarova et al., 2005). What is observed is a cell being able to produce specific responses for specific stimuli (Schaeffer & Weber, 1999). Kinetic insulation is one of the cell's mechanisms to pull this off (Behar, Dohlman, et al., 2007). It leverages the unique temporal behaviour of different pathways to establish specificity. So, in an example where there are two different pathways, X and Y, which share a common protein, P, the determination of whether the response originates from pathway X or pathway Y hinges on the temporal profile of P, meaning pathway X will only trigger a response if P's activation constitutes a transient signal (Locasale, 2008).

In contrast, pathway Y may respond exclusively to a slow P signal increase (Figure 1.11). The capability of each pathway to discern these distinct temporal profiles depends on the specific mechanisms inherent to each pathway. Some pathways utilise chaperoning proteins to create microcompartments, further insulating the pathway and increasing its specificity (Komarova et al., 2005). An example in *S. cerevisiae* is the FUS3, KSS1 and HOG1 pathways, which all share common proteins in the MAPK cascade even though they influence

vastly different cellular responses. FUS3, KSS1 and HOG1 function in the mating pheromone response, filamentous growth and high osmolarity response, respectively (Schaeffer & Weber, 1999; Schwartz & Madhani, 2004).

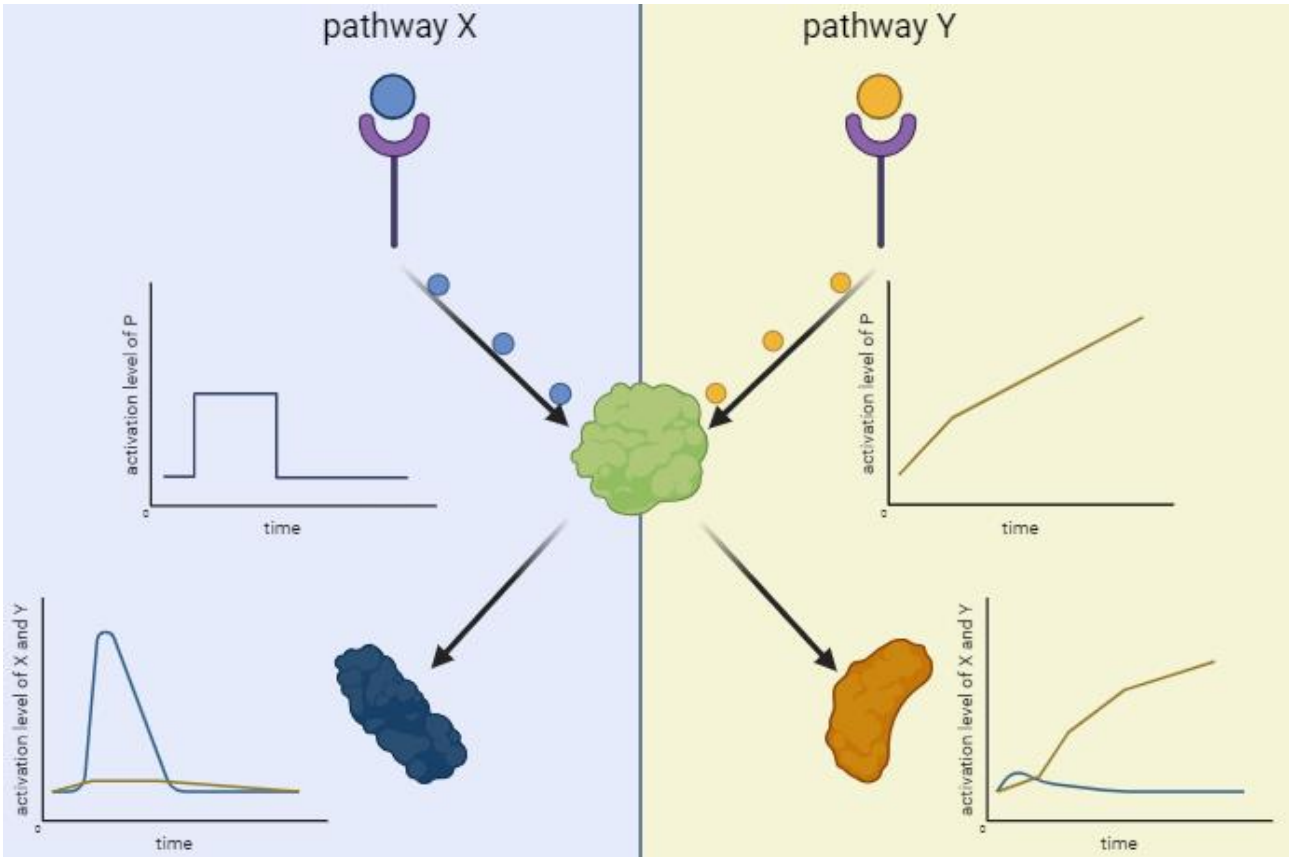

Figure 1.11: Kinetic insulation prevents cross-talk between pathways with a standard protein. Different pathways may share a common protein, and to prevent crosstalk, the activation profile of a common protein determines the activation signal profile for each pathway. Thus, each pathway has a separate outcome (Behar, Dohlman, et al., 2007)—*created with BioRender.com*.

Enhancing accuracy in biochemical reactions through kinetic proofreading

Kinetic proofreading utilises energy-consuming steps in a pathway to increase the fidelity of the reaction. This mechanism is used in T-cell activation, enabling T-cells to differentiate between “self” and “non-self” antigens (Iyengar & Perry, 2021). DNA repair systems also use kinetic proofreading to recognise errors in the DNA strand and replace them with the correct nucleotide. In protein synthesis, kinetic proofreading assures heightened accuracy in codon reading and adding the correct amino acid to the polypeptide chain, making the error rate for this reaction as low as 10^{-4} (Hopfield, 1974).

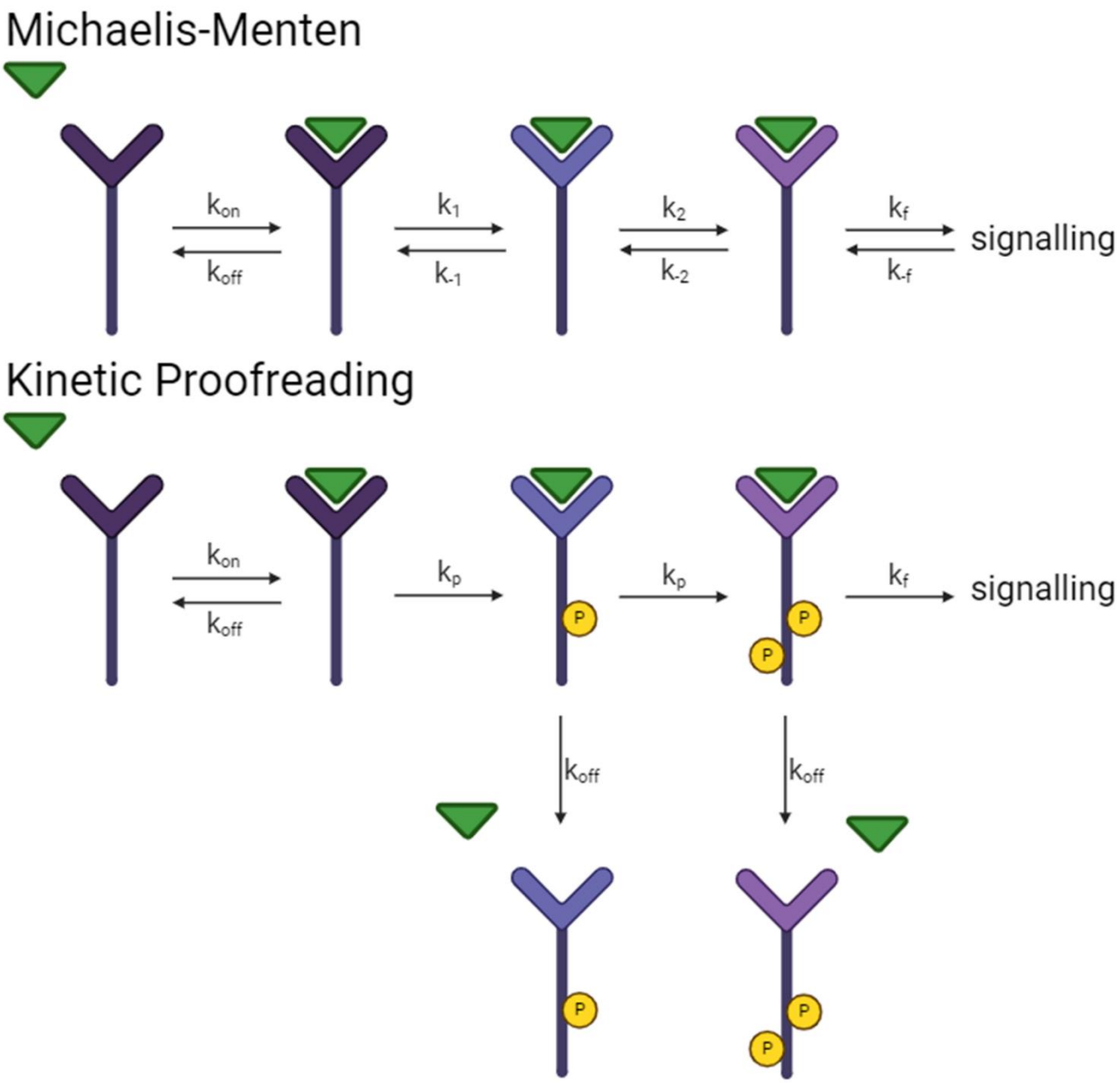

Figure 1.12: The kinetic proofreading mechanism compared to a reversible Michaelis-Menten process. The Michaelis-Menten reaction (top) progresses linearly and reversibly at each step, where the difference in the reverse reaction rate at each step (k_{off}, k_{-1}, k_{-2} and k_{-f}) for the correct and incorrect substrate or ligand determines the fidelity of the reaction. However, with kinetic proofreading (bottom), the phosphorylation modification of the receptor or enzyme (k_p), illustrated by the yellow circles, introduces a discriminating step. This step ensures that it cannot be reformed again if the complex disassociates (koff, different for the correct and incorrect ligand or enzyme). This increases the fidelity of the reaction—*created with BioRender.com*.

The kinetic proofreading mechanism is best understood when contrasted with a Michaelis-Menten reaction. Given a simple Michaelis-Menten reaction, the 'on' rates for incorrect and correct substrates are assumed to be similar. The 'off' rates differ, with the correct substrate having a lower off rate than the incorrect substrate (Hopfield, 1974). This allows the off rates to differentiate between the substrates, thus increasing the fidelity of the reaction. Adding steps increases the fidelity of the reaction even further. However, the trade-off would involve many steps to reach the same error rate observed for protein synthesis (Boeger, 2022).

Kinetic proofreading solves this problem by enzymatically coupling the reaction to another reaction that can provide energy, e.g. the hydrolysis of ATP or GTP (Hopfield, 1974). The energy step overcomes the thermodynamic limits and modifies the tRNA in protein synthesis. The modified tRNA either continues down the elongation process or dissociates from the codon; however, once dissociated, due to the phosphorylation, it cannot reassociate (Alon, 2019). The energy step provides a second discriminating step, which removes the dissociated tRNA from the pool of options, thus further increasing the fidelity of the reaction. In cell signalling, kinetic proofreading ensures that a false signal is not propagated and is a consequence of multiple reactions, which initiate the signal cascade (Goldstein et al., 2008).

Attenuation and amplification of the signal using high, low and band pass filters.

Cells are signal processors in a noisy environment and need processes to filter out unwanted noise, much like low pass, high pass, and bandpass filters do in electrical signalling processors. The removal of noise is essential because when a signal is transmitted, the environment will inevitably introduce noise to the signal, thus adding errors to the information (Magsi et al., 2018). Therefore, signal processors must be able to remove the noise and error and extract the original signal. Band pass, low pass, and high pass filters do this. A high pass filter attenuates frequencies below a lower threshold, only allowing frequencies above it to pass through, and a low pass filter attenuates frequencies above an upper threshold, allowing only frequencies below the threshold through. A bandpass filter combines the two, only allowing frequencies over a specific range through and attenuating all frequencies below and above the upper and lower threshold (Jaeger & Blalock, 2016).

These filters are utilised in biological systems. The thalamus acts as a low-pass filter, but the individual neurons act as a high-pass filter. For individual neurons of the thalamus to be fired, the input needs to be above a specific rate; however, for the thalamus to encode a specific stimulus, the neurons cannot be firing too rapidly as this will create ambiguity within the network and cause the thalamus not to be able to encode the stimuli at all. So, the thalamus only encodes the stimuli when the firing of the neurons happens below a given rate (Connelly et al., 2016). Synthetic biologists have also been able to design chemically responsive protein-based bandpass filters that only react to a drug over a specified concentration range (Shui et al., 2023). Similarly, the HOG pathway in *S. cerevisiae* acts as a low pass filter, where it averages out the stimuli when the osmolarity changes rapidly but accurately follows osmolarity stimulation when it is not rapidly changing (Hersen et al., 2008). These filtering properties within biological systems, networks, and pathways most likely emerge from their architecture. The fact that these properties are analogous to electrical

engineering concepts may make it easier to understand these complex systems, thus opening different avenues of investigation.

1.6. The aim and objectives

The principal objective of this study is to elucidate how multiple oxidation events within redox-regulated pathways contribute to the specificity of these pathways in responding to stimuli, hydrogen peroxide. To achieve this, we have developed and analysed a computational model of the Pap1-Tpx1-Trr1 pathway, investigating the impacts of multiple oxidations on the system's response to varying hydrogen peroxide concentrations. Further, our *in vitro* assembly of the Pap1-Tpx1-Trr1 pathway, coupled with targeted Pap1 protein mutations aimed at inhibiting multiple oxidations, may provide insight into the dynamic responses of the pathway to such events.

Chapter 2: The Computational Modelling of the Tpx1-Pap1 Pathway

2.1. Introduction

Computational modelling uses mathematical and logical approaches to model realistic or approximate solutions for biochemical and metabolic pathways (Klipp & Liebermeister, 2006). These approaches have been used to model several redox systems, providing insights into these systems. For example, it was established that a redox switch's oxidation-reduction ratio influences the switch's hydrogen peroxide sensitivity (Antunes & Brito, 2017). In the thioredoxin system, an analytical solution expanded upon the computational model's insights, demonstrating that the thioredoxin system is adaptable and has interconnectivity between thioredoxin-dependent pathways (Pillay et al., 2011). A large-scale model was used to study how redox couples (GSH/GSSG, Cys/CySS and thioredoxins) influence cell function, interact, and control each other (Kemp et al., 2008).

For experimental work and computational models investigating signalling pathways, the signal output can be described as a function of four parameters: dynamic range, amplitude, time, and duration (Figure 2.1) (Heinrich et al., 2002). The dynamic range is the pathway's responsiveness to the incremental changes in the input, which is vital in determining the outcome of the signal (Janes et al., 2008). Signal amplitude (S_i) is the average concentration of the activated protein, indicating the signal's strength. The average time it takes to activate the protein is described by the signal time (τ_i) while the signal duration (ϑ_i) is the average time the protein remains activated (Heinrich et al., 2002; Hornberg et al., 2005). These signal parameters are calculated from the total amount of activated protein (P_i) over the signal interval (t) and $\mathrm{T_i}$ is the total concentration of activated protein. Additionally, the equations have been formatted by colour to show how each variable in integrated into other equations.

The area under the curve ($P_i(t)$) is I_i and is calculated as such:

$$I_i = \int_0^\infty P_i(t)dt \tag{2.1}$$

and

$$T_i = \int_0^\infty t \cdot P_i(t)dt \tag{2.2}$$

Equations 2.1 and 2.2 are used to describe the signal time (τ_i):

$$\tau_i = \frac{T_i}{I_i} \tag{2.3}$$

The signal duration is calculated using equation 2.2:

$$\vartheta_i = \sqrt{\frac{\int_0^\infty t^2 P_i(t)\,dt}{I_i} - \tau_i^2} \tag{2.4}$$

The signal amplitude is calculated using equation 2.3:

$$S_i = \frac{I_i}{2\vartheta_i} \tag{2.5}$$

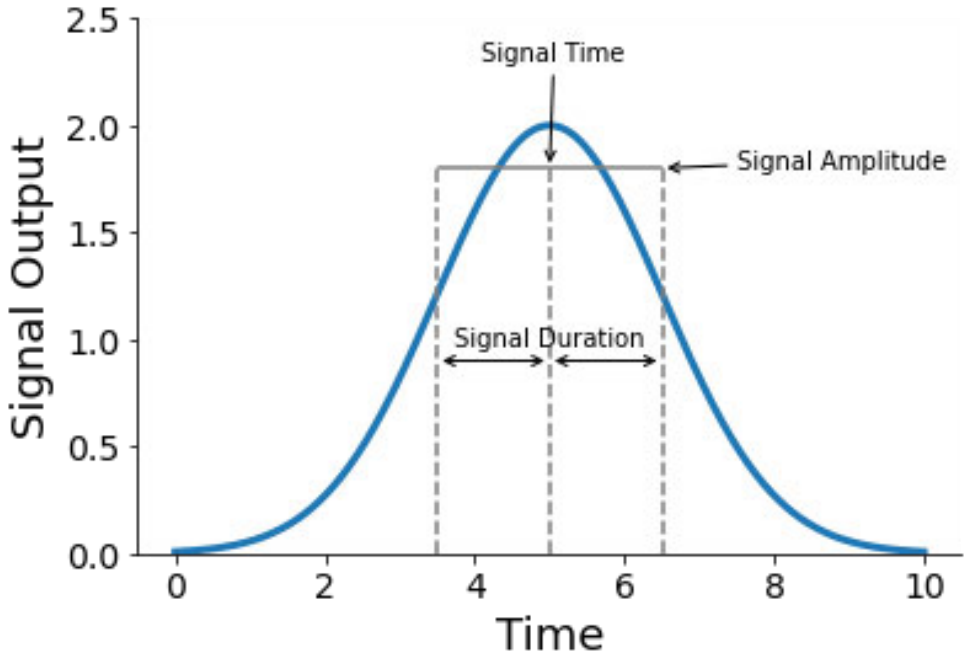

Figure 2.1: A graphical representation of signal time, duration and amplitude. The signal parameters can be calculated using equations 2.1, 2.2 and 2.3 from the signal output's time course.

This study investigated the purpose of multiple oxidation steps in adaptive redox pathways for transcription factor activation. Specifically, we focused on the Tpx1-Pap1 pathway and its response to the input signal, hydrogen peroxide. We employed *in silico* methodologies to determine the potential benefits of adding an extra oxidation step in enhancing the pathway's response. We constructed and analysed simplified analytical models for single-oxidation and double-oxidation functions to achieve this. Additionally, we developed a model of the Tpx1-Pap1-Trr1 pathway to investigate its behaviour and dynamics further under different hydrogen peroxide concentrations and when one or two oxidation steps are needed for the full activation of the pathway. Through these analyses, we aimed to understand better how multiple oxidation steps contribute to redox signalling pathways' overall functionality and adaptability.

2.1. Methods

The analytical modelling of a single and double oxidised redox transcription factor

Double and single oxidation models were constructed to investigate the fraction of oxidised transcription factor (TF_{ox}/TF_{tot}). TF_{ox}/TF_{tot} was solved using Maxima (https://maxima.sourceforge.io/) and was analysed using NumPy (Harris et al., 2020) and Matplotlib (Hunter, 2007). A histogram of TF_{ox}/TF_{tot} values for each quartile of a variable was generated using 30 bins.

Computational modelling of the Tpx1-Pap1-Trr1 pathway

The computational models for the Tpx1-Pap1 pathway were developed using SciTE, a text editor, and simulated using the Python Simulator for Cellular Systems (PySCeS) (Olivier et al., 2005) in a Jupyter notebook (https://jupyter.org/). The models were based on differential equations that described the molecular interactions within the pathway, incorporating data from the BRENDA database (https://www.brenda-enzymes.org/). All models are available in the Supplementary Information.

2.2. Results

Developing an analytical model for comparing single and multiple oxidation models in redox transcription factor activation.

We investigated the impact of multiple oxidation events on a theoretical redox transcription factor activation by comparing a model requiring a single oxidation event to activate the transcription factor to one requiring two.

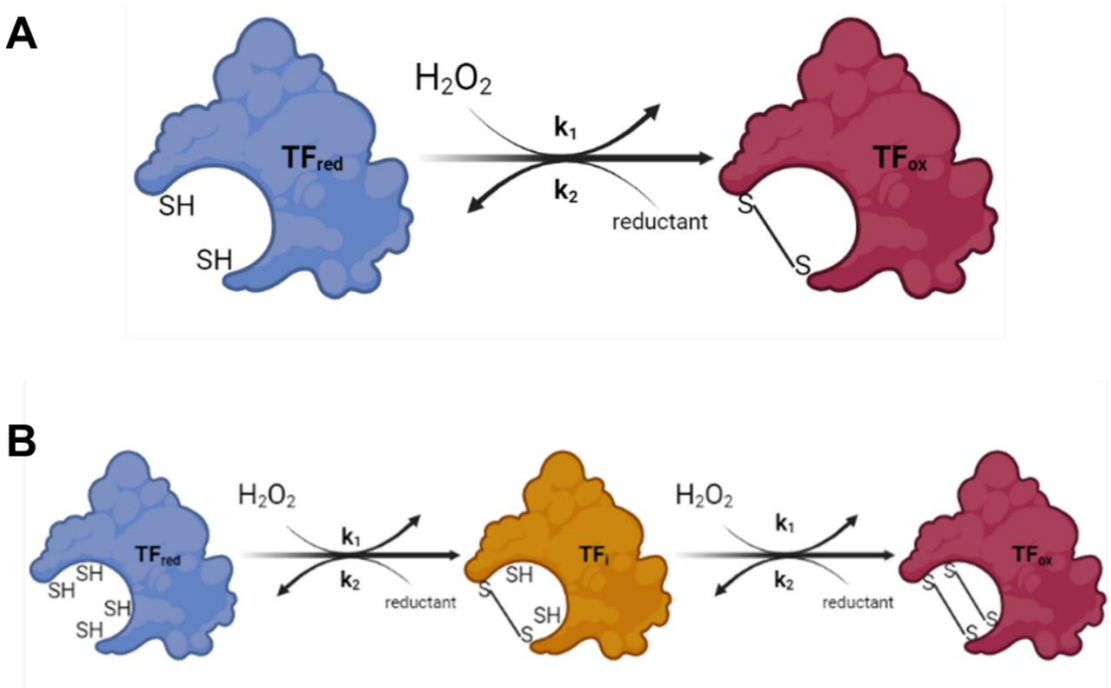

Figure 2.2: The oxidation and reduction of the simple hypothetical redox transcription factor. (A) Schematic representation of a redox transcription factor (TF) undergoing reversible oxidation from its reduced isoform (TF_{red}) to its oxidised, active form (TF_{ox}) by hydrogen peroxide (H_2O_2) with a rate constant of k_1 and the reducing reaction with a rate constant of k_2. **(B)** The TF_{red} undergoes two oxidation events to form an intermediary isoform (TF_i) and then the fully activated TF_{ox} isoform, both with a rate constant of k_1 and the reducing reaction with a rate constant of k_2—*created with BioRender.com.*

The analytical single oxidation and double oxidation models developed comprised two or four reactions, respectively, with the redox transcription factor (TF) being oxidised and reduced once or twice (Figure 2.2). The models made several assumptions: (i) at a steady state, the rates of oxidation and reduction of the TF were equal; (ii) auxiliary reactions which contribute to the oxidation or reduction of the TF were included in the k_1 and k_2 parameters, respectively; and (iii) TF_{ox} is the only active isoform of TF. In the models, the total concentration of the TF was conserved, and the reactions were also described with irreversible mass-action kinetics (Behar, Hao, et al., 2007; Cavadas et al., 2013; Klipp & Liebermeister, 2006).

The ODEs for the single-oxidation model:

$$\frac{dTF_{red}}{dt} = k_2 \cdot T\mathrm{F}_{\mathrm{ox}} \cdot \mathrm{reductant} - k_1 \cdot T\mathrm{Fred} \cdot H_2O_2 \quad (2.6)$$

$$\frac{dTF_{ox}}{dt} = k_1 \cdot TF_{red} \cdot H_2O_2 - k_2 \cdot TF_{ox} \cdot reductant \quad (2.7)$$

In the single oxidation event system, the rate equations are given by:

$$v_1 = k_1 \cdot TF_{red} \cdot H_2O_2 \quad (2.8)$$

$$v_2 = k_2 \cdot TF_{ox} \cdot reductant \quad (2.9)$$

The total TF moiety couple can be related to its sum as follows:

$$TF_{tot} = TF_{red} + TF_{ox}$$

$$TF_{red} = TF_{tot} - TF_{ox} \quad (2.10)$$

At steady state, $v_2 = v_1$, which gives us:

$$k_2 \cdot TF_{ox} \cdot reductant = k_1 \cdot TF_{red} \cdot H_2O_2 \quad (2.11)$$

Rearranging equation (2.11) yields:

$$TF_{ox} = \frac{k_1 \cdot TF_{red} \cdot H_2O_2}{k_2 \cdot reductant} \quad (2.12)$$

To solve for a fraction of the activated TF, we can substitute equation (2.10) into equation (2.12), which gives us the following:

$$\frac{TF_{ox}}{TF_{tot}} = \frac{k_1 \cdot H_2O_2}{k_1 \cdot H_2O_2 + k_2 \cdot reductant} \quad (2.13)$$

Thus, as the reductant approached zero, the fraction of activated TF tended toward one, resulting in the total oxidation of the TF at any hydrogen peroxide value greater than zero (eqn. 2.13). This solution was aligned with the literature as Pap1 is fully oxidised in *Δtrr1 S. pombe* cells (i.e.) cells where the reductant is zero (Vivancos et al., 2004). Conversely, as the reductant increased, the fraction of activated TF tended towards zero (eqn. 2.13) as the reductant reduced the oxidised form of the TF. The fraction of activated TF is zero if the hydrogen peroxide concentration is zero, showing that the system is inactive under normoxic conditions (eqn. 2.13). As the hydrogen peroxide concentration increases, the fraction of activated TF is also expected to increase, which is corroborated by OxyR studies demonstrating that the fraction of oxidised OxyR increased with increased hydrogen peroxide (Åslund et al., 1999).

The ODEs for the double-oxidation model:

$$\frac{dTF_{red}}{dt} = k_2 \cdot TF_i \cdot reductant - k_1 \cdot TF_{red} \cdot H_2O_2 \quad (2.14)$$

$$\frac{dTF_i}{dt} = k_1 \cdot TF_{red} \cdot H_2O_2 + k_2 \cdot TF_{ox} \cdot reductant - k_2 \cdot TF_i \cdot reductant - k_1 \cdot TF_i \cdot H_2O_2 \quad (2.15)$$

$$\frac{dTF_{ox}}{dt} = k_1 \cdot TF_i \cdot H_2O_2 - k_2 \cdot TF_{ox} \cdot reductant \quad (2.16)$$

Equations (2.17) through (2.20) define the rates of four chemical reactions in terms of rate constants and concentrations of reactants for the double oxidation model (Figure 2.2B):

$$v_1 = k_1 \cdot TF_{red} \cdot H_2O_2 \quad (2.17)$$

$$v_2 = k_2 \cdot TF_i \cdot reductant \quad (2.18)$$

$$v_3 = k_1 \cdot TF_i \cdot H_2O_2 \quad (2.19)$$

$$v_4 = k_2 \cdot TF_{ox} \cdot reductant \quad (2.20)$$

The total concentration of TF is defined in equation (2.21):

$$TF_{tot} = TF_{red} + TF_i + TF_{ox} \quad (2.21)$$

The intermediary isoform at steady state was described as $v_1 + v_4 = v_2 + v_3$, which was substituted and solved:

$$k_1 \cdot TF_{red} \cdot H_2O_2 + k_2 \cdot TF_{ox} \cdot reductant = k_2 \cdot TF_i \cdot reductant + k_1 \cdot TF_i \cdot H_2O_2$$

$$TF_i = \frac{k_1 \cdot TF_{red} \cdot H_2O_2 + k_2 \cdot TF_{ox} \cdot reductant}{k_2 \cdot reductant + k_1 \cdot H_2O_2} \quad (2.22)$$

The reduced isoform at steady was described as $v_2 = v_1$ at steady state, which was substituted and solved:

$$k_2 \cdot TF_i \cdot reductant = k_1 \cdot TF_{red} \cdot H_2O_2$$

$$TF_{red} = \frac{k_2 \cdot TF_i \cdot reductant}{k_1 \cdot H_2O_2} \quad (2.23)$$

The intermediary isoform was also described in terms of the total:

$$TF_i = TF_{tot} - TF_{red} - TF_{ox} \quad (2.24)$$

Equation (2.24) substituted into equation (2.23) and solving yields:

$$TF_{red} = \frac{k_2 \cdot (TF_{tot} - TF_{red} - TF_{ox}) \cdot reductant}{k_1 \cdot H_2O_2}$$

$$TF_{red} = \frac{(TF_{tot} - TF_{ox}) \cdot k_2 \cdot reductant}{k_2 \cdot reductant + k_1 \cdot H_2O_2} \quad (2.25)$$

At a steady state, the oxidised isoform can be described as $v_4 = v_3$, therefore:

$$k_2 \cdot TF_{ox} \cdot reductant = k_1 \cdot TF_i \cdot H_2O_2 \quad (2.26)$$

Equation (2.25) was substituted into equation (2.22), and it was substituted into equation (2.26) and solved:

$$k_2 \cdot TF_{ox} \cdot reductant = k_1 \cdot \left(\frac{k_1 \cdot \left(\frac{(TF_{tot} - TF_{ox}) \cdot k_2 \cdot reductant}{k_2 \cdot reductant + k_1 \cdot H_2O_2}\right) \cdot H_2O_2 + k_2 \cdot TF_{ox} \cdot reductant}{k_2 \cdot reductant + k_1 \cdot H_2O_2}\right) \cdot H_2O_2$$

$$\frac{TF_{ox}}{TF_{tot}} = \frac{{k_1}^2 \cdot {H_2O_2}^2}{{k_1}^2 \cdot {H_2O_2}^2 + k_1 \cdot k_2 \cdot H_2O_2 \cdot reductant + {k_2}^2 \cdot reductant^2} \quad (2.27)$$

The two equations for the single oxidation (2.13) and double oxidation (2.27) share similarities: the fraction of activated TF is directly proportional to the hydrogen peroxide concentration and inversely proportional to the reductant concentration. However, the single oxidation equation comprises linear polynomials in both the numerator and denominator with no critical points, whereas the double oxidation equation (eqn 2.27) comprises quadratic polynomials with critical points at (0, reductant). At the critical point, the slope of the graph is zero, and for quadratic polynomials, the absolute value of the rate of change increases the further away from the critical point (Marden, 1966). Additionally, when the absolute value of the rate of change is high, a slight change in the hydrogen peroxide concentration will cause a rapid increase in the fraction of activated TF. When it is low, the opposite is true. Therefore, for the double oxidation equation at low hydrogen peroxide concentrations, close to the critical point, TF activation is low and less responsive to hydrogen peroxide changes than the single oxidation model. Conversely, TF activation is highly responsive to high hydrogen peroxide changes at high concentrations. Thus, an additional oxidation reaction changes the system's behaviour to input hydrogen peroxide concentrations.

To visualise this effect, the two functions were plotted on contour plots:

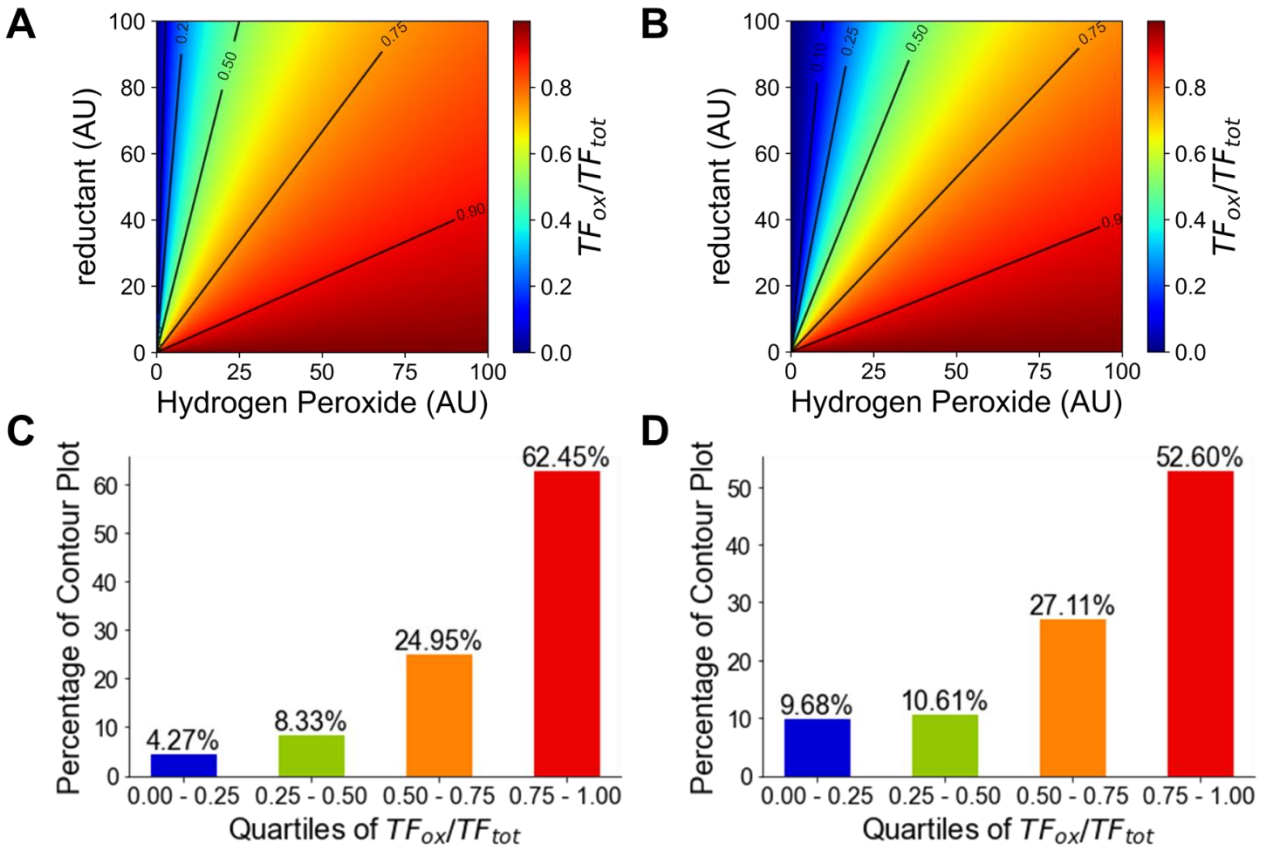

Figure 2.3: The transcription factor activation for a single and double oxidation equation. (A-B) The contour plots were constructed using equation (2.13) for the single oxidation equation and equation (2.27) for the double oxidation equation with the reductant and hydrogen peroxide concentrations quantified in arbitrary units (AU). The contour plots used a gradient scale to represent the fraction of activated transcription factor (TF_{ox}/TF_{tot}). Boundary lines (0.1, 0.25, 0.5, 0.75 and 0.9)

are drawn on the plot as black lines and labelled. **(A)** Represents the single oxidation function, and **(B)** represents the double oxidation function. **(C-D)** Bar plots representing the percentage of the contour plot (corresponding to (A) and (B) respectively) that fall within the quartiles of the fraction of activated transcription factor (Q1=0-0.25, Q2=0.25-0.5, Q3=0.5-0.75 and Q4=0.75-1.0).

Our results show that the double oxidation model (Figure 2.3B) can maintain a higher fraction of inactive TF over a broader range of hydrogen peroxide concentrations than the single oxidation model (Figure 2.3A). This is demonstrated by the rightward shift of the boundary lines (Figure 2.3B), particularly at low hydrogen peroxide concentrations. The shift in the TF activation levels was quantified by looking at the activation threshold of 0.5 for the activated transcription factor. In the single oxidation function, a modest proportion of the plot, 12.6% (4.27+8.33%, Figure 2.3C), fell below this threshold. However, in the case of the double oxidation function, this percentage increased to 20.29% (9.68 + 10.61%, Figure 2.3D). These findings suggested that the double oxidation function maintained relatively lower activation levels across varying concentrations of reductant and hydrogen peroxide than the single oxidation function.

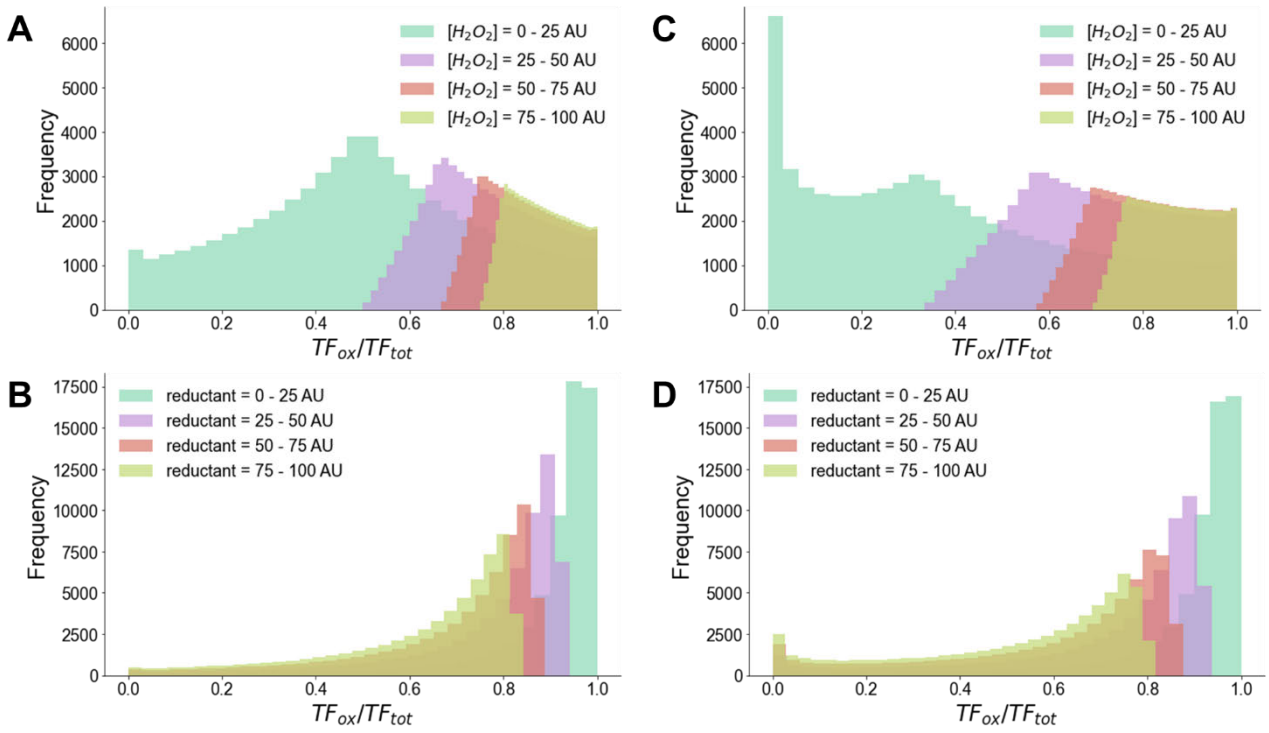

Figure 2.4: The distribution of the contour plot for the fraction of activated transcription factor. The TF_{ox}/TF_{tot} data points were categorised into their corresponding quartile based on the concentration of hydrogen peroxide or reducant. The histogram was generated by dividing the TFox/TFtot values range within each quartile into 30 bins. The number of data points within each bin was counted to obtain the frequency, making it unitless. **(A)** The distribution plot for the single oxidation function at the different quartiles of hydrogen peroxide. **(B)** The distribution plot for the single oxidation function at the different quartiles of the reductant. **(C)** The distribution plot for the double oxidation function at the different quartiles of hydrogen peroxide. **(D)** The distribution plot for the double oxidation function at the different quartiles of the reductant.

The double oxidation function also had a wider dynamic range of activation, as exhibited by its broader distribution of activated transcription factor. At lower hydrogen peroxide levels

(0–25 AU), the double oxidation model had a lower median (0.33 TF_{ox}/TF_{tot}) and mean (0.37 TF_{ox}/TF_{tot}) (Figure 2.4C) than the single oxidation model mean and median at 0.5 TF_{ox}/TF_{tot} (Figure 2.4A). Thus, most data is clustered towards the low activation levels for the double oxidation model, whereas the single oxidation model is normally distributed at low hydrogen peroxide levels. This suggests that the double oxidation model at low hydrogen peroxide concentrations is less responsive than the single oxidation model. However, the mean and median values of activated TF for both models at high hydrogen peroxide concentrations (75-100 AU) are similar, with the single oxidation model's being 0.88 and 0.87 and the double oxidation model's being 0.86 and 0.86. Therefore, both models respond similarly and highly at high concentrations of hydrogen peroxide.

The double oxidation function displays heightened sensitivity to the influence of the reductant on the activation of the transcription factor compared to the single oxidation function. Both functions exhibit similar central tendencies at low reductant concentrations (0–25 AU), with mean and median values of 0.9 and 0.94 for the single oxidation function (Figure 2.4B) and 0.88 and 0.94 for the double oxidation function (Figure 2.4D), respectively. In the highest quartile (75–100 AU), the mean and median of activated TF for the double oxidation function are 0.53 and 0.61, respectively, while for the single oxidation function, they are 0.62 and 0.70. Thus, the double oxidation model was more affected by the reductant than the single oxidation model at these levels.

The analytical modelling of the activation of a redox transcription factor showed that increasing the number of oxidation steps attenuated the activation of the pathway (i.e.) extra oxidation steps prevent pathway activation at low hydrogen peroxide concentrations. Furthermore, this attenuation of the double oxidation model seemed limited to lower hydrogen peroxide levels. Compared to the single oxidation model, there was no decrease in the double oxidation model's ability to respond highly to elevated levels of hydrogen peroxide. Therefore, an extra oxidation step results in a high-pass filter for the system. This filter is critical as the oxidative stress response reconfigures the cell's metabolome, transcriptome, and proteome to support antioxidant defence mechanisms (Gasch et al., 2000; Morano et al., 2012; Rusz et al., 2021). Therefore, these systems' unintentional and nonessential activation could be highly detrimental and wasteful for the organism.

The model of the Tpx1-Pap1 pathway indicates that the pathway acts as a high-pass filter.

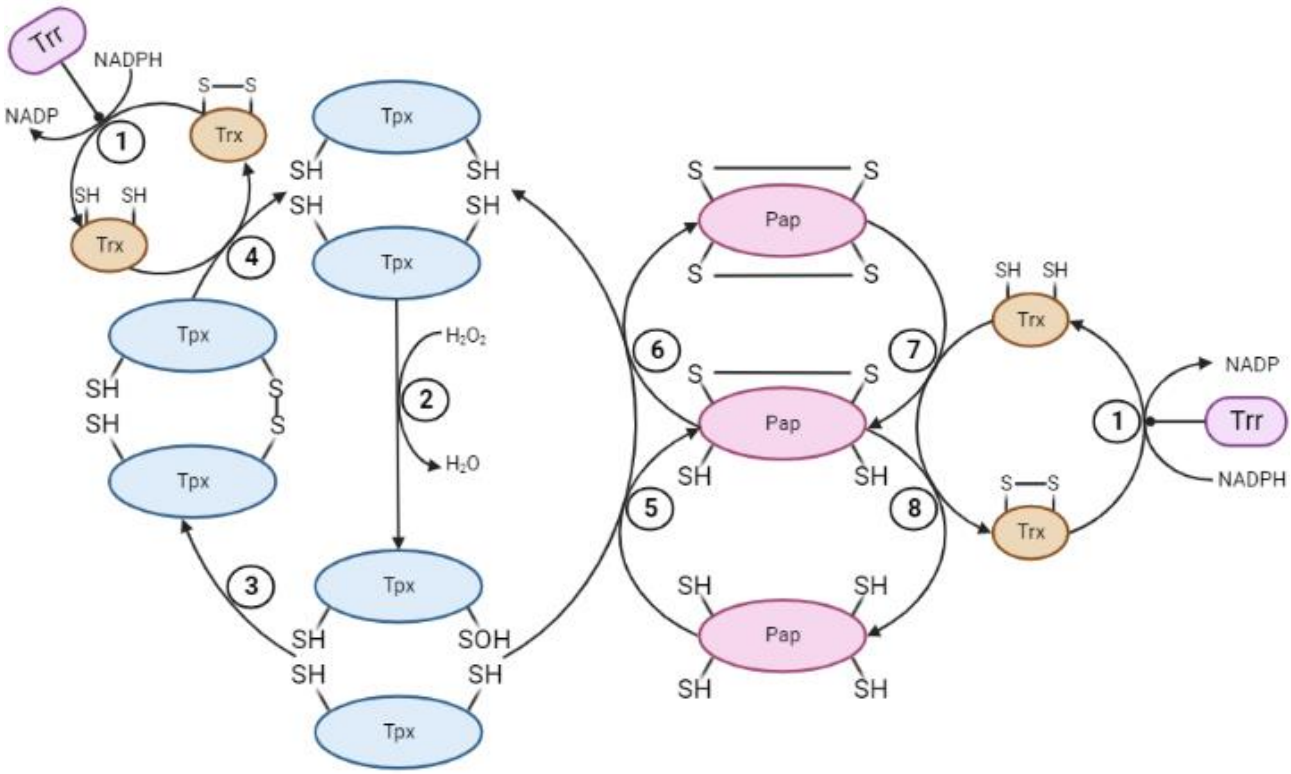

Figure 2.5: Schematic representation of the Tpx1-Pap1 pathway used for computational analysis. The reduction of Trx by Trr and NADPH is represented by reaction 1. The oxidant sensing component of the pathway is the oxidation of a Tpx dimer, reaction 2, which is modified to the sulfenic isoform. The sulfenic isoform then reacts with the other monomer within the dimer to form a disulfide bridge, reaction 3, which Trx then reduces in reaction 4. In the single oxidation model, Pap is oxidised once, as in reaction 5, and assumed to be fully oxidised (Model S1). The double oxidation model (Model S2) includes reaction 6, which occurs at a rate 10 times faster than reaction 5 and forms a partially oxidised intermediate. Reactions 7 and 8 reduce the oxidised Pap (Boronat et al., 2014; Klomsiri et al., 2011; Vivancos et al., 2005)—*created with BioRender.com*.

We constructed a model of *S. pombe's* Pap1 pathway to analyse the double and single oxidation models on a complete system of reactions (Figure 2.5). In order to investigate the Tpx1-Pap1 pathway, we simplified the model to include a maximum of eight reactions, including only those proteins and reactions directly involved in Pap1 activation. We assumed the second oxidation step occurred faster than the first, as the partially oxidised isoform is rarely observed in western blotting experiments (Vivancos et al., 2005). However, a double oxidation model was constructed in which the second Pap1 oxidation step occurs at the same rate as the first. All three models' hydrogen peroxide consumption (Figure S1) and Tpx1 oxidation states (Figure S3) were compared and found to be the same. This demonstrated that the differences observed in Pap1 oxidation for each model (Figure S2) were independent of the dynamics of the upstream molecules. The construction of the pathway was based on the information provided in Table 2.1.

The ODEs for the computational model of the Tpx1-Pap1-Trr1 pathway:

$$\frac{dTrxSS}{dt} = k_4 \cdot TpxSH_{TpxSS} \cdot TrxSH \; + k_7 \cdot PapSSSS \cdot TrxSH + k_8 \cdot PapSSSH \cdot TrxSH - \frac{k_{cat1} \cdot Trr\left(\frac{NADPH}{k_{1nadph}}\right)\left(\frac{TrxSS}{k_{1trx1ss}}\right)}{\left(\frac{1+NADPH}{k_{1nadph}}\right)\left(\frac{1+TrxSS}{k_{1trx1ss}}\right)} \quad (2.28)$$

$$\frac{dTrxSH}{dt} = \frac{k_{cat1} \cdot Trr\left(\frac{NADPH}{k_{1nadph}}\right)\left(\frac{TrxSS}{k_{1trx1ss}}\right)}{\left(\frac{1+NADPH}{k_{1nadph}}\right)\left(\frac{1+TrxSS}{k_{1trx1ss}}\right)} - k_4 \cdot TpxSH\_TpxSS \cdot TrxSH\ ) - k_7 \cdot PapSSSS \cdot TrxSH - k_8 \cdot PapSSSH \cdot TrxSH \quad (2.29)$$

$$\frac{dTpxSH}{dt} = k_4 \cdot TpxSH\_TpxSS \cdot TrxSH + k_5 \cdot TpxSH\_TpxSOH \cdot PapSHSH + k_6 TpxSH\_TpxSOH \cdot PapSSSH - k_2 \cdot TpxSH\_TpxSH \cdot H_2O_2 \quad (2.30)$$

$$\frac{dTpxSH\_TpxSOH}{dt} = k_2 \cdot TpxSH\_TpxSH \cdot H_2O_2 - k_3 \cdot TpxSH\_TpxSS - k_5 \cdot TpxSH\_TpxSOH \cdot PapSHSH\ ) - k_6 \cdot TpxSH\_TpxSOH \cdot PapSSSH \quad (2.31)$$

$$\frac{dTpxSH\_TpxSS}{dt} = k_3 \cdot TpxSH\_TpxSS - k_4 \cdot TpxSH\_TpxSS \cdot TrxSH\ ) \quad (2.32)$$

$$\frac{dPapSHSH}{dt} = k_8 \cdot PapSSSH \cdot TrxSH - k_5 \cdot TpxSH\_TpxSOH \cdot PapSHSH \quad (2.33)$$

$$\frac{dPapSSSH}{dt} = k_5 \cdot TpxSH\_TpxSOH \cdot PapSHSH \; + k_7 \cdot PapSSSS \cdot TrxSH - k_6 \cdot TpxSH\_TpxSOH \cdot PapSSSH - k_8 \cdot PapSSSH \cdot TrxSH \quad (2.34)$$

$$\frac{dPapSSSS}{dt} = k_6 \cdot TpxSH\_TpxSOH \cdot PapSSSH - k_7 \cdot PapSSSS \cdot TrxSH \quad (2.35)$$

Table 2.1: Kinetic parameters and species concentrations used to develop the computational models of Pap1 reduction and activation.

Model Reactions		Model Parameters			
Reaction Label	**Rate equation**	**Kinetic Parameters (s-1; µM; µM.s-1)**		**Species**	**Initial concentration (µM)**
R1	$\frac{k_{cat1} \cdot Trr \left(\frac{NADPH}{k_{1nadph}}\right)\left(\frac{TrxSS}{k_{1trx1ss}}\right)}{\left(\frac{1+NADPH}{k_{1nadph}}\right)\left(\frac{1+TrxSS}{k_{1trx1ss}}\right)}$	k_{cat1}	66	TrxSH	0.7 (Marguerat et al., 2012)
				TrxSS	0.00
		k_{1nadph}	1.3	NADPH	150 (Lee et al., 1995)
				NADP	0.00
		$k_{1trx1ss}$	4.4	Trr	0.5 (Lee et al., 1995)
R2	$k_2 \cdot TpxSH_{TpxSH} \cdot H_2O_2$	k_2	20	H2O2	[c]1.00
				H2O	0.00
R3	$k_3 \cdot TpxSH\_TpxSS$	k_3	1.7	TpxSH_TpSH	4 (Marguerat et al., 2012)
R4	$k_4 \cdot TpxSH\_TpxSS \cdot TrxSH$	k_4	0.2	TpxSH_TpxSOH	0.00
R5	$k_5 \cdot TpxSH\_TpxSOH \cdot PapSHSH$	k_5	0.04	TpxSH_TpxSS	0.00
*R6	$k_6 \cdot TpxSH\_TpxSOH \cdot PapSSSH$	[a]k_6	0.4	PapSHSH	0.0245 (Marguerat et al., 2012)
*R7	$k_7 \cdot PapSSSS \cdot TrxSH$	[a,b] k_7	0.01	PapSSSH	0.00
R8	$k_8 \cdot PapSSSH \cdot TrxSH$	[b]k_8	0.01	PapSSSS	0.00

* These reactions are not present in the single oxidation model.
[a] These parameters are not present in the single oxidation model.
[b] These parameters are changed when the reduction of Pap1 is a perturbation.
[c] The initial concentration of hydrogen peroxide (H_2O_2) is changed for each system perturbation

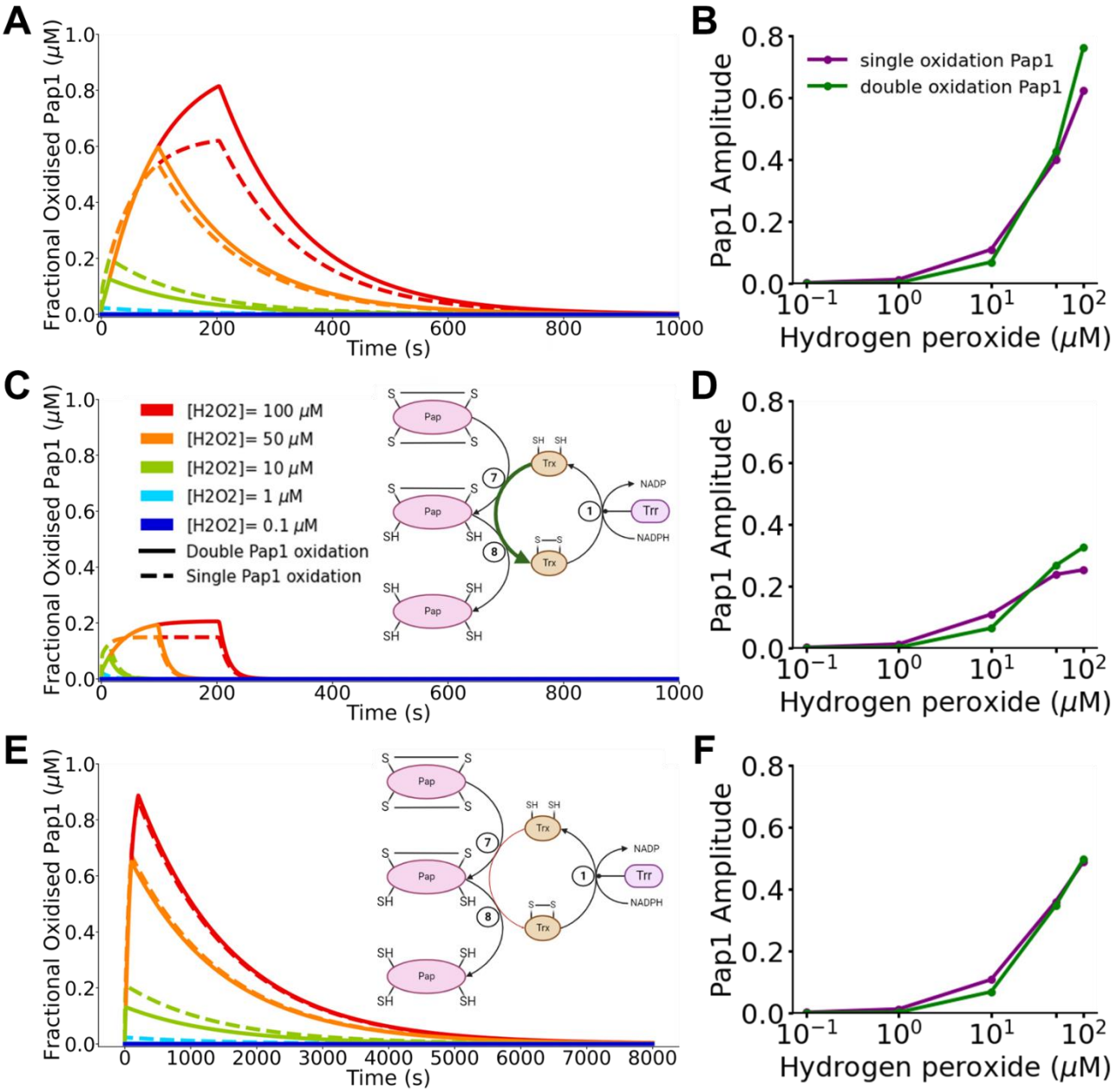

Figure 2.6:The double oxidation of Pap1 activity of the pathway at low and high hydrogen peroxide concentrations, respectively. The left panel **(A, C, E)** shows the time course for a fraction of oxidised Pap1 with increasing hydrogen peroxide concentrations for single and double oxidation models. The right panel **(B, D, F)** shows the amplitude for each model at the different concentrations of hydrogen peroxide. **(A – B)** the simulation results for the single and double oxidation models of Pap1 at different hydrogen peroxide concentrations, with the model reduction parameters left unchanged. **(C – D)** The single and double oxidation model with a 10-fold increase in Pap1 inactivation. **(E – F)** The single and double oxidation models with a 10-fold decrease in Pap1 inactivation. The plots in each figure show the fraction of activated Pap1 at different hydrogen peroxide concentrations over a specific time (16 min:40 sec for A and C, 2 hrs:13 min:20 for C).

The double oxidation of Pap1 exhibited an apparent attenuation of the pathway at low concentrations of hydrogen peroxide, resembling the behaviour of a high-pass filter. Under normoxic conditions (Figure 2.6A), when the hydrogen peroxide concentration is 10 μM or lower, the fraction of activated Pap1 in the double oxidation model is lower compared to the single oxidation model. However, starting from 50 μM of hydrogen peroxide, the double oxidation model displays a higher fraction of activated Pap1. This transition in the pathway's

behaviour, shifting from low activation to high activation, suggests the presence of a threshold in the double oxidation model. The amplitude analysis of the pathway at different hydrogen peroxide concentrations (Figure 2.6B), which quantifies the average concentration of activated Pap1, confirms the distinct behaviour of the double oxidation model compared to the single oxidation model. At low hydrogen peroxide concentrations, the double oxidation model shows a lower amplitude, therefore a lower concentration of activated Pap1 over the signal time, in the fraction of activated Pap1 than the single oxidation model. However, as the hydrogen peroxide concentration increases, the double oxidation model displays a larger amplitude value.

We analysed Pap1 activation for both models when Pap1's reduction rate is either increased or decreased. Increasing the reduction rate (Figure 2.6C-D) decreased the overall fraction of the activated Pap1, its signal time and the duration of both models. With the increased reduction rate, the pattern observed in Figure 2.6A is conserved, but the high pass properties are exaggerated. Lower Pap1 activation was observed for the double oxidation model at low hydrogen peroxide concentrations and higher Pap1 activation for the double oxidation model at high hydrogen peroxide concentrations. However, the overall attenuation of both models makes the pathway less activated (Figure 2.6D), which could result in an inadequate or non-existent response to hydrogen peroxide.

By decreasing the Pap1 inactivation rate (Figure 2.6E), the maximum fraction of activated Pap1 increases in the single oxidation model, reaching levels similar to those of the double oxidation model at 50 and 100 µM hydrogen peroxide. However, at lower hydrogen peroxide concentrations (10 µM or less), the double oxidation model still exhibits a smaller fraction of activated Pap1 than the single oxidation model. Interestingly, the decrease in the Pap1 inactivation rate does not appear to impact the maximum fraction of activated Pap1 significantly in the double oxidation model across all concentrations of hydrogen peroxide.

2.3. Discussion

In this study, we investigated the impact of an additional oxidation event on a redox pathway and its implications for transcription factor activation using an analytical model. Our findings revealed that including an extra oxidation step in the pathway conferred high-pass filter properties. The double oxidation models exhibited a greater attenuation of transcription factor activation at low concentrations of hydrogen peroxide and comparable activation levels at higher concentrations of hydrogen peroxide. The response to oxidative stress reconfigures the cell and can alter the cell's proteome by inducing reversible and irreversible post-translational modifications (Go & Jones, 2013). Transcriptomically, a wide array of genes are

induced by oxidative stress; these genes code for proteins involved in the antioxidant defence system, protein synthesis and carbohydrate metabolism, thus affecting the metabolome (Chen et al., 2003). Therefore, the accidental activation of the oxidative stress response pathways is detrimental to the cell. A high pass filter-like mechanism ensures that low levels of hydrogen peroxide, which may play a role in normal cell physiology, do not activate the pathway and the stress response. Multiple oxidation steps impart this property onto the pathway due to an increased number of steps at which the reductant can inhibit transcription factor activation. However, too many reductive steps could make the pathway less responsive as observed by the overall lowered Pap1 activation at high reductant capacity (cf. Figures 2.3, 2.6). Therefore, the number of redox steps in activating these pathways represents a trade-off between high-pass filtering and responsiveness.

In agreement with the literature, our model showed Tpx1 underwent oxidation at low hydrogen peroxide concentrations (20 and 50 µM), while Pap1 remains reduced and inactive (Domènech et al., 2018). At higher levels of hydrogen peroxide, our model showed increased Pap1 activation which was also in agreement with the literature (Quinn et al., 2002). However, our model is simplified and relies on estimated parameters as some parameter values are unknown. Consequently, certain discrepancies exist between the *in silico* model and the *in vivo* pathway. For instance, our model does not account for the bimodal function resulting from the recovery of the hyperoxidised Tpx1 isoform by Srx1 as gene expression was not included in the model (Vivancos et al., 2005).

Chapter 3: *In vitro* analysis of the Tpx1-Pap1-Trr1 system

3.1. Introduction

In vivo and *in vitro* approaches give complementary insights into redox biology and the systems involved, from the molecular to the organismal level. *In vivo* approaches allow researchers to study the system in a physiologically relevant context, including the system's environmental, genomic, and proteomic background, generating spatial and temporally dependent data. However, this plethora of data has downsides, making it challenging to disentangle all the different information flows, signalling and activity in a system (Rao et al., 2014). *In vitro* methods fill this gap by simplifying the system and enabling researchers to control the environment and the components involved; this allows for more acute manipulation of the system, which can provide mechanistic insights (Graudejus et al., 2018). However, this approach sacrifices critical components in each system, but together, these methods are synergistic with *validated in vitro studies* and complementing *in vivo* observations.

In vitro studies on transcription factors offer a targeted examination of these crucial proteins, which lie downstream of signalling cascades and can regulate the response of a system to stimuli. Notable studies have included studying the role of c-Fos and c-Jun in an *in vitro* system to analyse hydrogen peroxide's influence on its DNA binding and transcriptional activity (Ferguson, 2001). The DNA binding capability of NF-κB was studied *in vitro* and shown to be inhibited by alkylation and diamide oxidation, with the diamide oxidation inhibition being reversed by reducing agents (Toledano & Leonard, 1991). Moreover, the activation of OxyR is influenced by the ratio between hydrogen peroxide generation and degradation, and its preferential reduction by the glutaredoxin system was demonstrated in an *in vitro* experiment (Åslund et al., 1999).

There have been no *in vitro* studies of Pap1 activation, which is surprising given that there are conflicting theoretical models of Pap1 activation. The first two models assume that Tpx1 oxidises Pap1 directly (Figure 3.1 A-B), although it is unclear whether it is the sulfenic isoform of Tpx1 which interacts with Pap1 (Vivancos et al., 2005; Vivancos et al., 2006) or the disulphide Tpx1 isoform which oxidises Pap1 via a thiol-disulphide exchange (Calvo, Boronat, et al., 2013; He et al., 2016). The third model assumes Pap1 oxidation is driven by oxidised thioredoxin-1 (Trx1) (Brown et al., 2013) (Figure 3.1C). All three of these mechanisms could operate simultaneously, and an *in vitro* system could be used to test these models. However,

the resolution of the models is complicated because Tpx1 can exist in its monomeric and dimeric isoforms and other redox states. These redox states of some isoforms are similar in size, making it difficult to differentiate them by SDS-PAGE. For example, the Tpx1 homodimer can have a single or two disulphide bonds or the C_p of one Tpx1 molecule can be hyperoxidised to form C_pSO_2H (Tomalin et al., 2016). The monomeric isoform on a gel can represent the sulfenic acid Tpx1 and the hyperoxidised sulfinic acid isoform of Tpx1 (Day et al., 2012; Vivancos et al., 2005). The computational model (Figure 2.5) assumed that the sulfenic acid isoform of Tpx1 (Figure 3.1A) oxidised Pap1; the other two models were excluded.

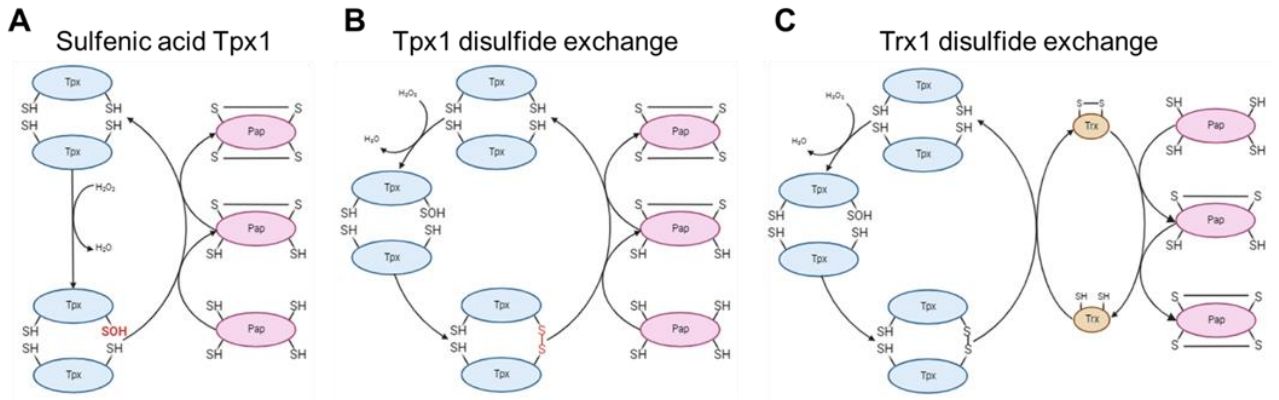

Figure 3.1: Theoretical Pap1 activation models. Pap1 is not directly oxidised by hydrogen peroxide, and thus, three hypothetical mechanisms propose distinct events that lead to the oxidation and activation of Pap1. **(A)** Hydrogen peroxide oxidises Tpx1 to form the sulfenic acid, which then oxidises Pap1. **(B)** Pap1 oxidation occurs through thiol-disulfide exchange with the disulfide isoform of Tpx1. **(C)** Oxidised Tpx1 oxidises Trx1, which undergoes a thiol-disulfide exchange with Pap1 to oxidise it (details in text)—*created with BioRender.com*.

Four critical cysteines regulate Pap1's redox activity. The two critical cysteines for Pap1 activation at the n-CRD are Cys-278 and Cys-285, as when these critical cysteines are mutated, no nuclear accumulation of Pap1 is observed *in vivo* (Calvo, Ayté, et al., 2013). Cells expressing this mutated Pap1 are as sensitive to hydrogen peroxide as *Δpap1* cells. At the c-CRD, there are three cysteines. However, only two are critical, and mutations of these critical cysteines, Cys-501 and Cys-532, disrupt Pap1 accumulation in the nucleus with a mutation at Cys-501 leading to a partial nuclear accumulation and a mutation at Cys-532 completely inhibiting the nuclear accumulation of Pap1. Interestingly, a mutation in Cys-532 leads to peroxide-sensitivity equivalent to *Δpap1* cells (Calvo, Ayté, et al., 2013; Castillo et al., 2002).

In this chapter, we expressed and purified the Tpx1-Pap1-Trr1 system. As a first step, we aimed to determine the mechanism underlying Pap1 activation and then used site-directed mutagenesis to create Pap1 mutants activated by a single disulfide bridge.

3.2. Methods and Materials

Materials

PCR reagents, including DreamTaq DNA polymerase, SnakeSkin™ dialysis tubing (3.5 K MWCO), PageRuler™ Plus prestained protein ladder, Pierce™ bicinchoninic acid (BCA) protein kit and GeneJET plasmid miniprep kit were obtained from Thermo Fisher Scientific (Johannesburg, South Africa). PCR primers and nickel-charged nitriloacetic acid (Ni-NTA) agarose were purchased from Whitehead Scientific (Pty) Ltd (Cape Town, South Africa). Hydrogen peroxide was obtained from Lab Care Supplies (Durban, South Africa). Bovine serum albumin (BSA) was purchased from Celtic Molecular Diagnostics (Pty)Ltd (Cape Town, South Africa). N-ethylmaleimide (NEM); iodoacetamide (IAM); acrylamide; *N,N'*-methylene-bisacrylamide, ammonium persulphate (APS); the secondary antibody produced in rabbit, anti-mouse IgG horseradish peroxidase conjugate antibody (Lot #106M4870V); kanamycin sulfate; dithiothreitol (DTT); 4-(2-aminoethyl) benzene sulfonyl fluoride hydrochloride (ABESF), phenylmethylsulfonyl fluoride (PMSF) and isopropyl ß-D-1-thiogalactopyranoside (IPTG) were obtained from Sigma Aldrich (Johannesburg, South Africa). *S. pombe* cytosolic thioredoxin (trx1, *SPAC7D4.07c*), thioredoxin peroxidase (tpx1, *SPCC576.03c*), thioredoxin reductase (trr1, *SPBC3F6.03*), and AP-1-like transcription factor (pap1, *SPAC1783.07c*) genes were synthesised and cloned into the pET28α expression vectors by GenScript Ltd (Hong Kong). The Q5 site-directed mutagenesis kit from New England Biolabs was obtained via Inqaba Biotechnical Industries (Pretoria, South Africa). The primary antibody, monoclonal mouse 6x-His tag, was kindly donated by Prof Dean Goldring (Pietermaritzburg, South Africa), and *E. coli* BL21 cells were available as lab stocks. Clarity™ western ECL substrate, nitrocellulose membrane (0.45 µM), *N,N,N',N'*-tetramethylethylenediamine (TEMED), and other general chemicals were bought from Merck (Johannesburg, South Africa).

Luria-Bertani agar and broth

The Luria-Bertani (LB) agar medium composition used in this study included agar (20 g/L), NaCl (10 g/L), tryptone (10 g/L), and yeast extract (5 g/L). For LB broth, the same components were used except for agar. All solid ingredients were dissolved in distilled water, and the pH of the solution was adjusted to 7.0 with NaOH. The media were sterilised by autoclaving, and once cooled, kanamycin was added at a concentration of 50 µg/mL.

1× Phosphate Buffered Saline

PBS consisted of KCl (2.7 mM), Na_2HPO_4, KHPO (10 mM) and NaCl (500 mM); the solutes were dissolved in distilled water, and the pH was adjusted to 7.4 using HCl. The buffer was autoclaved and stored at room temperature.

Lysis buffer

The lysis buffer consisted of KCl (2.7 mM), Na_2HPO_4 and KH_2PO_4 (10 mM), NaCl (500 mM), glycerol (20% v/v) and imidazole (20 mM). The buffer was made of distilled water and autoclaved; β-mercaptoethanol (10 mM) was added once cooled.

Equilibration Buffer

The equilibration buffer consisted of PBS (1×), imidazole (30 mM) and β-mercaptoethanol (10 mM).

Wash buffer

The wash buffer consisted of PBS (1×), imidazole (20 mM) and β-mercaptoethanol (10 mM).

Elution buffers at different imidazole concentrations

The elution buffers consisted of PBS (1×), β-mercaptoethanol (10 mM) and imidazole at different concentrations (40, 60, 80, 100, 120, 150 and 250 mM), which was made from 1 M imidazole.

30% Acrylamide solution

The acrylamide solution consisted of acrylamide (29% w/v) and N,N'-methylene bisacrylamide (1% w/v) dissolved in distilled water. The solution was filtered through a Whatman filter paper.

Separating buffer

The separating buffer consisted of Tris base (1.5 M) and SDS (0.8% w/v) and was dissolved in distilled water. The pH was calibrated to pH 8.8 with HCl, and the solution was filtered using a Minisart® syringe filter.

Stacking buffer

The stacking buffer consisted of Tris base (0.5 M) and SDS (0.4% w/v) and was dissolved in distilled water. The pH was adjusted to pH 6.8 with HCl and filtered using a Minisart® syringe filter.

10× SDS Tank Buffer

The SDS tank buffer consisted of Tris base (0.25 M), glycine (1.924 M), and SDS (0.03467 M) and was dissolved in distilled water.

Coomassie Blue Stain

Coomassie blue stain consisted of brilliant blue R250 (0.125% w/v), methanol (50% v/v) and acetic acid (10% v/v) and was made up of distilled water.

Destain Solution I and II

The destain solution was made with methanol (50% v/v), acetic acid (10% v/v), and distilled water, whilst destain solution II consisted of methanol (5% v/v) and acetic acid (7% v/v) and distilled water.

50× TAE

The TAE buffer consisted of tris base (2 M), acetic acid (1 M), and disodium EDTA (Na_2-EDTA) (50 mM), which were dissolved in distilled water.

10x Tris-buffered saline (TBS) and 1x Tris-buffered saline with 0.1% Tween® 20 detergent (TBST)

A stock solution of 10x TBS was made with a final concentration of 200 mM Tris base and 1.5 M NaCl, and its pH was adjusted to 7.6 with HCl, and 1x TBST was made from the 10x stock solution, and 0.1% (w/v) Tween® 20 detergent was added.

Blocking agent in TBST

The blocking agent used was BSA, dissolved as 10% (w/v) BSA in 1x TBST.

The primary and secondary antibody solution

The primary antibody was stored at -20°C. Before use, it was diluted 5000 X in 5% BSA in 1x TBST and kept at 4°C for reuse. The secondary antibody was stored at -20 °C and was freshly prepared before use by diluting it 5000 X in 5% BSA in 1x TBST.

Methods

Growing of E. coli BL21 cultures

LB (50 µg/mL kanamycin) stock plates were incubated at 37 °C, and broth cultures were incubated at that same temperature at 200 rpm.

Expression and purification of Tpx1 and Pap1 protein

The protocol used for the expression and purification of the recombinant proteins was adapted from Sivashanmugam et al. (2009).

Determining the optimal induction time for each protein

50 mL of LB broth was inoculated with 1 mL overnight *E. coli* BL21 culture containing the pET28α plasmid, housing the respective *S. pombe* genes. The culture was incubated at 37 °C and grown to OD_{600}=0.3 – 0.4. The culture was then induced with isopropyl β-D-1-thiogalactopyranoside (IPTG) at a final concentration of 0.5 mM and incubated (30°C at 200 rpm), and a 1 mL sample was collected pre-induction and every hour post-induction. All the samples were centrifuged (12 000 *x g* for 5 minutes), and the supernatant was discarded. The pellets were resuspended in sterile distilled water dependent on the OD600 of each sample (according to equation 3.1); this step normalised the cell number.

$$amount\ of\ sterile\ dH_2O = 1000\ \mu L \left(\frac{OD_{600}\ value}{10}\right) \quad (3.1)$$

These samples were then run on an SDS-PAGE gel to check the optimal induction time.

Expression of Protein

A 50 mL LB broth was inoculated with 1 mL of overnight culture and incubated at 37 °C until reaching an optical density at 600 nm (OD_{600}) of 0.3–0.4. The culture was then induced with IPTG at a final concentration of 0.5 mM and incubated at 30 °C with agitation at 200 rpm for a predetermined optimal induction time. After the induction period, the cells were harvested by centrifugation (9299 *x g*, 4 °C, 10 minutes), the supernatant was discarded, and the cell pellets were stored at -20 °C if necessary.

Sonication-dependent extraction of expressed soluble proteins from E. coli cell culture

The induced cell pellets were resuspended in 10 mL of lysis buffer containing either AEBSF (final concentration of 0.2 mM) or PMSF (final concentration of 2 mM). The cell suspension was subjected to sonication using 7 cycles of 1-minute pulses with a minimum of 1-minute intervals between pulses, operating at 30% amplitude. Following sonication, the samples were centrifuged (9299 x *g*, 4 °C, 10 minutes), and the supernatant was stored.

Ni-NTA Affinity His-Tagged Protein Purification

The Ni-NTA column was first washed with 30% (v/v) ethanol, and the eluate was discarded. The column was then equilibrated with the equilibration buffer to prepare it for sample loading. The sonicated supernatant containing the target proteins was carefully loaded onto the column and incubated overnight at 4°C on a bench-top tube rotator.

Determining the Optimal Imidazole Concentration for Protein Elution

At each elution step, 1 mL of the eluate was collected for further analysis. The crude supernatant containing unbound proteins was first eluted, followed by two wash steps using the wash buffer. After each wash step, the eluate was collected. Next, a series of gradient

wash steps with increasing concentrations of imidazole (40, 60, 80, 100, 120, 150, and 250 mM) were performed. The eluate was collected at each step of the gradient wash. Once all the desired elution samples were collected, the column was incubated with 0.5 M NaOH for a minimum of 30 minutes, and the solution was then discarded, in order to strip the column of protein and enable its reuse. The column was stored in 30% (v/v) ethanol at 4°C. The eluted samples were analysed by running them on an SDS-PAGE gel to assess the purity and yield of the target proteins.

The Batch Ni-NTA Affinity His-Tagged Purification of Proteins

The batch purification of the proteins was done post optimal imidazole determination, using the determined optimal imidazole concentration. The crude supernatant containing the target protein was eluted from the Ni-NTA column, and 1 mL of the eluate was collected. The column was then washed using the wash buffer, and the corresponding eluate was collected after each wash step. Two times the column volume of the predetermined elution buffer was added to elute the target proteins. All of the eluates were collected for further analysis. The fractions collected during the elution steps were then analysed by running them on an SDS-PAGE gel to assess the purity and yield of the target protein. The eluting buffer was exchanged for 1x PBS buffer via SnakeSkin tubing dialysis, PD-10 columns or Amicon 15-ultra filter.

Pierce™ BCA Protein Assay Kit

The BCA working reagent (WR) was made using equation 3.2 and was prepared to mix 50 parts of Reagent A and 1 part of Reagent B.

$$\text{volume of WR} = (\#\text{samples} + 2) \times 3 \times 0.2 \tag{3.2}$$

The microplate procedure with the sample-to-WR ratio of 1:8 was used. Thus, 25 µL of each sample triplicate was pipetted, and 200 µL WR was put into a microplate well. The plate was closed with a cover plate, incubated at 37°C for 30 minutes, and then cooled to room temperature. The absorbance was measured at 562 nm on a plate reader.

The contents of one Albumin Standard (BSA) ampule were diluted into several clean microcentrifuge tubes using the same diluent as the samples used. The dilution of BSA standards was prepared and aliquoted to the microplate in triplicates. The standard curve was created by plotting the average blank–corrected 562 nm measurement for each BSA standard vs. its concentration in µg/mL, done in triplicates.

The molar concentration (µM) was calculated using equation 3.3 to covert from µg/mL.

$$molar\ concentration\ (\mu M) = \frac{1}{protein\ size\ (kDa)} \times mass\ concentration\ (\mu g/mL) \tag{3.3}$$

The site-directed mutagenesis of the pap1 gene

Plasmid isolation of pET28α Pap1 plasmid

The GeneJet plasmid isolation kit and its protocol were used for isolating the pET28α Pap1 plasmid from *E. coli* BL21cultures stored in the lab. The DNA's purity was assessed using spectroscopy at A_{260}/A_{280} and stored at -20 °C.

Q5® site-directed mutagenesis of pET28α Pap1 plasmid

The Q5® site-directed mutagenesis kit and its protocol (dx.doi.org/10.17504/protocols.io.cjpumm) were used to mutate Pap1: Cys-278 to Ala-278 (Cys278Ala), Cys-285 to Ala-285, Cys-501 to Ser-501 (Cys501Ser) and Cys-532 to Ser-532 (Cys532Ser). The primers for the mutation (Table 3.1) were developed using NEBaseChanger® (https://nebasechanger.neb.com).

Table 3.1: Oligonucleotide primers for Pap1 site-directed mutagenesis. The primers and their annealing temperatures were constructed and calculated using NEBaseChanger®.

Primer	Sequence	Annealing Temperature
Cys278Ala forward	CAA GCA GTT CGC GCA AAA ACT GAG CAC CGC G	66
Cys278Ala reverse	CCA TCC GCA ACG TCC TCG	
Cys285Ala forward	GAG CAC CGC GAG CGG TAG CAT TG	69
Cys285Ala reverse	AGT TTT TGG CAG AAC TGC TTG CC	
Cys501Ala forward	GTATCTGAGCAGCCCGAAAGTGTGGAG	71
Cys501Ser reverse	GCA CGC TCC TTC GCC GGA	
Cys532Ser forward	CAA GGC GAA AAG CAG CAG CAG CG	69
Cys532Ser reverse	TTT TTC AGC TTG CTG CAC AGA TCG	

Visualisation of proteins

SDS-PAGE Acrylamide Gel Electrophoresis

For SDS-PAGE gel electrophoresis, protein samples were prepared by adding the loading buffer to the protein samples at a ratio of 2:5 and boiling them for 8-10 minutes. The resolving gel and stacking gel were prepared according to the method of Laemmli (1970). The gels were run in a 1x SDS tank buffer at 150 V. After electrophoresis, the gels were incubated overnight on an orbital shaker in a Coomassie Blue stain solution. Subsequently, the gels were destained, and protein bands were visualised using a G-BOX Chemi-XR5 GeneSys imaging system.

Western blotting

Following SDS-PAGE electrophoresis, a nitrocellulose membrane on top of the gel was sandwiched between transfer stacks (Trans-blot, Bio-rad). Protein transfer was performed

using the semi-dry method with an ice-cold transfer buffer. The gel was stained with Coomassie blue to confirm the successful transfer of proteins.

Following protein transfer, the nitrocellulose membrane was blocked by incubating it with a 10% (w/v) BSA solution in 1x TBST (Tris-buffered saline with Tween 20) for 30 minutes. After blocking, the membrane was incubated overnight (4°C, 60 rpm, RT) with the primary antibody (10 mL). The next day, the membrane was washed four times with 1x TBST for 5 minutes each to remove any unbound primary antibodies and other impurities. The membrane was then incubated with a diluted secondary antibody solution (1:20 000 dilution, 10 mL) for 1 hour at room temperature. Following the incubation with the secondary antibody, the membrane was washed four times with 1x TBST for 5 minutes each to remove any unbound secondary antibody. The membrane was dried for 10 minutes and incubated with an ECL reagent for 30 seconds. The membrane was imaged using the G-BOX Chemi-XR5 GeneSys imaging. The protein bands on the membrane were sized by comparing them to a PageRuler™ standard.

The Western blot images were processed into 8-bit images, and the intensities of the reduced Pap1 bands (Pap_{red}) and oxidised Pap1 bands (Pap_{ox}) were measured using the gel analysis function of ImageJ. To determine the overall concentration of Pap1, the intensities of Pap_{red} and Pap_{ox} were added together, resulting in the total Pap1 intensity (Pap_{total}). The fractional activation of Pap1 was calculated by dividing the intensity of Pap_{ox} by the Pap_{total}. A plot was created with the time course period on the x-axis and the fractional activation on the y-axis.

The assembling of the Tpx1-Pap1 system with hydrogen peroxide perturbation

Working solutions comprised 1.5 µM of Pap1, 4.5 µM of Tpx1 and 200 mM iodoacetamide (IAM) in phosphate-buffered saline (PBS) buffer. The proteins were reduced by 20 mM DTT (1 hour, RT), the DTT was removed using PD-10 columns or Amicon 15-ultra filters, and the 1x PBS buffer used in the reaction mixtures was degassed. Subsequently, the proteins Pap1 and Tpx1 were mixed within the reaction tube, followed by the addition of hydrogen peroxide (0.4 µM, 4 µM and 40 µM) to initiate the reaction, which was allowed to progress for time intervals of 0 s, 1 s, 5 s, 15 s, 30 s, and 60 s from the initial addition of hydrogen peroxide. The reaction was stopped at each time point by adding an aliquot of IAM (200 mM), and then the samples were prepared for electrophoresis.

3.3. Results

The IPTG expression and purification of the Tpx1-Pap1 pathway proteins

The *tpx1, pap1, trx1* and *trr1* genes were synthesised on a pET28α plasmid backbone and expressed utilising the *E. coli* BL21 expression system (Hutchens & Yip, 1990). IPTG induction successfully expressed the Tpx1-Pap1-Trr1 pathway proteins (Figure 3.2). The data suggested that the optimal induction time for Tpx1 was overnight, with the 4-hour time point producing an intense band (Figure 3.2A), which was corroborated by densitometry analysis (Figure 3.2B). The expression of Pap1 remained consistent throughout the induction period, with the overnight time point having the most pronounced band (Figure 3.2C). The densitometry analysis corroborated this, though the 1-hour time point was slightly above the other time points in terms of the yield of Pap1 (Figure 3.2D). Trr1 also had consistent expression across all time points, with marginally denser bands observed from the 4-hour time point (Figure 3.2E). The overnight expression of Trr1 produced the most significant yield (Figure 3.2F). The gel indicated that for Trx1, the 1, 5-hour, and overnight time points had the most intense bands (Figure 3.2G), which agreed with the densitometry analysis (Figure 3.2H). Pap1 and Tpx1 expression experiments were done in triplicates as they were our most important proteins. Trx1 and Trr1 expression was prioritised when we proved our concept with the Tpx1-Pap1 system.

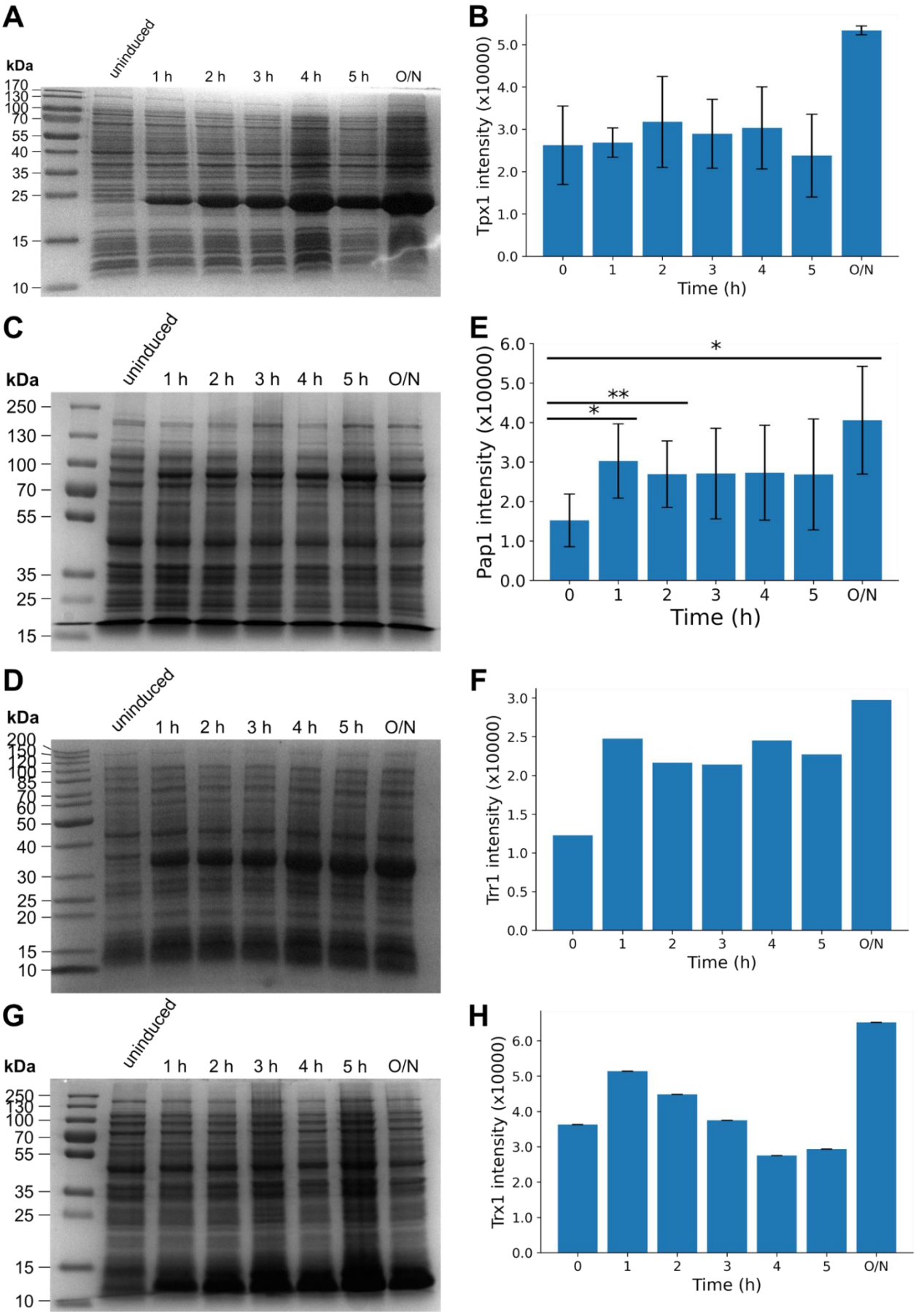

Figure 3.2: The expression and purification of Tpx1-Pap1-Trr1 system proteins. The induction of Tpx1-Pap1-Trr1 system proteins in the *E. coli* BL21 strain using the pET28α plasmid and IPTG induction. The induction was conducted for at least 16 hours, to observe if maximal induction

occurs overnight, for sufficient protein expression and was done in triplicate for Pap1 and Tpx1 induction. **(A)** Optimisation of induction time for Tpx1. **(B)** Determination of optimal expression time for Tpx1 using densitometry. **(C)** Optimisation of induction time for Pap1. **(D)** Determination of optimal expression time for Pap1 using densitometry. Standard error bars are shown as a two-tailed *t*-test was used to compare the induction times ('*', $p<0.10$ and '**' $p<0.05$). **(E)** Determination of the optimal time for Trr1 induction. **(F)** Determination of optimal expression time for Trr1 using densitometry. **(G)** Determination of the optimal time for Trx1 induction. **(H)** Determination of optimal expression time for Trx1 using densitometry.

The expression of the Tpx1-Pap1-Trr1 proteins revealed that the overnight induction time yielded the highest protein quantities for all four proteins; however, a trade-off between time efficacy and protein yield had to be considered. Consequently, it was determined that the second-best time point would be the preferred option for protein expression unless a maximum yield were deemed necessary. This meant that for Tpx1, a 2-hour induction time and for Pap1, Trr1, and Trx1, a 1-hour induction time were utilised for protein expression.

Imidazole elution successfully purified the proteins off Ni-NTA columns (Figure 3.3). The most significant yield of Tpx1 elute was at 150 mM imidazole elute buffer (Figure 3.3A). Pap1 was eluted at 60 mM imidazole elution buffer through to 250 mM imidazole elution buffer, and some Pap1 was eluted at the crude and wash 1 step (Figure 3.3C). When batch expressing, a small amount of Pap1 was eluted off at the crude and washed 1 elute, but the remaining Pap1 was eluted at 150 mM (Figure 3.3D). Trr1 purification demonstrated that it eluted off at the crude and wash 1 step and then at 80 mM to 150 mM. Unfortunately, much of the protein was observed within the debris pellet (Figure 3.3E). At 150 mM, after two washes, most of the Trr1 was eluted off the column, with a minimal amount coming off 250 mM and still a significant amount of the protein was trapped in the sonicated pellet (Figure 3.3F). In the batch expression, Trx1 was eluted in only the first two 150 mM imidazole buffer washes, with faint bands observed at the 60 and 250 mM washes (Figure 3.3G).

This purification protocol prevented co-elution of contaminating proteins, but some proteins remained trapped within the sonicated pellet, and the protocol will need further optimisation to enhance the solubility of the protein. Given the high yield of purified Tpx1, we used this protein for our range-finding experiments.

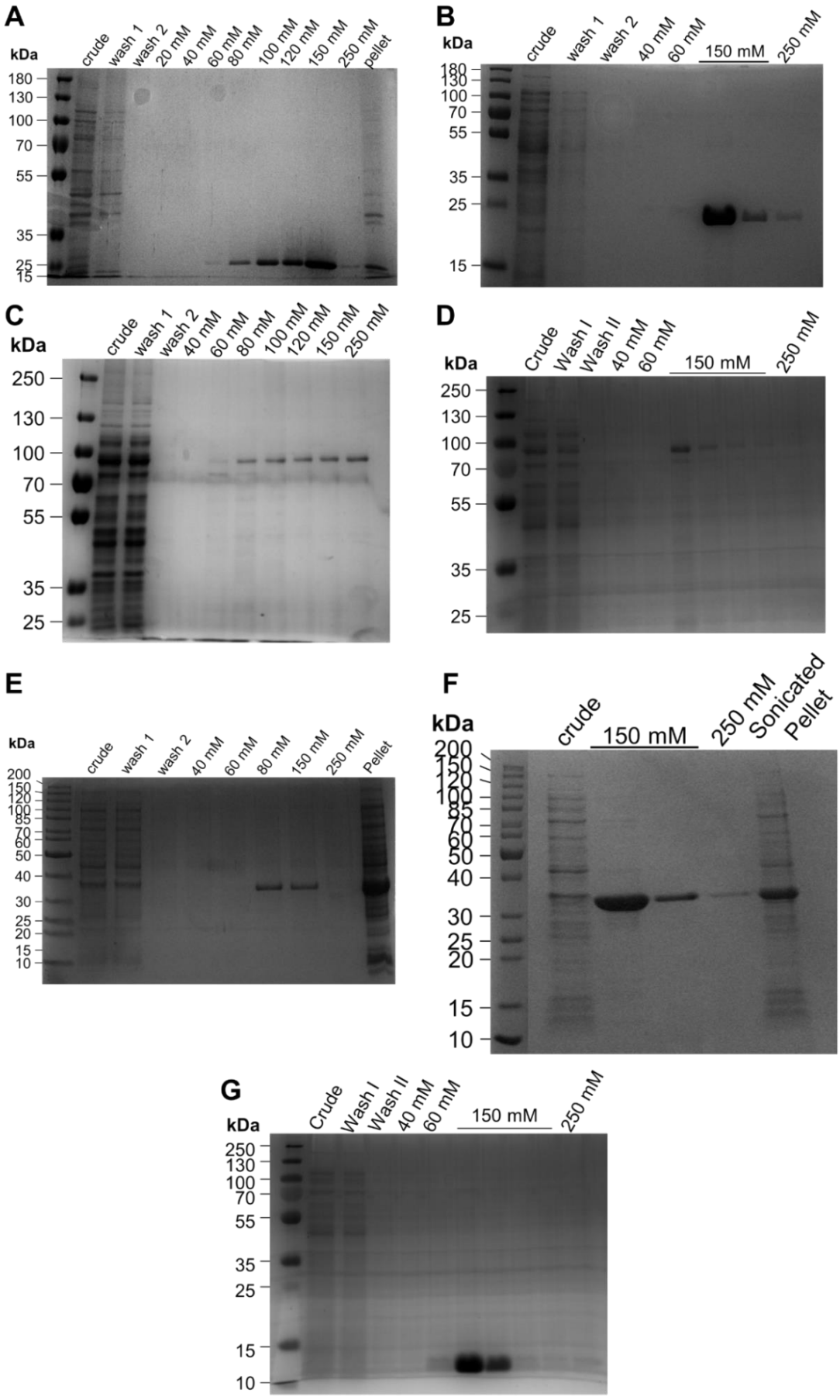

Figure 3.3: The purification of Tpx1-Pap1-Trr1 system proteins. Protein purification was done using Ni-NTA affinity chromatography and imidazole wash buffers for elution. **(A)** Determination of the optimal imidazole concentration for Tpx1 elution from a Ni-NTA agarose column. **(B)** Assessment of Tpx1 sample purity. **(C)** Determination of the optimal imidazole concentration for Pap1 elution from

a Ni-NTA agarose column. **(D)** Assessment of Pap1 sample purity. **(E)** Determination of the optimal imidazole concentration for Trr1 elution from a Ni-NTA agarose column. **(F)** Purity assessment of the batch expressed and purified Trr1 samples. **(G)** Purity assessment of the batch expressed and purified Trx1 samples.

Range finding experiments.

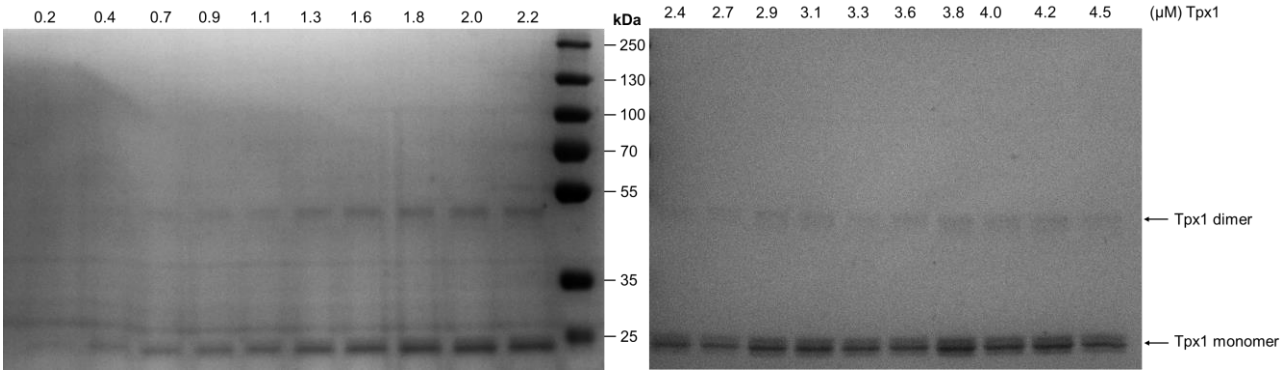

Figure 3.4: The optimisation of Tpx1 protein visualisation with Coomassie blue stain. A gradient concentration of Tpx1 was run on a reducing 12% SDS-PAGE gel ranging from 0.2 to 4.5 μM and visualised using Coomassie blue stain. Due to the reducing agent, Tpx1 was fully reduced, and only the monomeric isoform was visible.

We examined Tpx1 concentration gradients ranging from 0.2 to 4.5 μM on a reducing 12% SDS-PAGE gel to determine the minimum concentration required for successful visualisation using the Coomassie Blue stain (Figure 3.4). The intensity of the bands increased with increasing Tpx1 concentration, but from 2.0 μM upwards, there was no drastic increase in the intensity of the bands. A 2.2 μM Tpx1 concentration was used for further range-finding experiments.

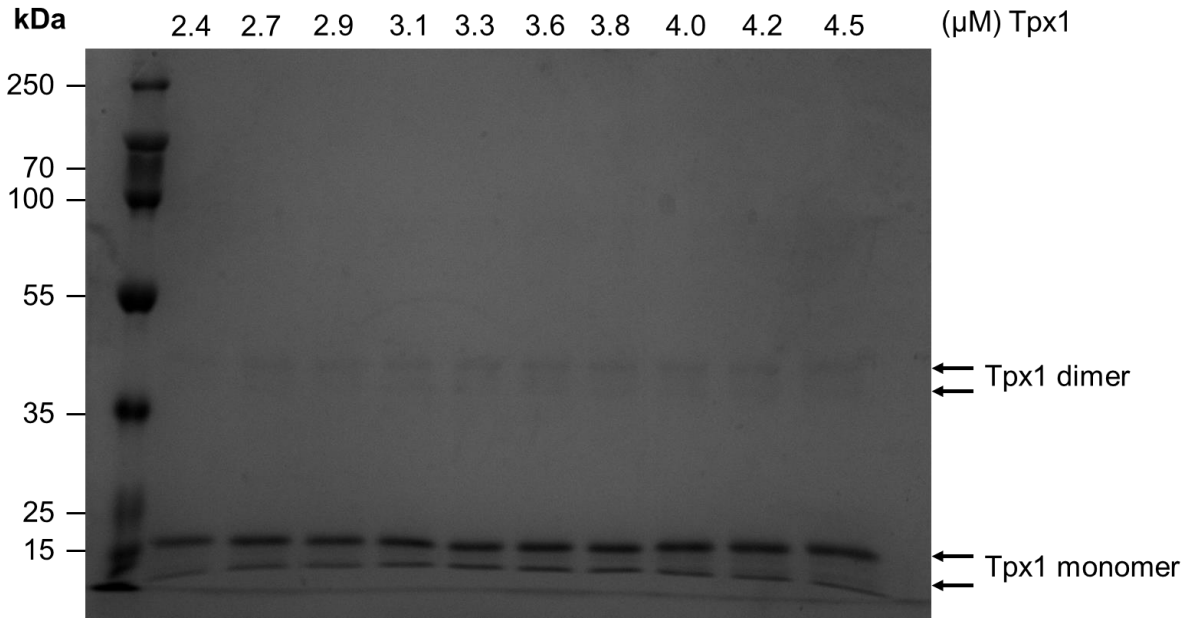

Figure 3.5: Visualisation of the Tpx1 isoforms. Gradient concentration of Tpx1 on a reducing 12% urea-SDS-PAGE gel ranging from 2.4 – 4.5 μM. The dimeric isoform can consist of the single and double disulphide bridge redox state of Tpx1, and the monomeric isoform comprises the free thiol and sulfinic isoform of Tpx1.

We utilised a modified gel with 9M urea (Smith, 1994) to enhance the separation of distinct Tpx1 isoforms (Figure 3.5). Two bands below 25 kDa and two above 35 kDa were observed in this gel, representing the monomer and dimer isoforms of Tpx1. The urea SDS-PAGE gel also successfully separated the different Tpx1 isoforms without affecting the clarity of the bands. However, it must be emphasised that precise and accurate classification of the isoforms requires an α-sulfenic acid-modified cysteine antibody which labels sulfenic acid-modified cysteine residues (Stöcker et al., 2018; Tomalin et al., 2016). This result highlighted a limitation of this assay: increasing the concentration of hydrogen peroxide led to an increase in oxidised Tpx1 in both dimeric and sulfinylated monomeric isoforms, which complicated the interpretation of SDS-PAGE results.

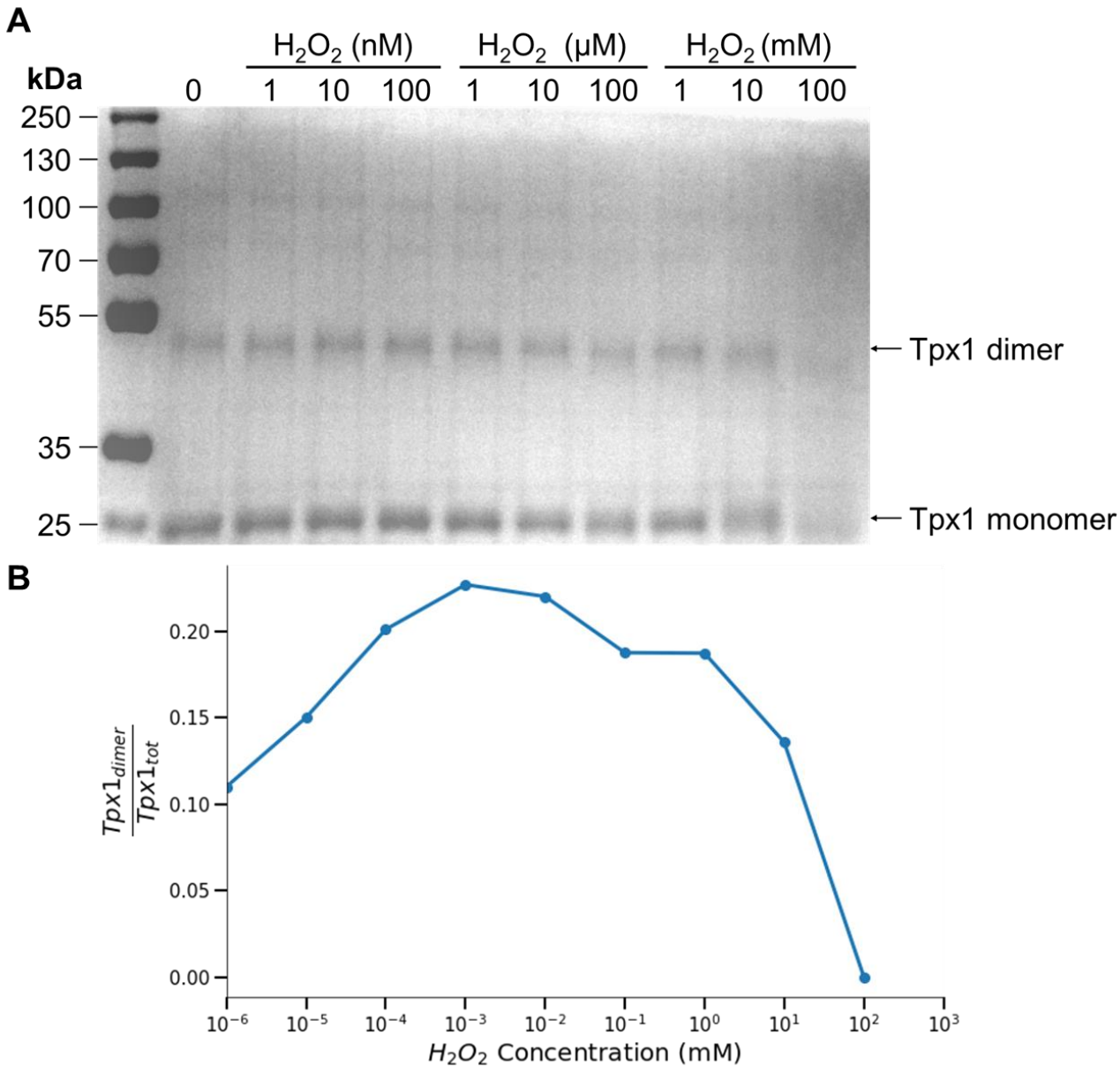

Figure 3.6: The effect of hydrogen peroxide on Tpx1 protein. (A) SDS-PAGE analysis of 2.2 µM Tpx1 protein exposed to a hydrogen peroxide gradient, ranging from 1 nM to 100 mM for 10 minutes. The gel reveals the presence of monomeric and dimeric Tpx1 at various hydrogen peroxide

concentrations. **(B)** Densitometry analysis of the dimeric to the monomeric ratio of Tpx1 at different hydrogen peroxide concentrations.

A 2.2 µM Tpx1 sample was exposed to hydrogen peroxide concentrations ranging from 1 nM to 100 mM hydrogen peroxide this was done as a range finding experiment on what would be the minimum and maximum concentration of hydrogen peroxide that could be used. What was observed is that hydrogen peroxide reacted with Tpx1, increasing the dimer formation of Tpx1, which was dose-dependent (Figure 3.6). Interestingly, some dimeric formation at zero hydrogen peroxide exposure suggested that protein handling protocols might cause oxidation by trace amounts of hydrogen peroxide in the buffer and exposure to oxygen (Figure 3.6A). Therefore, proteins needed to be pre-reduced before conducting assays with them. Densitometry analysis showed an increase in the fraction of oxidised (dimer) Tpx1 with increasing hydrogen peroxide from 1 nM to 1 µM, reaching a maximum dimer fraction at 1 µM, decreasing from 10 µM to 10 mM slightly, with theTpx1 dimer substantially decreased at 100 mM (Figure 3.6B).

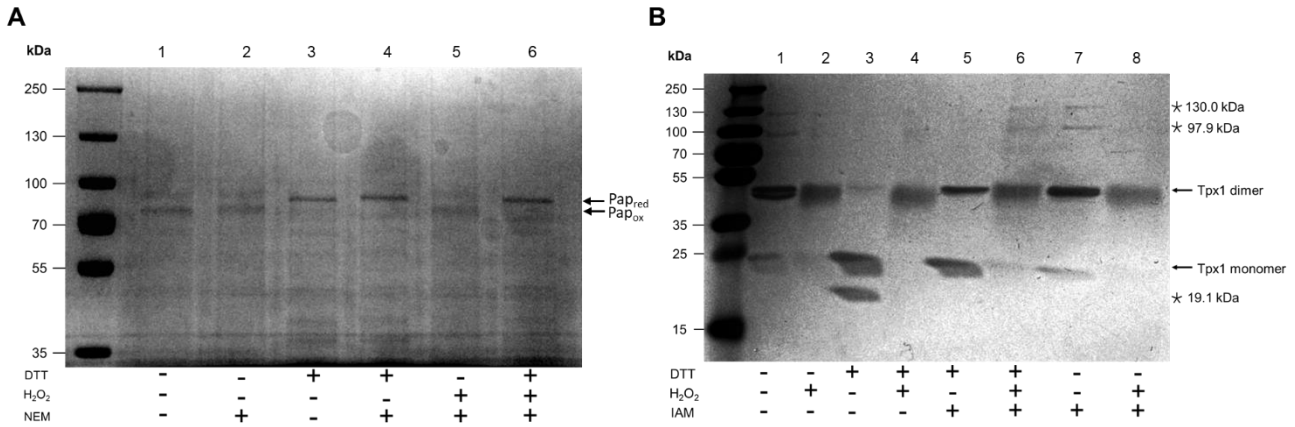

Figure 3.7: The optimisation of protein alkylation in the Tpx1-Pap1 System. This figure shows the optimisation of protein alkylation in the Tpx1-Pap1 system using a non-reducing 9% SDS-PAGE gel. The concentrations of Pap1 and Tpx1 were 1.1 and 4.8 µM, respectively. The reagents were added in this order: 10 mM DTT, 500 µM H_2O_2 and 17 mM IAM or 18 mM NEM. **(A)** The alkylation of the Pap1 protein shows the results obtained by treating Pap1 with NEM in the presence of H_2O_2 and DTT. **(B)** The alkylation of the Tpx1 protein shows the results obtained when Tpx1 is subjected to alkylation using IAM, H_2O_2, and DTT.

Thiol alkylation is used to preserve proteins in their current oxidation state, inhibiting further oxidation. As this system had not been previously analysed *in vitro*, it was necessary to test how the alkylation of Pap1 and Tpx1 affected the assay (Figure 3.7). Pap1 exhibited a reduced and oxidised isoform fraction in the untreated control, with the more intense band found in the oxidised isoform. Additionally, adding NEM did not change the redox state of Pap1 (Figure 3.7A). The pre-reduction of Pap1 entirely reduced it so that only the reduced Pap1 band was observed; the addition of NEM led to a slight shift upwards of the reduced band on the gel. When hydrogen peroxide and NEM were added to unreduced Pap1, the banding pattern was not different from the untreated control. Therefore, hydrogen peroxide

did not oxidise Pap1. Only the reduced band was visible when pre-reduced Pap1 was exposed to hydrogen peroxide and then alkylated with NEM (Figure 3.7A).

Tpx1 reacted differently to the three reagents: DTT, hydrogen peroxide and IAM (Figure 3.7B). The negative control of Tpx1 had Tpx1 mainly in its dimeric isoform, with some in the monomeric isoform. The addition of hydrogen peroxide dimerised all of the Tpx1. In contrast, the DTT reduction of Tpx1 completely reduced the protein. Additionally, a band was observed at 19.9 kDa, which most likely was reduced Tpx1. Pre-reduced Tpx1 and hydrogen peroxide had a similar banding to lane 2. The alkylation of Tpx1 using IAM on pre-reduced protein had a similar banding pattern to the negative control. Thus, the alkylating agent does not drastically affect how the protein runs on the gel. Hydrogen peroxide exposure oxidised most of the Tpx1 to form the dimeric isoform, and 97.9 kDa and 130.0 kDa bands were observed. These bands could be higher order Tpx1 isoforms (Jang et al., 2004), with 97.9 kDa being a dimer of dimers and 130.0 kDa a tetramer of dimers.

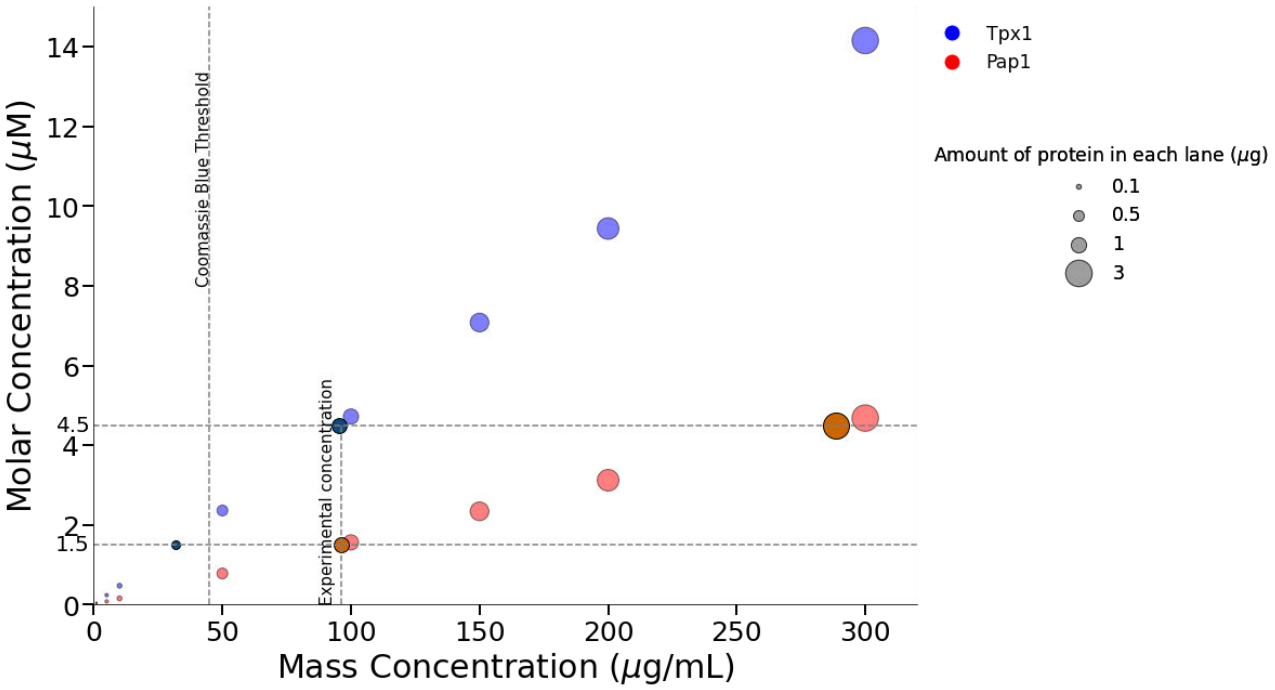

Figure 3.8: Protein Concentration Comparison in the Tpx1-Pap1-Trr1 System. A bubble plot was constructed depicting the molar (µM), mass concentration (µg/mL) and mass per lane (µg) of Pap1 and Tpx1. The plot demonstrated the minimum for Coomassie Blue visualisation and the actual experimental concentrations used in the experiments.

Protein-protein interactions are molar concentration-dependent which are protein size-dependent. However, Coomassie blue staining and western blotting are mass-dependent which results in a potential discrepancy between the reaction and visualisation conditions. For example, the smaller Tpx1 (21.191 kDa) protein has a larger molar concentration than Pap1 (61.532 kDa) at the same mass concentration (Figure 3.8). Additionally, the molar ratio of Pap1 and Tpx1 in an *S. pombe* cell is 1:54 (Marguerat et al., 2012).This limited our assays

capability to faithfully replicate *in vivo* reaction conditions. Therefore, in our assays, the molar concentration for Tpx1 and Pap1 was 4.5 µM and 1.5 µM (Figure 3.8), respectively

Assembling the Tpx1-Pap1 system

Assembling the Tpx1-Pap1 system provided insight into hydrogen peroxide signal transduction through Tpx1 to Pap1 and information on Pap1 signal dynamics at different hydrogen peroxide concentrations. Pap1 oxidation by hydrogen peroxide was dose-dependent and was shown by western blotting and densitometry analysis. Increasing the hydrogen peroxide concentration increased the prevalence of oxidised Pap1 (Figure 3.9A), with the most intense bands at 5 and 15 s at 40 µM hydrogen peroxide. The densitometry analysis corroborated these observations (Figure 3.9B). At 0.4 µM hydrogen peroxide (green), Pap1 oxidation was low but gradually increased over time. However, at 4 µM hydrogen peroxide (orange), Pap1 oxidation rapidly increased and then dropped at 30 s. whereas, at 40 µM (red), Pap1 increased and decreased immediately after but continued to increase. Moreover, the amplitude of Pap1, the average amount of oxidised Pap1 throughout the time course, increased with increased hydrogen peroxide (Figure 3.9C). This suggested that this simplified *in vitro* Tpx1-Pap1 system can sense and respond to hydrogen peroxide and differentiate between different concentrations.

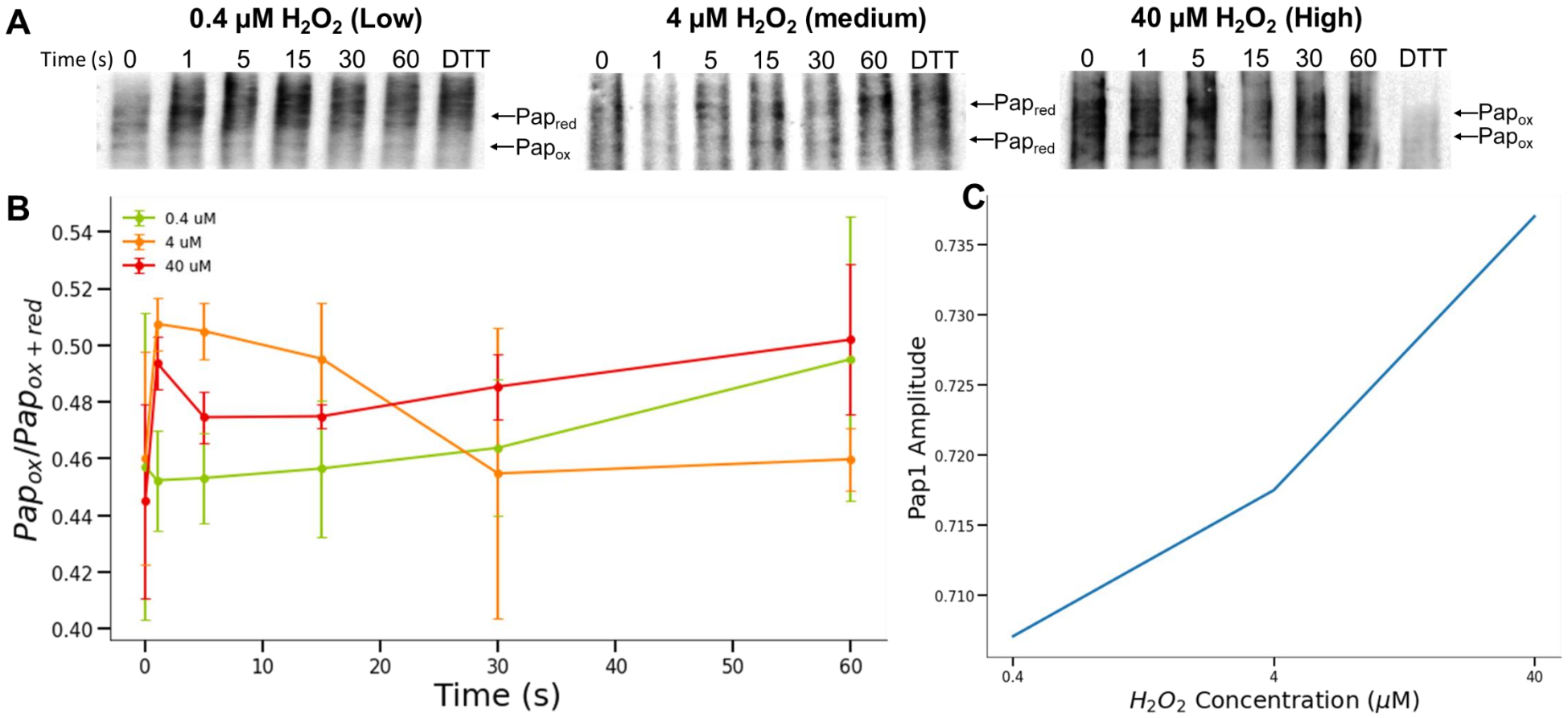

Figure 3.9: The oxidation of Pap1 in vitro over 1 minute at different hydrogen peroxide concentrations. The Tpx1-Pap1 system was assembled using recombinant Tpx1 (4.5 µM) and Pap1 (1.5 µM) protein and exposed to relatively low (0.4 µM), medium (4 µM) and high (40 µM) concentrations of hydrogen peroxide, over a 1-minute time range. **(A)** The representative western bolts for the *in vitro* Tpx1-Pap1 system at 0.4, 4 and 40 µM hydrogen peroxide, respectively. **(B)** The densitometry analysis-based fraction of oxidised Pap1 at the different time points for A (Table S1, S2 and S3). **(C)** The amplitude of oxidised Pap1 at the low, medium and high hydrogen peroxide concentrations obtained from the signals in B.

Site-Directed Mutagenesis of Pap1

The purpose of Figure 3.10 was to compare the wild-type and mutated versions of the Pap1 protein using the Pymol visualisation software. The Pap1 protein's structure was obtained from AlphaFold (accession code: Q01663). 87% of the protein's tertiary structure was predicted, with the bZIP region having been crystallised by Fujii et al. (2000). The pLDDT average over all 552 amino acid residues being 55.70, with the pLDDT for the n-CRD and c-CRD were and for Cys–278, Cys–284, Cys–501 and Cys–532 was 90.40, 81.22, 91.90 and 90.90 respectively (Jumper et al., 2021; Varadi et al., 2023). The protein mutations were conducted in PyMol, where the rotamer was altered to minimise clashes of amino acids. This comparison showed how mutations in critical cysteine residues disrupt the formation of essential disulfide bonds in Pap1 as the disulphide bridge cannot be formed.

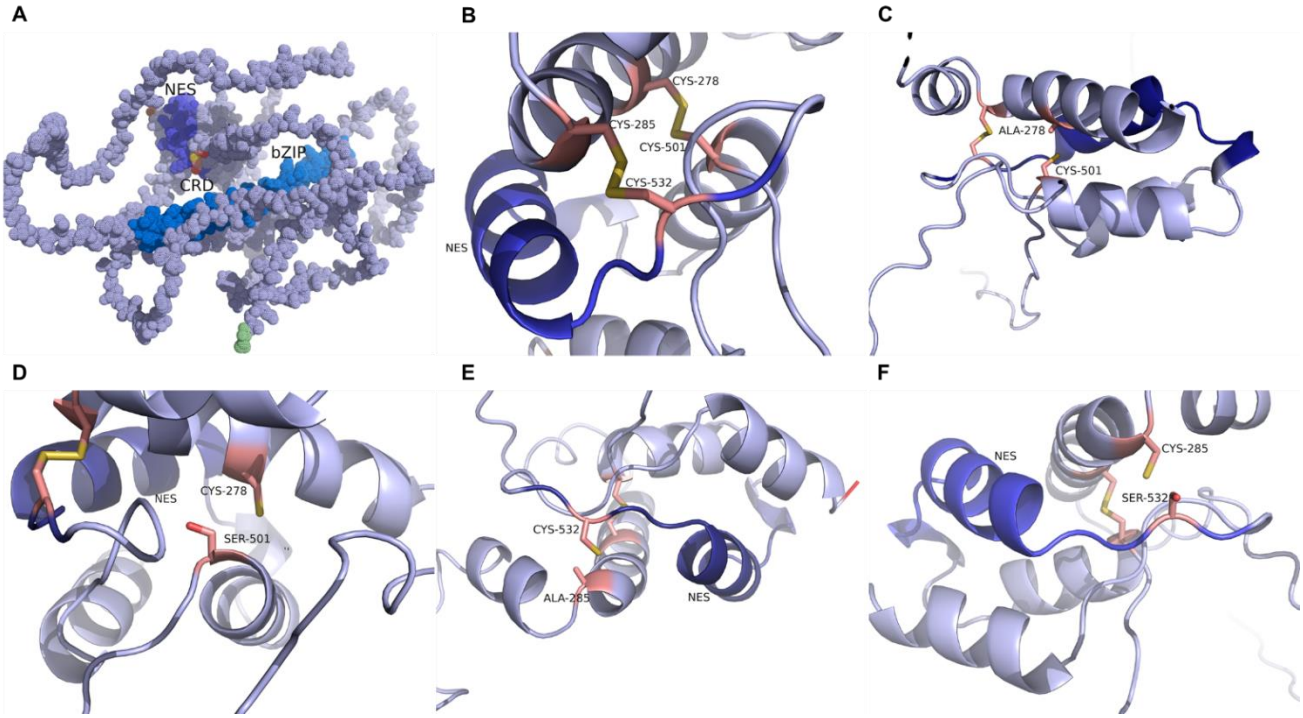

Figure 3.10: A comparative analysis of the wild-type and mutated versions of the Pap1 protein, visualised using Pymol visualisation software. The structure of the Pap1 protein is depicted as cartoon ribbons in light blue, while the critical cysteines are shown as sticks in salmon, with their sulfuric side chains coloured yellow and the hydroxymethyl side chain of serine in red. The nuclear export signal region and the basic leucine zipper domain of Pap1 are coloured in deep and marine blue, respectively, and the N-terminus and C-terminus are represented in green and brick red, respectively. **(A)** The wild-type oxidised Pap1 protein is displayed as a dot surface to illustrate the packing and steric hindrance of the oxidised protein. **(B)** The fully oxidised Pap1 exhibits two disulfide bridges formed at the cysteine residues Cys-278—Cys-501 and Cys-285—Cys-532. **(C)** The mutated Pap1 shows the substitution of Cys-278 with an alanine (Ala-278), disrupting one of the disulfide bridges. **(D)** Mutated Pap1 with Cys-285 was replaced by an alanine amino acid (Ala-285), disrupting the other disulfide bridge. **(E)** Pap1 mutated at Cys-501 to Ser-501 to break one of the disulfide bridges. **(F)** Pap1 mutated at Cys-532 to Ala-532, thus causing the disulfide bridge.

The mutating of the critical cysteines in Pap1 disabled their ability to form the disulfide bonds; however, it does not appear to alter the predicted tertiary structure of the protein

(Figure 3.10). Pap1 has 4 functional domains: the bZip domain, located near the n terminus of the protein, facilitating Pap1-DNA binding (Ellenberger, 1994); the n-CRD and c-CRD, located more towards the c terminus of Pap1, which contain the redox-sensitive critical cysteines involved in Pap1 hydrogen peroxide activation and the NES, found between the n-CRD and c-CRD, which enables Pap1 to interact with Crm1 (Kudo et al., 1999) (Figure 3.10A). The importance of the cysteines in the CRDs is that when Pap1 is oxidised, they form disulfide bonds across the c-CRD and n-CRD, locking the NES and CRDs in a very rigid conformation (Figure 3.10B). The mutating of Cys-278 or Cys-501 to alanine (Cys278Ala) and serine (Cys501Ser), respectively, inhibits the formation of this disulfide bond at the n-terminus of the NES (Figure 3.10C and Figure 3.10D), whilst the mutation of Cys-285 and Cys-532 to alanine (Cys285Ala) and serine (Cys532Ser) inhibits the formation of the disulfide bond at the c-terminus of the NES (Figure 3.10E and Figure 3.10F).

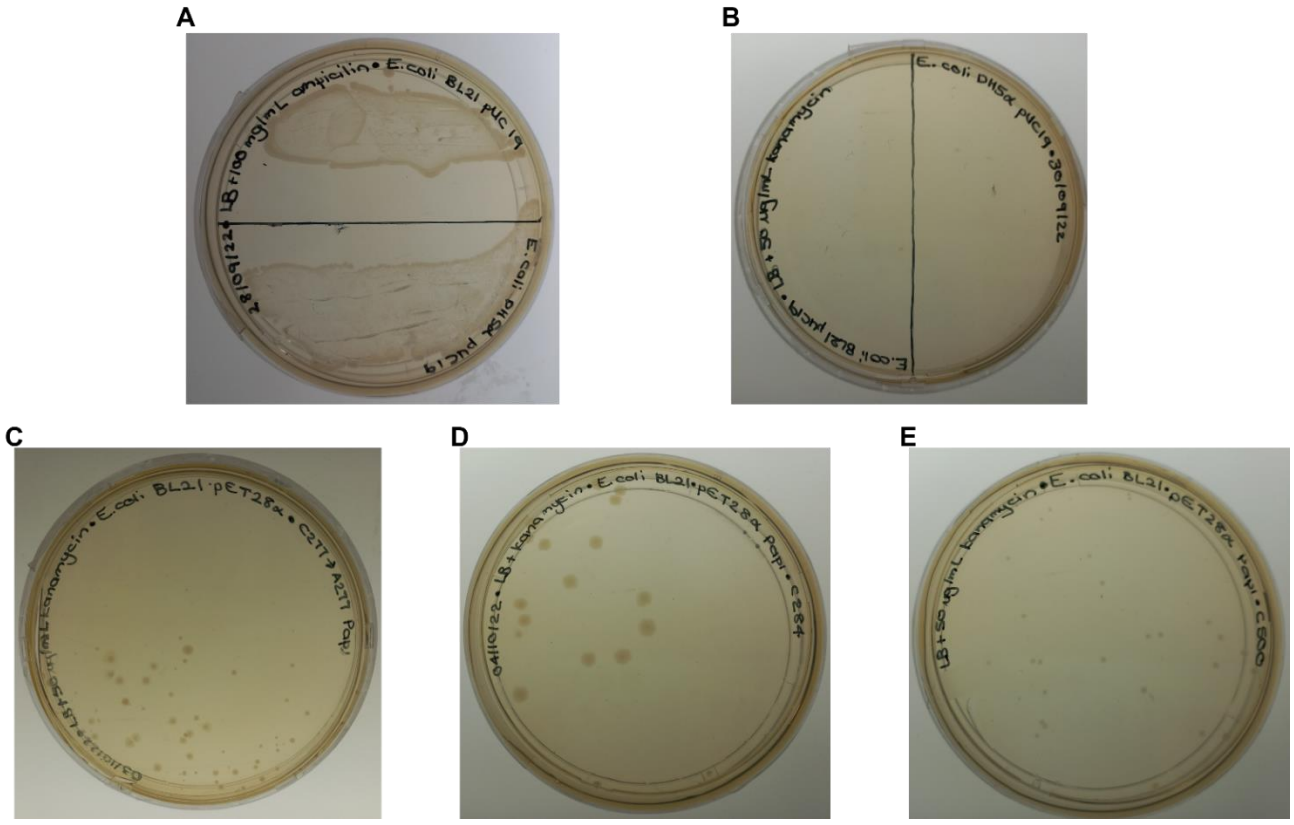

Figure 3.11: Transformation plates from Q5 site-directed mutagenesis of critical cysteines in Pap1. This figure presents the transformation plates obtained after performing Q5 site-directed mutagenesis on three critical cysteines in Pap1. The transformation plates demonstrate the successful introduction of mutations into the Pap1 gene and their subsequent transformation into *E. coli* cells. **(A)** the pUC19 transformation of DH5α and BL21 *E. coli* competent cells on an ampicillin (100 µg/mL) plate. **(B)** The pUC19 transformation of DH5a and BL21 *E. coli* competent cells is displayed on a kanamycin (50 µg/mL) plate. **(C)**, **(D)** and **(E)** represent the mutated Cys-278.

The mutations of Pap1 were obtained using the Q5® site-directed mutagenesis kit. In this method, the forward primer contains the mutagenic sequence, and the nonoverlapping reverse primer flanks it and amplifies the plasmid (Decero et al., 2020). The transformation

of the pET28α plasmid into *E. coli* BL21 competent cells were successful. The positive control (Figure 3.11A) resulted in a dense growth of cells, and the negative control (Figure 3.11B) exhibited no colony formation or growth. There was colony formation for *E. coli* BL21 transformed with pET28α housing the mutated Pap1 gene: Cys278Ala (Figure 3.11C), Cys285Ala (Figure 3.11D) and Cys501Ser (Figure 3.11E).

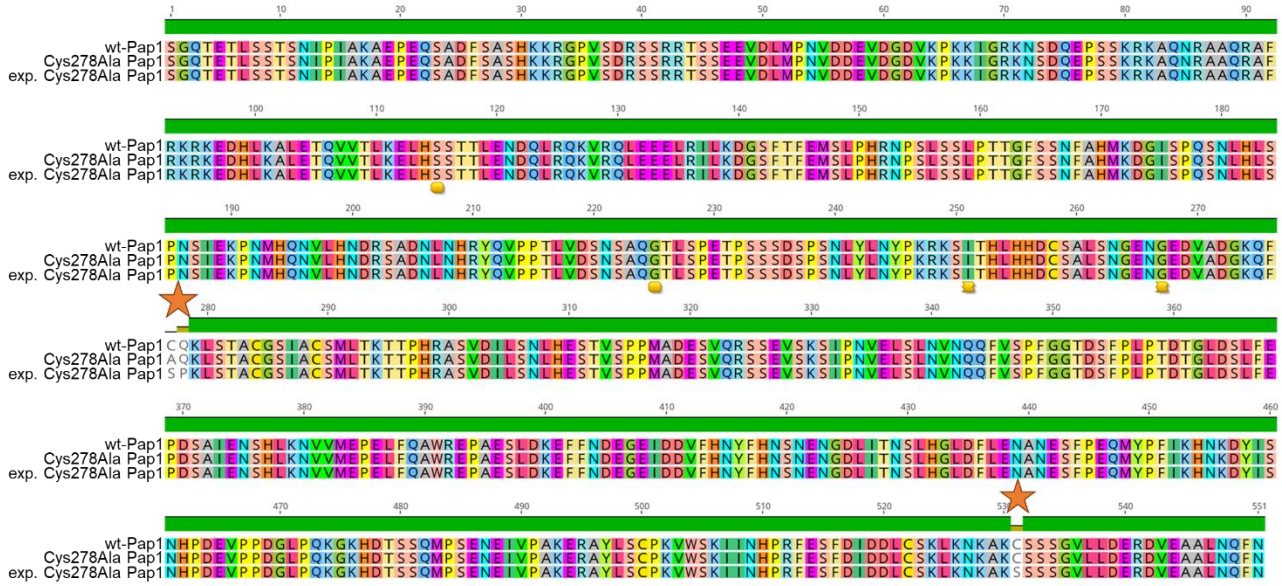

Figure 3.12: Comparison of Cys278Ala mutated Pap1 sequence to wild-type and theoretical sequences. This figure illustrates a comparison of the Cys278Ala mutated Pap1 sequence (bottom) with the native wild-type Pap1 sequence (top) and the theoretical Cys278Ala mutated Pap1 sequence (middle). The top sequence displays the native wild-type Pap1 sequence, representing the original sequence of the protein without any mutations or alterations. The middle sequence showcases the theoretical Cys278Ala mutated Pap1 sequence based on the specific mutation at residue Ala-278. This sequence represents the expected outcome of the mutation at position 278. The bottom sequence depicts the experimental Cys278Ala mutated Pap1 sequence obtained from sequencing with the orange stars showing the location of the incorrect mutations. This sequence represents the observed sequence resulting from the mutation at residue Ala-278.

Unfortunately, the site-directed mutagenesis of Pap1 was unsuccessful, as three unintended mutations were introduced into the sequence (Figure 3.12). The expected mutation, Cys278Ala, illustrated by comparing wild-type Pap1 to the theoretically mutated Pap1 sequence, failed. Instead, the NEB Q5® site-directed mutated Pap1 sequence had mutations at three residues: 278, 279 and 531, which resulted in serine, phenylalanine, and serine substitutions, respectively. These discrepancies suggested potential errors in the mutagenesis experiment, such as accidental primer mixing or issues with the sequencing data.

3.4. Discussion

In this study, we reconstituted a simplified recombinant Tpx1-Pap1 system *in vitro*, perturbed it at different hydrogen peroxide concentrations, and attempted to mutate Pap1 at

the four critical cysteines. However, this simplification does not ideally mimic the system as the system lacks the reducing component, the Trr1 system. The western blotting analysis showed that the Tpx1-Pap1 system has different signalling profiles at different hydrogen peroxide concentrations. Furthermore, oxidized, activated Pap1 was linked to increasing hydrogen peroxide. A direct comparison between our *in vitro* system and the bolus addition of hydrogen peroxide to cell culture cannot be made, as our in vitro system will mimic an individual cell's response. This is different from a cell culture analysis as this gives us the average response across the entire culture. However, observed similarities can be noted. Cell culture studies have demonstrated that Pap1 activation is hydrogen peroxide dose-dependent, with Pap1 in a cell culture being activated at 70 µM hydrogen peroxide (Chen et al., 2008; Vivancos et al., 2004), which is similar to our results. Knockout studies have shown that Pap1's activation requires Tpx1 for hydrogen peroxide signalling (Quinn et al., 2002; Vivancos et al., 2006), which was consistent with our results (Figure 3.7A).

Since Pap1 cannot be oxidised directly by hydrogen peroxide, the necessity for the highly sensitive peroxiredoxin, Tpx1, becomes more evident. The affinity of Tpx1 for hydrogen peroxide is such that it reacted with trace hydrogen peroxide amounts in the reaction buffer, which makes it an excellent antioxidant in *S. pombe* but also makes it a suitable hydrogen peroxide sensor for signal transduction to Pap1 (Marinho et al., 2014). However, for Pap1 activation, the downside of utilising Tpx1 as a redox relay sensor means that the system is subject to hyperoxidation of Tpx1, which shuts down its signal transduction capacity at high hydrogen peroxide concentrations (Tomalin et al., 2016). Therefore, we attributed the decrease in dimeric Tpx1 to hyperoxidation at high hydrogen peroxide concentrations; this redox state of Tpx1 accumulates in its monomeric isoform (Jara et al., 2007). Our study also showed Pap1's inability to be directly oxidised by hydrogen peroxide, *in vitro*, is an inherent property of the protein itself and is not due to mechanistically dependent.

We simplified the Tpx1-Pap1-Trr1 pathway to only Tpx1 and Pap1 for assembling this *in vitro* system. The exclusion of the Trr1 system, such as Trx1, has been shown to affect the dynamics of redox transcription factor activation by disallowing the reduction of the oxidised protein (Day et al., 2012). This removes the capability of the system to shut off *in vivo*. Additionally, the reducing component of these systems maintains Pap1 in a soluble, peroxide-responsive state (Brown et al., 2013). Utilising western blotting as our critical visualisation methodology allows for accurate protein identification; however, it requires optimisation, mainly if the downstream densitometry analysis will be quantitatively utilised.

Some of these limitations can be mitigated with further work, such as adding the Trr1 component to the *in vitro* system. This will better mimic the *in vivo* pathway and allow for a

more accurate model, and the further optimisation of the western blotting will improve the precision of the data, enhancing our certainty in the accuracy of the data and decreasing our standard errors. Optimisation of the western blotting will require antibody optimisation and additional protocols, including whole protein normalisation, for quantitative western blotting (Pillai-Kastoori et al., 2020). Acquiring α-Pap1 and α-Tpx1 antibodies will allow for more precise identification of the proteins and the interesting complexes they may form. Due to the failure of the mutagenesis work using NEB Q5® site-directed mutagenesis kit, another approach for introducing the mutations at the critical cysteines will need to be considered: gene synthesis and Gibson assembly are two approaches that will be considered.

Chapter 4: General Discussion

This thesis explored whether multiple oxidation events in redox pathways confer increased specificity to the respective pathway. We combined *in silico* and *in vitro* methods to model and assemble the Tpx1-Pap1-Trr1 pathway to address this. The first step involved the construction of simplified redox pathways, described through equations, which were plotted for further analysis. This was followed by constructing a simplified Tpx1-Pap1-Trr1 pathway that was computationally modelled and scrutinised for its different characteristics under different conditions. The *in vitro* component of the study involved the expression and purification of Tpx1, Pap1, Trr1 and Trx1 proteins, which were done utilising the *E. coli* BL21 and IPTG system and Ni-NTA chromatography. Tpx1 and Pap1 were assembled in a system and subjected to different concentrations of hydrogen peroxide, and the oxidation state of Pap1 was determined using western blotting and densitometry analysis. Finally, the Q5® Site-Directed Mutagenesis Kit was used to mutate *pap1*, and the results were sequenced.

Adding an extra oxidation step enhanced the system's capability to attenuate the signal, especially at low hydrogen peroxide concentrations. The analytical modelling of simplified generic redox pathways showed that the extra step increased the influence of the reduction steps in the system. In tandem, the computational modelling of the Tpx1-Pap1-Trr1 system revealed that the double oxidation system, compared to the single oxidation model, exhibited greater attenuation of the signal at low hydrogen peroxide and amplification at higher hydrogen peroxide concentrations. This is evidenced by the non-linear relationship between the Pap1 amplitude and the hydrogen peroxide concentration (Figure 2.6B). The non-linearity observed in the computational model is very similar to the in vitro Pap1 amplitude in response to hydrogen peroxide (Figure 3.9C). In the in vitro assay, a greater attenuation of the system was exhibited at 0.4 µM of hydrogen peroxide and amplification at 40 µM of hydrogen peroxide. Specificity is the ratio between correct and incorrect pathway responses (Komarova et al., 2005). In that case, a pathway that can minimise incorrect pathway responses and increase correct pathway responses will increase its specificity.

A redox pathway with high pass filter-like properties will counteract the effect of low physiological concentrations of hydrogen peroxide by preventing the pathway's activation under these conditions. However, the attenuation of the signal increases with an increase in the number of oxidative events but at the cost of weaker pathway activation. This insight highlights the interplay between the number of oxidation steps and the system's response across varying hydrogen peroxide concentrations. The computational model created in this study was acknowledged to be simplified, with some of the parameters approximated from

analogous systems. The assumptions of the computational model could produce results that were an artefact of the model and not an approximation of the in vitro or in vivo pathway. This necessitated the *in vitro* assay to verify the modelling findings, and in the future, *in vivo* data would also be necessary.

Using recombinant Tpx1 and Pap1 demonstrated Pap1's Tpx1-dependent mechanism for hydrogen peroxide sensing, as observed in the literature. This is inherent to Pap1, not the pathway's mechanism. This was illustrated by Tpx1's oxidation in the presence of hydrogen peroxide, whilst Pap1 remained reduced even when exposed to hydrogen peroxide (Figure 3.7A). The Tpx1 and Pap1 were assembled to form the *in vitro* Tpx1-Pap1 system - an untried assay with these proteins within the field. Interestingly, the Tpx1-Pap1 system responded to hydrogen peroxide without Trr1 and Trx1, indicating that Pap1 oxidation can occur via Tpx1-hydrogen peroxide oxidation, thus answering a question about how Pap1 is oxidised, but not to the exclusion of the other mechanisms. Additionally, the system's signalling dynamics had distinct profiles at different hydrogen peroxide concentrations, with the average concentration of oxidised Pap1 rising with the increase in hydrogen peroxide concentration. These *in vitro* experiments contributed to the field by showing Tpx1-mediated oxidation of Pap1, illustrating Pap1's innate hydrogen peroxide insensitivity and demonstrating that assembling an *in vitro* system is possible and can provide insights into the mechanisms of the pathway.

The development of the *in vitro* assay ran into some issues, such as the oxidised state of the system prior to the hydrogen peroxide exposure, even though the proteins were reduced. It is concerning as it may distort our findings on the effect of hydrogen peroxide on the system. Therefore, in the future, a protocol must be developed to reduce the system better than our attempts. Coomassie Blue was initially considered a sufficient visualisation method for this system. However, challenges arose with Pap1 visualisation. Therefore, we turned to western blotting but could not optimise the protocol under time constraints. However, western blotting has the advantage of differentiating proteins when specialised antibodies are used, allowing for further elucidation of the system. Our attempts to mutate *pap1* were unsuccessful; therefore, we have now turned to alternative methods of acquiring the mutated *pap1* gene. We have looked into ordering the plasmids from GenScript and creating our own using Gibson assembly, whichever is both time and financially feasible. Thus, future studies will entail the optimisation of the final assembly of the system, the generation of mutated *pap1* and the addition of the other proteins in the pathway to the *in vitro* system. In retrospect, there have been fewer published *in vitro* studies than *in* vivo studies on redox signalling, possibly due to the challenges with studying these systems *in vitro.* The development of genetically encoded redox sensors which may be activated by single or multiple disulphide bridges, could

represent an alternate approach to confirm our computational modelling analyses both *in vitro* and *in vivo* (Meyer & Dick, 2010).

Chapter 5: References

Aiyer, K. (2022). *The Great Oxidation event: How cyanobacteria changed life*. The American Society for Microbiology. Retrieved 2 January from https://asm.org/Articles/2022/February/The-Great-Oxidation-Event-How-Cyanobacteria-Change

Alon, U. (2019). *An Introduction to Systems Biology: Design Principles of Biological Circuits*. CRC press.

Ameyar, M., Wisniewska, M., & Weitzman, J. B. (2003). A role for AP-1 in apoptosis: the case for and against. *Biochimie*, *85*(8), 747-752. https://doi.org/https://doi.org/10.1016/j.biochi.2003.09.006

Antelmann, H., & Helmann, J. D. (2011). Thiol-Based Redox Switches and Gene Regulation. *Antioxidants & redox signaling*, *14*(6), 1049-1063. https://doi.org/10.1089/ars.2010.3400

Antunes, F., & Brito, P. M. (2017). Quantitative biology of hydrogen peroxide signaling. *Redox Biology*, *13*, 1-7. https://doi.org/10.1016/j.redox.2017.04.039

Apel, K., & Hirt, H. (2004). Reactive oxygen species: metabolism, oxidative stress, and signal transduction. *Annual Review of Plant Biology*, *55*, 373-399.

Aruoma, O. I. (1998). Free radicals, oxidative stress, and antioxidants in human health and disease. *Journal of the American Oil Chemists' Society*, *75*(2), 199-212. https://doi.org/10.1007/s11746-998-0032-9

Åslund, F., Zheng, M., Beckwith, J., & Storz, G. (1999). Regulation of the OxyR transcription factor by hydrogen peroxide and the cellular thiol—disulfide status. *Proceedings of the National Academy of Sciences*, *96*(11), 6161-6165. https://doi.org/10.1073/pnas.96.11.6161

Auten, R. L., & Davis, J. M. (2009). Oxygen Toxicity and Reactive Oxygen Species: The Devil Is in the Details. *Pediatric Research*, *66*(2), 121-127. https://doi.org/10.1203/pdr.0b013e3181a9eafb

Bahn, G., Park, J.-S., Yun, U. J., Lee, Y. J., Choi, Y., Park, J. S., Baek, S. H., Choi, B. Y., Cho, Y. S., Kim, H. K., Han, J., Sul, J. H., Baik, S.-H., Lim, J., Wakabayashi, N., Bae, S. H., Han, J.-W., Arumugam, T. V., Mattson, M. P., & Jo, D.-G. (2019). NRF2/ARE pathway negatively regulates BACE1 expression and ameliorates cognitive deficits in mouse Alzheimer's models. *Proceedings of the National Academy of Sciences*, *116*(25), 12516-12523. https://doi.org/10.1073/pnas.1819541116

Baird, L., Llères, D., Swift, S., & Dinkova-Kostova, A. T. (2013). Regulatory flexibility in the Nrf2-mediated stress response is conferred by conformational cycling of the Keap1-Nrf2 protein complex. *Proceedings of the National Academy of Sciences*, *110*(38), 15259-15264. https://doi.org/10.1073/pnas.1305687110

Baird, L., Swift, S., Llères, D., & Dinkova-Kostova, A. T. (2014). Monitoring Keap1–Nrf2 interactions in single live cells. *Biotechnology Advances*, *32*(6), 1133-1144. https://doi.org/https://doi.org/10.1016/j.biotechadv.2014.03.004

Balaban, R. S., Nemoto, S., & Finkel, T. (2005). Mitochondria, Oxidants, and Aging. *Cell*, *120*(4), 483-495. https://doi.org/10.1016/j.cell.2005.02.001

Battin, E. E., & Brumaghim, J. L. (2009). Antioxidant activity of sulfur and selenium: a review of reactive oxygen species scavenging, glutathione peroxidase, and metal-binding antioxidant mechanisms. *Cell biochemistry and biophysics*, *55*(1), 1-23.

Baudouin-Cornu, P., & Thomas, D. (2007). Oxygen at life's boundaries. *Nature*, *445*(7123), 35-36. https://doi.org/10.1038/nature05521

Beckman, J. S., Beckman, T. W., Chen, J., Marshall, P. A., & Freeman, B. A. (1990). Apparent hydroxyl radical production by peroxynitrite: implications for endothelial injury from nitric oxide and superoxide. *Proceedings of the National Academy of Sciences*, *87*(4), 1620-1624.

Behar, M., Dohlman, H. G., & Elston, T. C. (2007). Kinetic insulation as an effective mechanism for achieving pathway specificity in intracellular signaling networks. *Proceedings of the National Academy of Sciences*, *104*(41), 16146-16151. https://doi.org/10.1073/pnas.0703894104

Behar, M., Hao, N., Dohlman, H. G., & Elston, T. C. (2007). Mathematical and Computational Analysis of Adaptation via Feedback Inhibition in Signal Transduction Pathways. *Biophysical Journal*, *93*(3), 806-821. https://doi.org/10.1529/biophysj.107.107516

Bender, D., & Hildt, E. (2019). Effect of Hepatitis Viruses on the Nrf2/Keap1-Signaling Pathway and Its Impact on Viral Replication and Pathogenesis. *International Journal of Molecular Sciences*, *20*(18), 4659. https://doi.org/10.3390/ijms20184659

Bersweiler, A., D'Autréaux, B., Mazon, H., Kriznik, A., Belli, G., Delaunay-Moisan, A., Toledano, M. B., & Rahuel-Clermont, S. (2017). A scaffold protein that chaperones a cysteine-sulfenic acid in H_2O_2 signaling. *Nature Chemical Biology*, *13*(8), 909-915. https://doi.org/10.1038/nchembio.2412

Biteau, B., Labarre, J., & Toledano, M. B. (2003). ATP-dependent reduction of cysteine–sulphinic acid by *S. cerevisiae* sulphiredoxin. *Nature*, *425*(6961), 980-984. https://doi.org/10.1038/nature02075

Boeger, H. (2022). Kinetic Proofreading. *Annual Review of Biochemistry*, *91*(1), 423-447. https://doi.org/10.1146/annurev-biochem-040320-103630

Boronat, S., Domènech, A., Paulo, E., Calvo, I. A., García-Santamarina, S., García, P., Encinar del Dedo, J., Barcons, A., Serrano, E., Carmona, M., & Hidalgo, E. (2014). Thiol-based H_2O_2 signalling in microbial systems. *Redox Biology*, *2*, 395-399. https://doi.org/https://doi.org/10.1016/j.redox.2014.01.015

Bozonet, S. M., Findlay, V. J., Day, A. M., Cameron, J., Veal, E. A., & Morgan, B. A. (2005). Oxidation of a eukaryotic 2-Cys peroxiredoxin is a molecular switch controlling the transcriptional response to increasing levels of hydrogen peroxide. *Journal of Biological Chemistry*, *280*(24), 23319-23327.

Brigelius-Flohé, R., & Flohé, L. (2011). Basic Principles and Emerging Concepts in the Redox Control of Transcription Factors. *Antioxidants & redox signaling*, *15*(8), 2335-2381. https://doi.org/10.1089/ars.2010.3534

Brown, J. D., Day, A. M., Taylor, S. R., Tomalin, L. E., Morgan, B. A., & Veal, E. A. (2013). A Peroxiredoxin Promotes H_2O_2 Signaling and Oxidative Stress Resistance by Oxidizing a Thioredoxin Family Protein. *Cell Reports*, *5*(5), 1425-1435. https://doi.org/10.1016/j.celrep.2013.10.036

Cadenas, E., & Davies, K. J. A. (2000). Mitochondrial free radical generation, oxidative stress, and aging. *Free Radical Biology and Medicine*, *29*(3), 222-230. https://doi.org/https://doi.org/10.1016/S0891-5849(00)00317-8

Calvo, I. A., Ayté, J., & Hidalgo, E. (2013). Reversible thiol oxidation in the H_2O_2-dependent activation of the transcription factor Pap1. *Journal of Cell Science*, *126*(10), 2279-2284. https://doi.org/10.1242/jcs.124370

Calvo, I. A., Boronat, S., Domènech, A., García-Santamarina, S., Ayté, J., & Hidalgo, E. (2013). Dissection of a Redox Relay: H_2O_2-Dependent Activation of the Transcription Factor Pap1 through the Peroxidatic Tpx1-Thioredoxin Cycle. *Cell Reports*, *5*(5), 1413-1424. https://doi.org/10.1016/j.celrep.2013.11.027

Calvo, I. A., García, P., Ayté, J., & Hidalgo, E. (2012). The transcription factors Pap1 and Prr1 collaborate to activate antioxidant, but not drug tolerance, genes in response to H_2O_2. *Nucleic Acids Research*, *40*(11), 4816-4824. https://doi.org/10.1093/nar/gks141

Carballo, M., Conde, M., El Bekay, R., MartíN-Nieto, J., Camacho, M. A. J., MonteseiríN, J., Conde, J., Bedoya, F. J., & Sobrino, F. (1999). Oxidative Stress Triggers STAT3 Tyrosine Phosphorylation and Nuclear Translocation in Human Lymphocytes.

Journal of Biological Chemistry, *274*(25), 17580-17586. https://doi.org/10.1074/jbc.274.25.17580
Carlberg, I., & Mannervik, B. (1985). Glutathione reductase. In *Methods in Enzymology* (Vol. 113, pp. 484-490). Academic Press. https://doi.org/https://doi.org/10.1016/S0076-6879(85)13062-4
Carlson, J., Price, L., & Deng, H. (2020). Nrf2 and the Nrf2-Interacting Network in Respiratory Inflammation and Diseases. In (pp. 51-76). Springer International Publishing. https://doi.org/10.1007/978-3-030-44599-7_3
Carter, M. E., & Brunet, A. (2007). FOXO transcription factors. *Current Biology*, *17*(4), R113-R114.
Castillo, E. A., Ayte, J., Chiva, C., Moldon, A., Carrascal, M., Abian, J., Jones, N., & Hidalgo, E. (2002). Diethylmaleate activates the transcription factor Pap1 by covalent modification of critical cysteine residues. *Molecular Microbiology*, *45*(1), 243-254. https://doi.org/10.1046/j.1365-2958.2002.03020.x
Cavadas, M. A., Nguyen, L. K., & Cheong, A. (2013). Hypoxia-inducible factor (HIF) network: insights from mathematical models. *Cell Communication and Signaling*, *11*(1), 42. https://doi.org/10.1186/1478-811x-11-42
Chae, H. Z., Robison, K., Poole, L. B., Church, G., Storz, G., & Rhee, S. G. (1994). Cloning and sequencing of thiol-specific antioxidant from mammalian brain: alkyl hydroperoxide reductase and thiol-specific antioxidant define a large family of antioxidant enzymes. *Proceedings of the National Academy of Sciences*, *91*(15), 7017-7021. https://doi.org/10.1073/pnas.91.15.7017
Chen, D., Toone, W. M., Mata, J., Lyne, R., Burns, G., Kivinen, K., Brazma, A., Jones, N., & Bähler, J. (2003). Global Transcriptional Responses of Fission Yeast to Environmental Stress. *Molecular biology of the cell*, *14*(1), 214-229. https://doi.org/10.1091/mbc.e02-08-0499
Chen, D., Wilkinson, C. R. M., Watt, S., Penkett, C. J., Toone, W. M., Jones, N., & Bähler, J. (2008). Multiple Pathways Differentially Regulate Global Oxidative Stress Responses in Fission Yeast. *Molecular biology of the cell*, *19*(1), 308-317. https://doi.org/10.1091/mbc.e07-08-0735
Christman, M. F., Morgan, R. W., Jacobson, F. S., & Ames, B. N. (1985). Positive control of a regulon for defenses against oxidative stress and some heat-shock proteins in *Salmonella typhimurium*. *Cell*, *41*(3), 753-762. https://doi.org/10.1016/S0092-8674(85)80056-8
Chu, F.-F., Esworthy, R. S., Chu, P. G., Longmate, J. A., Huycke, M. M., Wilczynski, S., & Doroshow, J. H. (2004). Bacteria-induced intestinal cancer in mice with disrupted Gpx1 and Gpx2 genes. *Cancer Research*, *64*(3), 962-968. https://doi.org/10.1158/0008-5472.can-03-2272
Cobley, J. N. (2018). Synapse Pruning: Mitochondrial ROS with Their Hands on the Shears. *BioEssays*, *40*(7), 1800031. https://doi.org/10.1002/bies.201800031
Connelly, W. M., Laing, M., Errington, A. C., & Crunelli, V. (2016). The Thalamus as a Low Pass Filter: Filtering at the Cellular Level does Not Equate with Filtering at the Network Level. *Frontiers in Neural Circuits*, *9*. https://doi.org/10.3389/fncir.2015.00089
D'Autréaux, B., & Toledano, M. B. (2007). ROS as signalling molecules: mechanisms that generate specificity in ROS homeostasis. *Nature reviews. Molecular cell biology*, *8*(10), 813-824. http://search.ebscohost.com/login.aspx?direct=true&db=mnh&AN=17848967&site=ehost-live&scope=site
Day, A. M., Brown, J. D., Taylor, S. R., Rand, J. D., Morgan, B. A., & Veal, E. A. (2012). Inactivation of a Peroxiredoxin by Hydrogen Peroxide Is Critical for Thioredoxin-Mediated Repair of Oxidized Proteins and Cell Survival. *Molecular Cell*, *45*(3), 398-408. https://doi.org/10.1016/j.molcel.2011.11.027

Decero, S. A., Winslow, C. H., & Coburn, J. (2020). Method to Overcome Inefficiencies in Site-Directed Mutagenesis of A/T-Rich DNA. *Journal of Biomolecular Techniques 3*(3), 94-99. https://doi.org/10.7171/jbt.20-3103-003

Delaunay, A., Isnard, A.-D., & Toledano, M. B. (2000). H_2O_2 sensing through oxidation of the Yap1 transcription factor. *The EMBO journal*, *19*(19), 5157-5166. https://doi.org/10.1093/emboj/19.19.5157

Demple, B., & Halbrook, J. (1983). Inducible repair of oxidative DNA damage in *Escherichia coli*. *Nature*, *304*(5925), 466-468. https://doi.org/10.1038/304466a0

Dinkova-Kostova, A. T., & Abramov, A. Y. (2015). The emerging role of Nrf2 in mitochondrial function. *Free Radical Biology and Medicine*, *88*, 179-188. https://doi.org/https://doi.org/10.1016/j.freeradbiomed.2015.04.036

Dinkova-Kostova, A. T., Holtzclaw, W. D., Cole, R. N., Itoh, K., Wakabayashi, N., Katoh, Y., Yamamoto, M., & Talalay, P. (2002). Direct evidence that sulfhydryl groups of Keap1 are the sensors regulating induction of phase 2 enzymes that protect against carcinogens and oxidants. *Proceedings of the National Academy of Sciences*, *99*(18), 11908-11913. https://doi.org/10.1073/pnas.172398899

Domènech, A., Ayté, J., Antunes, F., & Hidalgo, E. (2018). Using in vivo oxidation status of one- and two-component redox relays to determine H_2O_2 levels linked to signaling and toxicity. *BMC Biology*, *16*(1). https://doi.org/10.1186/s12915-018-0523-6

Ellenberger, T. (1994). Getting a grip on DNA recognition: structures of the basic region leucine zipper, and the basic region helix-loop-helix DNA-binding domains. *Current Opinion in Structural Biology*, *4*(1), 12-21. https://doi.org/https://doi.org/10.1016/S0959-440X(94)90054-X

Enomoto, A. (2001). High Sensitivity of Nrf2 Knockout Mice to Acetaminophen Hepatotoxicity Associated with Decreased Expression of ARE-Regulated Drug Metabolizing Enzymes and Antioxidant Genes. *Toxicological Sciences*, *59*(1), 169-177. https://doi.org/10.1093/toxsci/59.1.169

Estrada, C. P., Covacu, R., Sankavaram, S. R., Svensson, M., & Brundin, L. (2014). Oxidative Stress Increases Neurogenesis and Oligodendrogenesis in Adult Neural Progenitor Cells. *Stem Cells and Development*, *23*(19), 2311-2327. https://doi.org/10.1089/scd.2013.0452

Falkowski, P. G., Katz, M. E., Milligan, A. J., Fennel, K., Cramer, B. S., Aubry, M. P., Berner, R. A., Novacek, M. J., & Zapol, W. M. (2005). The Rise of Oxygen over the Past 205 Million Years and the Evolution of Large Placental Mammals. *Science*, *309*(5744), 2202-2204. https://doi.org/10.1126/science.1116047

Fenton, H. J. H. (1894). LXXIII.—Oxidation of tartaric acid in presence of iron. *J. Chem. Soc., Trans.*, *65*(0), 899-910. https://doi.org/10.1039/ct8946500899

Ferguson, H. A. (2001). Expression and purification of recombinant human c-Fos/c-Jun that is highly active in DNA binding and transcriptional activation *in vitro*. *Nucleic Acids Research*, *29*(20), 98e-98. https://doi.org/10.1093/nar/29.20.e98

Fernandes, A. P., & Holmgren, A. (2004). Glutaredoxins: glutathione-dependent redox enzymes with functions far beyond a simple thioredoxin backup system. *Antioxidants & redox signaling*, *6*(1), 63-74. https://doi.org/10.1089/152308604771978354

Fichman, Y., Rowland, L., Nguyen, T. T., Chen, S.-J., & Mittler, R. (2024). Propagation of a rapid cell-to-cell H_2O_2 signal over long distances in a monolayer of cardiomyocyte cells. *Redox Biology*, *70*, 2213-2317. https://doi.org/10.1101/2023.12.19.572374

Fichman, Y., Rowland, L., Oliver, M. J., & Mittler, R. (2023). ROS are evolutionary conserved cell-to-cell stress signals. *Proceedings of the National Academy of Sciences*, *120*(31). https://doi.org/10.1073/pnas.2305496120

Fischer, R., & Maier, O. (2015). Interrelation of Oxidative Stress and Inflammation in Neurodegenerative Disease: Role of TNF. *Oxidative Medicine and Cellular Longevity*, *2015*, 1-18. https://doi.org/10.1155/2015/610813

Fisher, A. B. (2011). Peroxiredoxin 6: A Bifunctional Enzyme with Glutathione Peroxidase and Phospholipase A2 Activities. *Antioxidants & redox signaling*, *15*(3), 831-844. https://doi.org/10.1089/ars.2010.3412
Forman, H. J., Maiorino, M., & Ursini, F. (2010). Signaling Functions of Reactive Oxygen Species. *Biochemistry*, *49*(5), 835-842. https://doi.org/10.1021/bi9020378
Fourquet, S., Guerois, R., Biard, D., & Toledano, M. B. (2010). Activation of NRF2 by Nitrosative Agents and H_2O_2 Involves KEAP1 Disulfide Formation. *Journal of Biological Chemistry*, *285*(11), 8463-8471. https://doi.org/10.1074/jbc.m109.051714
Fujii, Y., Shimizu, T., Toda, T., Yanagida, M., & Hakoshima, T. (2000). Structural basis for the diversity of DNA recognition by bZIP transcription factors. *Nature Structural Biology*, *7*(10), 889-893. https://doi.org/10.1038/82822
Gasch, A. P., Spellman, P. T., Kao, C. M., Carmel-Harel, O., Eisen, M. B., Storz, G., Botstein, D., & Brown, P. O. (2000). Genomic Expression Programs in the Response of Yeast Cells to Environmental Changes. *Molecular biology of the cell*, *11*(12), 4241-4257. https://doi.org/10.1091/mbc.11.12.4241
Ghezzi, P., Jaquet, V., Marcucci, F., & Schmidt, H. H. H. W. (2017). The oxidative stress theory of disease: levels of evidence and epistemological aspects. *British Journal of Pharmacology*, *174*(12), 1784-1796. https://doi.org/10.1111/bph.13544
Gilbert, D. L. (Ed.). (2012). *Oxygen and Living Processes: An Interdisciplinary Approach* (1 ed.). Springer Science & Business Media.
Go, Y.-M., & Jones, D. P. (2013). The Redox Proteome. *Journal of Biological Chemistry*, *288*(37), 26512-26520. https://doi.org/10.1074/jbc.r113.464131
Goldstein, B. C., Daniel , Faeder, J. R., & Hlavacek, W. S. (2008). Kinetic proofreading model. *Advances in Experimental Medicine and Biology*, *640*, 82-94. https://doi.org/10.1007/978-0-387-09789-3_8
Goncalves, R. L. S., Quinlan, C. L., Perevoshchikova, I. V., Hey-Mogensen, M., & Brand, M. D. (2015). Sites of superoxide and hydrogen peroxide production by muscle mitochondria assessed *ex vivo* under conditions mimicking rest and exercise. *Journal of Biological Chemistry*, *290*(1), 209-227. https://doi.org/10.1074/jbc.m114.619072
Govindjee, & Shevela, D. (2011). Adventures with cyanobacteria: a personal perspective. *Frontiers in Plant Science*, *2*. https://doi.org/10.3389/fpls.2011.00028
Graudejus, O., Ponce Wong, R. D., Varghese, N., Wagner, S., & Morrison, B. (2018). Bridging the gap between *in vivo* and *in vitro* research: Reproducing in vitro the mechanical and electrical environment of cells *in vivo*. *Frontiers in Cellular Neuroscience*, *12*.
Gray, M. J., Wholey, W.-Y., & Jakob, U. (2013). Bacterial Responses to Reactive Chlorine Species. *Annual Review of Microbiology*, *67*(1), 141-160. https://doi.org/10.1146/annurev-micro-102912-142520
Gromer, S., Urig, S., & Becker, K. (2004). The thioredoxin system—From science to clinic. *Medicinal Research Reviews*, *24*(1), 40-89. https://doi.org/10.1002/med.10051
Gupta, V., & Carroll, K. S. (2014). Sulfenic acid chemistry, detection and cellular lifetime. *Biochimica et Biophysica Acta (BBA) - General Subjects*, *1840*(2), 847-875. https://doi.org/10.1016/j.bbagen.2013.05.040
Hall, A., Karplus, P. A., & Poole, L. B. (2009). Typical 2-Cys peroxiredoxins – structures, mechanisms and functions. *The FEBS Journal*, *276*(9), 2469-2477. https://doi.org/10.1111/j.1742-4658.2009.06985.x
Halliwell, B. (2006a). Oxidative stress and cancer: have we moved forward? *Biochemical Journal*, *401*(1), 1-11. https://doi.org/10.1042/bj20061131
Halliwell, B. (2006b). Reactive species and antioxidants. Redox biology is a fundamental theme of aerobic life. *Plant physiology*, *141*(2), 312-322.
Halliwell, B., & Gutteridge, J. M. C. (2015a). *Free radicals in biology and medicine* (5th ed.). Oxford University Press.

Halliwell, B., & Gutteridge, J. M. C. (2015b). Oxidative stress and redox regulation: adaptation, damage, repair, senescence, and death. In *Free Radicals in Biology and Medicine* (5th ed., pp. 199–283). Oxford University Press. https://doi.org/10.1093/acprof:oso/9780198717478.003.0005

Hanschmann, E.-M., Godoy, J. R., Berndt, C., Hudemann, C., & Lillig, C. H. (2013). Thioredoxins, Glutaredoxins, and Peroxiredoxins—Molecular Mechanisms and Health Significance: from Cofactors to Antioxidants to Redox Signaling. *Antioxidants & redox signaling*, *19*(13), 1539-1605. https://doi.org/10.1089/ars.2012.4599

Harman, D. (1956). Aging: A Theory Based on Free Radical and Radiation Chemistry. *Journal of Gerontology*, *11*(3), 298-300. https://doi.org/10.1093/geronj/11.3.298

Harris, C. R., Millman, K. J., Van Der Walt, S. J., Gommers, R., Virtanen, P., Cournapeau, D., Wieser, E., Taylor, J., Berg, S., Smith, N. J., Kern, R., Picus, M., Hoyer, S., Van Kerkwijk, M. H., Brett, M., Haldane, A., Del Río, J. F., Wiebe, M., Peterson, P., . . . Oliphant, T. E. (2020). Array programming with NumPy. *Nature*, *585*(7825), 357-362. https://doi.org/10.1038/s41586-020-2649-2

Harvey, C. J., Thimmulappa, R. K., Sethi, S., Kong, X., Yarmus, L., Brown, R. H., Feller-Kopman, D., Wise, R., & Biswal, S. (2011). Targeting Nrf2 signaling improves bacterial clearance by alveolar macrophages in patients with COPD and in a mouse model. *Science translational medicine*, *3*(78), 78ra32-78ra32.

Hayles, J., & Nurse, P. (2018). Introduction to Fission Yeast as a Model System. *Cold Spring Harbor Protocols*, *2018*(5). https://doi.org/10.1101/pdb.top079749

He, Y., Chen, Y., Song, W., Zhu, L., Dong, Z., & Ow, D. W. (2016). A Pap1–Oxs1 signaling pathway for disulfide stress in *Schizosaccharomyces pombe*. *Nucleic Acids Research*, *45*(1), 106-114. https://doi.org/10.1093/nar/gkw818

Hegde, M. L., Mantha, A. K., Hazra, T. K., Bhakat, K. K., Mitra, S., & Szczesny, B. (2012). Oxidative genome damage and its repair: Implications in aging and neurodegenerative diseases. *Mechanisms of Ageing and Development*, *133*(4), 157-168. https://doi.org/10.1016/j.mad.2012.01.005

Heinrich, R., Neel, B. G., & Rapoport, T. A. (2002). Mathematical Models of Protein Kinase Signal Transduction. *Molecular Cell*, *9*(5), 957-970. https://doi.org/10.1016/s1097-2765(02)00528-2

Hersen, P., McClean, M. N., Mahadevan, L., & Ramanathan, S. (2008). Signal processing by the HOG MAP kinase pathway. *Proceedings of the National Academy of Sciences*, *105*(20), 7165-7170. https://doi.org/10.1073/pnas.0710770105

Higgins, L. G., Kelleher, M. O., Eggleston, I. M., Itoh, K., Yamamoto, M., & Hayes, J. D. (2009). Transcription factor Nrf2 mediates an adaptive response to sulforaphane that protects fibroblasts in vitro against the cytotoxic effects of electrophiles, peroxides and redox-cycling agents. *Toxicology and Applied Pharmacology*, *237*(3), 267-280. https://doi.org/https://doi.org/10.1016/j.taap.2009.03.005

Hodgskiss, M. S. W., Crockford, P. W., Peng, Y., Wing, B. A., & Horner, T. J. (2019). A productivity collapse to end Earth's Great Oxidation. *Proceedings of the National Academy of Sciences*, *116*(35), 17207-17212. https://doi.org/10.1073/pnas.1900325116

Hoffman, C. S., Wood, V., & Fantes, P. A. (2015). An Ancient Yeast for Young Geneticists: A Primer on the *Schizosaccharomyces pombe* Model System. *Genetics*, *201*(2), 403-423. https://doi.org/10.1534/genetics.115.181503

Hopfield, J. J. (1974). Kinetic Proofreading: A New Mechanism for Reducing Errors in Biosynthetic Processes Requiring High Specificity. *Proceedings of the National Academy of Sciences*, *71*(10), 4135-4139. https://doi.org/10.1073/pnas.71.10.4135

Hornberg, J. J., Bruggeman, F. J., Binder, B., Geest, C. R., De Vaate, A. J. M. B., Lankelma, J., Heinrich, R., & Westerhoff, H. V. (2005). Principles behind the multifarious control of signal transduction. *The FEBS Journal*, *272*(1), 244-258. https://doi.org/10.1111/j.1432-1033.2004.04404.x

Howes, R. M. (2006). The Free Radical Fantasy. *Annals of the New York Academy of Sciences*, *1067*(1), 22-26. https://doi.org/https://doi.org/10.1196/annals.1354.004
Hunter, J. D. (2007). Matplotlib: A 2D Graphics Environment. *Computing in Science & Engineering*, *9*(3), 90-95. https://doi.org/10.1109/mcse.2007.55
Hutchens, T. W., & Yip, T.-T. (1990). Differential interaction of peptides and protein surface structures with free metal ions and surface-immobilized metal ions. *Journal of Chromatography A*, *500*, 531-542. https://doi.org/https://doi.org/10.1016/S0021-9673(00)96090-4
Jaeger, R. C., & Blalock, T. N. (2016). *Microelectronic circuit design* (5th ed.). McGraw-Hill Education.
Janes, K. A., Reinhardt, H. C., & Yaffe, M. B. (2008). Cytokine-Induced Signaling Networks Prioritize Dynamic Range over Signal Strength. *Cell*, *135*(2), 343-354. https://doi.org/10.1016/j.cell.2008.08.034
Jang, H. H., Lee, K. O., Chi, Y. H., Jung, B. G., Park, S. K., Park, J. H., Lee, J. R., Lee, S. S., Moon, J. C., Yun, J. W., Choi, Y. O., Kim, W. Y., Kang, J. S., Cheong, G.-W., Yun, D.-J., Rhee, S. G., Cho, M. J., & Lee, S. Y. (2004). Two Enzymes in One. *Cell*, *117*(5), 625-635. https://doi.org/10.1016/j.cell.2004.05.002
Jara, M., Vivancos, A. P., Calvo, I. A., Moldón, A., Sansó, M., & Hidalgo, E. (2007). The Peroxiredoxin Tpx1 Is Essential as a H_2O_2 Scavenger during Aerobic Growth in Fission Yeast. *Molecular biology of the cell*, *18*(6), 2288-2295. https://doi.org/10.1091/mbc.e06-11-1039
Jumper, J., Evans, R., Pritzel, A., Green, T., Figurnov, M., Ronneberger, O., Tunyasuvunakool, K., Bates, R., Žídek, A., Potapenko, A., Bridgland, A., Meyer, C., Kohl, S. A. A., Ballard, A. J., Cowie, A., Romera-Paredes, B., Nikolov, S., Jain, R., Adler, J., . . . Hassabis, D. (2021). Highly accurate protein structure prediction with AlphaFold. *Nature*, *596*(7873), 583-589. https://doi.org/10.1038/s41586-021-03819-2
Jun, H., Kieselbach, T., & Jönsson, L. J. (2012). Comparative proteome analysis of *Saccharomyces cerevisiae*: A global overview of *in vivo* targets of the yeast activator protein 1. *BMC Genomics*, *13*(1), 230. https://doi.org/10.1186/1471-2164-13-230
Kasting, J. F. (2014). 6.6 - Modeling the Archean Atmosphere and Climate. In H. D. Holland & K. K. Turekian (Eds.), *Treatise on Geochemistry (Second Edition)* (pp. 157-175). Elsevier. https://doi.org/https://doi.org/10.1016/B978-0-08-095975-7.01306-1
Kemp, M., Go, Y.-M., & Jones, D. P. (2008). Non-equilibrium thermodynamics of thiol/disulfide redox systems: A perspective on redox systems biology. *Free Radical Biology and Medicine*, *44*(6), 921-937. https://doi.org/10.1016/j.freeradbiomed.2007.11.008
Kimura, H., Sawada, T., Oshima, S., Kozawa, K., Ishioka, T., & Kato, M. (2005). Toxicity and roles of reactive oxygen species. *Current Drug Targets-Inflammation & Allergy*, *4*(4), 489-495.
Kırlı, K., Karaca, S., Dehne, H. J., Samwer, M., Pan, K. T., Lenz, C., Urlaub, H., & Görlich, D. (2015). A deep proteomics perspective on CRM1-mediated nuclear export and nucleocytoplasmic partitioning. *eLife*, *4*. https://doi.org/10.7554/elife.11466
Klipp, E., & Liebermeister, W. (2006). Mathematical modeling of intracellular signaling pathways. *BMC Neuroscience*, *7*(S1), S10. https://doi.org/10.1186/1471-2202-7-s1-s10
Klomsiri, C., Karplus, P. A., & Poole, L. B. (2011). Cysteine-Based Redox Switches in Enzymes. *Antioxidants & redox signaling*, *14*(6), 1065-1077. https://doi.org/10.1089/ars.2010.3376
Klotz, L.-O., Kröncke, K.-D., & Sies, H. (2003). Singlet oxygen-induced signaling effects in mammalian cells. *Photochemical & Photobiological Sciences*, *2*(2), 88-94. https://doi.org/10.1039/b210750c
Knoops, B., Goemaere, J., Van der Eecken, V., & Declercq, J.-P. (2011). Peroxiredoxin 5: Structure, Mechanism, and Function of the Mammalian Atypical 2-Cys

Peroxiredoxin. *Antioxidants & redox signaling*, *15*(3), 817-829. https://doi.org/10.1089/ars.2010.3584
Komarova, N. L., Zou, X., Nie, Q., & Bardwell, L. (2005). A theoretical framework for specificity in cell signaling. *Molecular Systems Biology*, *1*(1), E1-E5. https://doi.org/10.1038/msb4100031
Kudo, N., Taoka, H., Toda, T., Yoshida, M., & Horinouchi, S. (1999). A Novel Nuclear Export Signal Sensitive to Oxidative Stress in the Fission Yeast Transcription Factor Pap1. *Journal of Biological Chemistry*, *274*(21), 15151-15158. https://doi.org/10.1074/jbc.274.21.15151
Kuge, S. (1997). Regulation of yAP-1 nuclear localization in response to oxidative stress. *The EMBO journal*, *16*(7), 1710-1720. https://doi.org/10.1093/emboj/16.7.1710
Laemmli, U. K. (1970). Cleavage of structural proteins during the assembly of the head of bacteriophage T4. *Nature*, *227*(5259), 680-685.
Lapointe, J., & Hekimi, S. (2010). When a theory of aging ages badly. *Cellular and Molecular Life Sciences*, *67*(1), 1-8. https://doi.org/10.1007/s00018-009-0138-8
Lee, J., Dawes, I. W., & Roe, J. H. (1995). Adaptive response of *Schizosaccharomyces pombe* to hydrogen peroxide and menadione. *Microbiology*, *141*(12), 3127-3132. https://doi.org/10.1099/13500872-141-12-3127
Lee, J., Godon, C., Lagniel, G., Spector, D., Garin, J., Labarre, J., & Toledano, M. B. (1999). Yap1 and Skn7 Control Two Specialized Oxidative Stress Response Regulons in Yeast. *The Journal of Biological Chemistry*, *274*(23), 16040-16046. https://doi.org/10.1074/jbc.274.23.16040
Levine, R., Moskovitz, J., & Stadtman, E. (2001). Oxidation of Methionine in Proteins: Roles in Antioxidant Defense and Cellular Regulation. *IUBMB Life*, *50*(4), 301-307. https://doi.org/10.1080/713803735
Li, L., Cheung, S.-H., Evans, E. L., & Shaw, P. E. (2010). Modulation of Gene Expression and Tumor Cell Growth by Redox Modification of STAT3. *Cancer Research*, *70*(20), 8222-8232. https://doi.org/10.1158/0008-5472.can-10-0894
Lillig, C. H., Berndt, C., & Holmgren, A. (2008). Glutaredoxin systems. *Biochimica et Biophysica Acta (BBA) - General Subjects*, *1780*(11), 1304-1317. https://doi.org/https://doi.org/10.1016/j.bbagen.2008.06.003
Lin, M. T., & Flint Beal, M. (2003). The oxidative damage theory of aging. *Clinical Neuroscience Research*, *2*(5), 305-315. https://doi.org/https://doi.org/10.1016/S1566-2772(03)00007-0
Lloyd, D. R., Phillips, D. H., & Carmichael, P. L. (1997). Generation of Putative Intrastrand Cross-Links and Strand Breaks in DNA by Transition Metal Ion-Mediated Oxygen Radical Attack. *Chemical Research in Toxicology*, *10*(4), 393-400. https://doi.org/10.1021/tx960158q
Locasale, J. W. (2008). Signal duration and the time scale dependence of signal integration in biochemical pathways. *BMC Systems Biology*, *2*(1), 108. https://doi.org/10.1186/1752-0509-2-108
Lu, J., & Holmgren, A. (2014). The thioredoxin antioxidant system. *Free Radical Biology and Medicine*, *66*, 75-87. https://doi.org/10.1016/j.freeradbiomed.2013.07.036
Lyons, T. W., Reinhard, C. T., & Planavsky, N. J. (2014). The rise of oxygen in Earth's early ocean and atmosphere. *Nature*, *506*(7488), 307-315. https://doi.org/10.1038/nature13068
Madrid, M., Soto, T., Franco, A., Paredes, V., Vicente, J., Hidalgo, E., Gacto, M., & Cansado, J. (2004). A Cooperative Role for Atf1 and Pap1 in the Detoxification of the Oxidative Stress Induced by Glucose Deprivation in *Schizosaccharomyces pombe*. *Journal of Biological Chemistry*, *279*(40), 41594-41602. https://doi.org/10.1074/jbc.m405509200
Magsi, H., Sodhro, A. H., Chachar, F. A., & Abro, S. A. K. (2018, 2018). Analysis of signal noise reduction by using filters.

Mani, S. (2015). Production of Reactive Oxygen Species and Its Implication in Human Diseases. In V. Rani & U. C. S. Yadav (Eds.), *Free Radicals in Human Health and Disease* (1st ed., pp. 3-15). Springer India. https://doi.org/10.1007/978-81-322-2035-0_1

Marden, M. (1966). *Geometry of Polynomials* (2 ed., Vol. 3). American Mathematical Society. https://books.google.co.za/books?id=raZwAAAAQBAJ

Marguerat, S., Schmidt, A., Codlin, S., Chen, W., Aebersold, R., & Bähler, J. (2012). Quantitative Analysis of Fission Yeast Transcriptomes and Proteomes in Proliferating and Quiescent Cells. *Cell*, *151*(3), 671-683. https://doi.org/10.1016/j.cell.2012.09.019

Marinho, H. S., Real, C., Cyrne, L., Soares, H., & Antunes, F. (2014). Hydrogen peroxide sensing, signaling and regulation of transcription factors. *Redox Biology*, *2*, 535-562. https://doi.org/https://doi.org/10.1016/j.redox.2014.02.006

Mashamaite, L. N., Rohwer, J. M., & Pillay, C. S. (2015). The glutaredoxin mono- and di-thiol mechanisms for deglutathionylation are functionally equivalent: implications for redox systems biology. *Bioscience Reports*, *35*(1), 1-10. https://doi.org/10.1042/bsr20140157

Meister, A., & Anderson, M. E. (1983). Glutathione. *Annual Review of Biochemistry*, *52*(1), 711-760. https://doi.org/10.1146/annurev.bi.52.070183.003431

Meyer, A. J., & Dick, T. P. (2010). Fluorescent Protein-Based Redox Probes. *Antioxidants & redox signaling*, *13*(5), 621-650. https://doi.org/10.1089/ars.2009.2948

Mignolet-Spruyt, L., Xu, E., Idänheimo, N., Hoeberichts, F. A., Mühlenbock, P., Brosché, M., Van Breusegem, F., & Kangasjärvi, J. (2016). Spreading the news: subcellular and organellar reactive oxygen species production and signalling. *Journal of Experimental Botany*, *67*(13), 3831-3844. https://doi.org/10.1093/jxb/erw080

Mittler, R. (2017). ROS Are Good. *Trends in Plant Science*, *22*(1), 11-19. https://doi.org/10.1016/j.tplants.2016.08.002

Morano, K. A., Grant, C. M., & Moye-Rowley, W. S. (2012). The Response to Heat Shock and Oxidative Stress in *Saccharomyces cerevisiae*. *Genetics*, *190*(4), 1157-1195. https://doi.org/10.1534/genetics.111.128033

Moye-Rowley, W. S., Harshman, K. D., & Parker, C. S. (1989). Yeast YAP1 encodes a novel form of the jun family of transcriptional activator proteins. *Genes & Development*, *3*(3), 283-292. https://doi.org/10.1101/gad.3.3.283

Munck, A., Guyre, P. M., & Holbrook, N. J. (1984). Physiological Functions of Glucocorticoids in Stress and Their Relation to Pharmacological Actions*. *Endocrine Reviews*, *5*(1), 25-44. https://doi.org/10.1210/edrv-5-1-25

Nagarajan, N., Oka, S., & Sadoshima, J. (2017). Modulation of signaling mechanisms in the heart by thioredoxin 1. *Free Radical Biology and Medicine*, *109*, 125-131. https://doi.org/https://doi.org/10.1016/j.freeradbiomed.2016.12.020

Nitti, M., Marengo, B., Furfaro, A. L., Pronzato, M. A., Marinari, U. M., Domenicotti, C., & Traverso, N. (2022). Hormesis and Oxidative Distress: Pathophysiology of Reactive Oxygen Species and the Open Question of Antioxidant Modulation and Supplementation. *Antioxidants*, *11*(8), 1613. https://doi.org/10.3390/antiox11081613

O'Neill, J. S., & Reddy, A. B. (2011). Circadian clocks in human red blood cells. *Nature*, *469*(7331), 498-503. https://doi.org/10.1038/nature09702

Okazaki, S., Tachibana, T., Naganuma, A., Mano, N., & Kuge, S. (2007). Multistep Disulfide Bond Formation in Yap1 Is Required for Sensing and Transduction of H_2O_2 Stress Signal. *Molecular Cell*, *27*(4), 675-688. https://doi.org/10.1016/j.molcel.2007.06.035

Okegbe, C., Sakhtah, H., Sekedat, M. D., Price-Whelan, A., & Dietrich, L. E. P. (2012). Redox Eustress: Roles for Redox-Active Metabolites in Bacterial Signaling and Behavior. *Antioxidants & redox signaling*, *16*(7), 658-667. https://doi.org/10.1089/ars.2011.4249

Olivier, B. G., Rohwer, J. M., & Hofmeyr, J. H. S. (2005). Modelling cellular systems with PySCeS. *Bioinformatics*, *21*(4), 560-561. https://doi.org/10.1093/bioinformatics/bti046

Otsu, K., Sato, K., Ikeda, Y., Imai, H., Nakagawa, Y., Ohba, Y., & Fujii, J. (2005). An abortive apoptotic pathway induced by singlet oxygen is due to the suppression of caspase activation. *Biochemical Journal*, *389*(1), 197-206. https://doi.org/10.1042/bj20042067

Paek, A., Jose, E., March-Steinman, W., Wilson, B., & Shanks, L. (2023). *Temporal Coordination of the Transcription Factor Response to H_2O_2 stress*. Research Square Platform LLC. https://dx.doi.org/10.21203/rs.3.rs-2791121/v1

Papadakis, M. A., & Workman, C. T. (2015). Oxidative stress response pathways: Fission yeast as archetype. *Critical Reviews in Microbiology*, *41*(4), 520-535. https://doi.org/10.3109/1040841x.2013.870968

Park, S., & Imlay, J. A. (2003). High Levels of Intracellular Cysteine Promote Oxidative DNA Damage by Driving the Fenton Reaction. *Journal of Bacteriology*, *185*(6), 1942-1950. https://doi.org/10.1128/jb.185.6.1942-1950.2003

Pavlov, A. A., & Kasting, J. F. (2002). Mass-Independent Fractionation of Sulfur Isotopes in Archean Sediments: Strong Evidence for an Anoxic Archean Atmosphere. *Astrobiology*, *2*(1), 27-41. https://doi.org/10.1089/153110702753621321

Pemberton, L. F., & Paschal, B. M. (2005). Mechanisms of Receptor-Mediated Nuclear Import and Nuclear Export. *Traffic*, *6*(3), 187-198. https://doi.org/10.1111/j.1600-0854.2005.00270.x

Pignatello, J. J., Oliveros, E., & MacKay, A. (2006). Advanced Oxidation Processes for Organic Contaminant Destruction Based on the Fenton Reaction and Related Chemistry. *Critical Reviews in Environmental Science and Technology*, *36*(1), 1-84. https://doi.org/10.1080/10643380500326564

Pillai-Kastoori, L., Schutz-Geschwender, A. R., & Harford, J. A. (2020). A systematic approach to quantitative Western blot analysis. *Analytical Biochemistry*, *593*, 113608. https://doi.org/https://doi.org/10.1016/j.ab.2020.113608

Pillay, C. S., Hofmeyr, J.-H. S., & Rohwer, J. M. (2011). The logic of kinetic regulation in the thioredoxin system. *BMC Systems Biology*, *5*(1), 15. https://doi.org/10.1186/1752-0509-5-15

Pomposiello, P. J., & Demple, B. (2001). Redox-operated genetic switches: the SoxR and OxyR transcription factors. *Trends in Biotechnology*, *19*(3), 109-114. https://doi.org/https://doi.org/10.1016/S0167-7799(00)01542-0

Poole, L. B., Hall, A., & Nelson, K. J. (2011). Overview of Peroxiredoxins in Oxidant Defense and Redox Regulation. *Current Protocols in Toxicology*, *49*(1), 7.9.1-7.9.15. https://doi.org/10.1002/0471140856.tx0709s49

Poole, L. B., & Nelson, K. J. (2016). Distribution and Features of the Six Classes of Peroxiredoxins. *Molecules and Cells*, *39*(1), 53-59. https://doi.org/10.14348/molcells.2016.2330

Pulliam, D. A., Bhattacharya, A., & Van Remmen, H. (2013). Mitochondrial Dysfunction in Aging and Longevity: A Causal or Protective Role? *Antioxidants & redox signaling*, *19*(12), 1373-1387. https://doi.org/10.1089/ars.2012.4950

Quinn, J., Findlay, V. J., Dawson, K., Millar, J. B. A., Jones, N., Morgan, B. A., & Toone, W. M. (2002). Distinct regulatory proteins control the graded transcriptional response to increasing H_2O_2 levels in fission yeast *Schizosaccharomyces pombe*. *Molecular biology of the cell*, *13*(3), 805-816.

Ralser, M., Wamelink, M. M., Kowald, A., Gerisch, B., Heeren, G., Struys, E. A., Klipp, E., Jakobs, C., Breitenbach, M., Lehrach, H., & Krobitsch, S. (2007). Dynamic rerouting of the carbohydrate flux is key to counteracting oxidative stress. *Journal of Biology*, *6*(4), 10. https://doi.org/10.1186/jbiol61

Rao, V. S., Srinivas, K., Sujini, G. N., & Kumar, G. N. S. (2014). Protein-Protein Interaction Detection: Methods and Analysis. *International Journal of Proteomics*, *2014*, 1-12. https://doi.org/10.1155/2014/147648

Ravanat, J.-L., & Cadet, J. (1995). Reaction of Singlet Oxygen with 2'-Deoxyguanosine and DNA. Isolation and Characterization of the Main Oxidation Products. *Chemical Research in Toxicology*, *8*(3), 379-388. https://doi.org/10.1021/tx00045a009

Raymond, J., & Segrè, D. (2006). The Effect of Oxygen on Biochemical Networks and the Evolution of Complex Life. *Science*, *311*(5768), 1764-1767. https://doi.org/doi:10.1126/science.1118439

Reczek, C. R., & Chandel, N. S. (2015). ROS-dependent signal transduction. *Current opinion in cell biology*, *33*, 8-13. https://doi.org/10.1016/j.ceb.2014.09.010

Reczek, C. R., & Chandel, N. S. (2017). The Two Faces of Reactive Oxygen Species in Cancer. *Annual Review of Cancer Biology*, *1*(1), 79-98. https://doi.org/10.1146/annurev-cancerbio-041916-065808

Rhee, S. G. (2016). Overview on Peroxiredoxin. *Molecules and Cells*, *39*(1), 1-5. https://doi.org/10.14348/molcells.2016.2368

Rhee, S. G., Kang, S. W., Chang, T.-S., Jeong, W., & Kim, K. (2001). Peroxiredoxin, a Novel Family of Peroxidases. *IUBMB Life (International Union of Biochemistry and Molecular Biology: Life)*, *52*(1), 35-41. https://doi.org/10.1080/15216540252774748

Rigoulet, M., Yoboue, E. D., & Devin, A. (2011). Mitochondrial ROS generation and its regulation: mechanisms involved in H_2O_2 signaling. *Antioxidants & redox signaling*, *14*(3), 459-468.

Roos, G., Foloppe, N., & Messens, J. (2012). Understanding the pKa of Redox Cysteines: The Key Role of Hydrogen Bonding. *Antioxidants & redox signaling*, *18*(1), 94-127. https://doi.org/10.1089/ars.2012.4521

Rusz, M., Del Favero, G., El Abiead, Y., Gerner, C., Keppler, B. K., Jakupec, M. A., & Koellensperger, G. (2021). Morpho-metabotyping the oxidative stress response. *Scientific Reports*, *11*(1). https://doi.org/10.1038/s41598-021-94585-8

Schaeffer, H. J., & Weber, M. J. (1999). Mitogen-Activated Protein Kinases: Specific Messages from Ubiquitous Messengers. *Molecular and Cellular Biology*, *19*(4), 2435-2444. https://doi.org/10.1128/MCB.19.4.2435

Schwartz, M. A., & Madhani, H. D. (2004). Principles of MAP Kinase Signaling Specificity in *Saccharomyces cerevisiae*. *Annual Review of Genetics*, *38*(1), 725-748. https://doi.org/10.1146/annurev.genet.39.073003.112634

Selye, H. (1936). A Syndrome produced by Diverse Nocuous Agents. *Nature*, *138*(3479), 32-32. https://doi.org/10.1038/138032a0

Selye, H. (1950). Stress and the General Adaptation Syndrome. *British Medical Journal*, *1*(4667), 1383-1392. https://doi.org/10.1136/bmj.1.4667.1383

Shaulian, E., & Karin, M. (2001). AP-1 in cell proliferation and survival. *Oncogene*, *20*(19), 2390-2400. https://doi.org/10.1038/sj.onc.1204383

Shigenaga, M. K., Hagen, T. M., & Ames, B. N. (1994). Oxidative damage and mitochondrial decay in aging. *Proceedings of the National Academy of Sciences of the United States of America*, *91*(23), 10771-10778. https://doi.org/10.1073/pnas.91.23.10771

Shui, S., Scheller, L., & Correia, B. E. (2023). *Rationally designed protein bandpass filters for controlling cellular signaling with chemical inputs*. Cold Spring Harbor Laboratory. https://dx.doi.org/10.1101/2023.02.10.528077

Sies, H. (1993). Strategies of antioxidant defense. *European Journal of Biochemistry*, *215*(2), 213-219. https://doi.org/10.1111/j.1432-1033.1993.tb18025.x

Sies, H. (2018). On the history of oxidative stress: Concept and some aspects of current development. *Current Opinion in Toxicology*, *7*, 122-126. https://doi.org/https://doi.org/10.1016/j.cotox.2018.01.002

Sies, H. (2019a). *Oxidative stress: eustress and distress* (H. Sies, Ed. 1st ed.). Academic Press.
Sies, H. (2019b). Oxidative Stress: Eustress and Distress in Redox Homeostasis. In G. Fink (Ed.), *Stress: Physiology, Biochemistry, and Pathology* (1st ed., pp. 153-163). Academic Press. https://doi.org/https://doi.org/10.1016/B978-0-12-813146-6.00013-8
Sies, H. (2020). Oxidative eustress and oxidative distress: Introductory remarks. In H. Sies (Ed.), *Oxidative stress: eustress and distress* (pp. 3-12). Academic Press. https://doi.org/https://doi.org/10.1016/B978-0-12-818606-0.00001-8
Sies, H. (2021). Oxidative eustress: On constant alert for redox homeostasis. *Redox Biology*, *41*, 101867. https://doi.org/https://doi.org/10.1016/j.redox.2021.101867
Sies, H., Berndt, C., & Jones, D. P. (2017). Oxidative Stress. *Annual Review of Biochemistry*, *86*(1), 715-748. https://doi.org/10.1146/annurev-biochem-061516-045037
Sies, H., & Jones, D. (2007). Oxidative Stress. In G. Fink (Ed.), *Encyclopedia of Stress (Second Edition)* (2nd ed., pp. 45-48). Academic Press. https://doi.org/https://doi.org/10.1016/B978-012373947-6.00285-3
Simon, A. R., Rai, U., Fanburg, B. L., & Cochran, B. H. (1998). Activation of the JAK-STAT pathway by reactive oxygen species. *American Journal of Physiology-Cell Physiology*, *275*(6), C1640-C1652. https://doi.org/10.1152/ajpcell.1998.275.6.C1640
Sivashanmugam, A., Murray, V., Cui, C., Zhang, Y., Wang, J., & Li, Q. (2009). Practical protocols for production of very high yields of recombinant proteins usingEscherichia coli. *Protein Science*, *18*(5), 936-948. https://doi.org/10.1002/pro.102
Sivitz, W. I., & Yorek, M. A. (2010). Mitochondrial Dysfunction in Diabetes: From Molecular Mechanisms to Functional Significance and Therapeutic Opportunities. *Antioxidants & Redox Signaling*, *12*(4), 537-577. https://doi.org/10.1089/ars.2009.2531
Smith, B. J. (1994). Acetic Acid-Urea Polyacrylamide Gel Electrophoresis of Proteins. In J. M. Walker (Ed.), *Basic Protein and Peptide Protocols* (pp. 39-47). Humana Press. https://doi.org/10.1385/0-89603-268-x:39
Song, J.-Y., & Roe, J.-H. (2008). The role and regulation of Trxl, a cytosolic thioredoxin in *Schizosaccharomyces pombe*. *The Journal of Microbiology*, *46*(4), 408-414. https://doi.org/10.1007/s12275-008-0076-4
Srivastava, S. (2017). The Mitochondrial Basis of Aging and Age-Related Disorders. *Genes*, *8*(12), 398. https://doi.org/10.3390/genes8120398
Stöcker, S., Maurer, M., Ruppert, T., & Dick, T. P. (2018). A role for 2-Cys peroxiredoxins in facilitating cytosolic protein thiol oxidation. *Nature Chemical Biology*, *14*(2), 148-155. https://doi.org/10.1038/nchembio.2536
Stone, J. R., & Yang, S. (2006). Hydrogen Peroxide: A Signaling Messenger. *Antioxidants & redox signaling*, *8*(3-4), 243-270. https://doi.org/10.1089/ars.2006.8.243
Storz, G., & Tartaglia, L. A. (1992). OxyR: a regulator of antioxidant genes. *The Journal of nutrition*, *122*(suppl_3), 627-630.
Ströher, E., & Dietz, K. J. (2006). Concepts and Approaches Towards Understanding the Cellular Redox Proteome. *Plant Biology*, *8*(4), 407-418. https://doi.org/10.1055/s-2006-923961
Suzen, S., Tucci, P., Profumo, E., Buttari, B., & Saso, L. (2022). A Pivotal Role of Nrf2 in Neurodegenerative Disorders: A New Way for Therapeutic Strategies. *Pharmaceuticals*, *15*(6), 692. https://doi.org/10.3390/ph15060692
Taguchi, K., Motohashi, H., & Yamamoto, M. (2011). Molecular mechanisms of the Keap1-Nrf2 pathway in stress response and cancer evolution. *Genes to Cells*, *16*(2), 123-140. https://doi.org/10.1111/j.1365-2443.2010.01473.x
Talwar, D., Miller, C. G., Grossmann, J., Szyrwiel, L., Schwecke, T., Demichev, V., Mikecin Drazic, A.-M., Mayakonda, A., Lutsik, P., Veith, C., Milsom, M. D., Müller-Decker, K., Mülleder, M., Ralser, M., & Dick, T. P. (2023). The GAPDH redox switch safeguards

reductive capacity and enables survival of stressed tumour cells. *Nature Metabolism*, *5*(4), 660-676. https://doi.org/10.1038/s42255-023-00781-3

Terzi, A., & Suter, D. M. (2020). The role of NADPH oxidases in neuronal development. *Free Radical Biology and Medicine*, *154*, 33-47. https://doi.org/https://doi.org/10.1016/j.freeradbiomed.2020.04.027

Thomas, C., Mackey, M. M., Diaz, A. A., & Cox, D. P. (2009). Hydroxyl radical is produced via the Fenton reaction in submitochondrial particles under oxidative stress: implications for diseases associated with iron accumulation. *Redox Report*, *14*(3), 102-108. https://doi.org/10.1179/135100009x392566

Timme-Laragy, A. R., Hahn, M. E., Hansen, J. M., Rastogi, A., & Roy, M. A. (2018). Redox stress and signaling during vertebrate embryonic development: Regulation and responses. *Seminars in Cell & Developmental Biology*, *80*, 17-28. https://doi.org/10.1016/j.semcdb.2017.09.019

Toledano, M. B., & Leonard, W. J. (1991). Modulation of transcription factor NF-kappa B binding activity by oxidation-reduction *in vitro*. *Proceedings of the National Academy of Sciences*, *88*(10), 4328-4332. https://doi.org/10.1073/pnas.88.10.4328

Tomalin, L. E., Day, A. M., Underwood, Z. E., Smith, G. R., Dalle Pezze, P., Rallis, C., Patel, W., Dickinson, B. C., Bähler, J., Brewer, T. F., Chang, C. J.-L., Shanley, D. P., & Veal, E. A. (2016). Increasing extracellular H_2O_2 produces a bi-phasic response in intracellular H_2O_2, with peroxiredoxin hyperoxidation only triggered once the cellular H_2O_2-buffering capacity is overwhelmed. *Free Radical Biology and Medicine*, *95*, 333-348. https://doi.org/https://doi.org/10.1016/j.freeradbiomed.2016.02.035

Toone, W. M., Morgan, B. A., & Jones, N. (2001). Redox control of AP-1-like factors in yeast and beyond. *Oncogene*, *20*(19), 2336-2346. https://doi.org/10.1038/sj.onc.1204384

Turner-Ivey, B., Manevich, Y., Schulte, J., Kistner-Griffin, E., Jezierska-Drutel, A., Liu, Y., & Neumann, C. A. (2013). Role for Prdx1 as a specific sensor in redox-regulated senescence in breast cancer. *Oncogene*, *32*(45), 5302-5314. https://doi.org/10.1038/onc.2012.624

Varadi, M., Bertoni, D., Magana, P., Paramval, U., Pidruchna, I., Radhakrishnan, M., Tsenkov, M., Nair, S., Mirdita, M., Yeo, J., Kovalevskiy, O., Tunyasuvunakool, K., Laydon, A., Žídek, A., Tomlinson, H., Hariharan, D., Abrahamson, J., Green, T., Jumper, J., . . . Velankar, S. (2023). AlphaFold Protein Structure Database in 2024: providing structure coverage for over 214 million protein sequences. *Nucleic Acids Research*, *52*(D1), D368-D375. https://doi.org/10.1093/nar/gkad1011

Varatnitskaya, M., Degrossoli, A., & Leichert, L. I. (2021). Redox regulation in host-pathogen interactions: thiol switches and beyond. *Biological chemistry*, *402*(3), 299-316. https://doi.org/10.1515/hsz-2020-0264

Veal, E. A., Ross, S. J., Malakasi, P., Peacock, E., & Morgan, B. A. (2003). Ybp1 Is Required for the Hydrogen Peroxide-induced Oxidation of the Yap1 Transcription Factor. *Journal of Biological Chemistry*, *278*(33), 30896-30904. https://doi.org/10.1074/jbc.m303542200

Veal, E. A., Underwood, Z. E., Tomalin, L. E., Morgan, B. A., & Pillay, C. S. (2018). Hyperoxidation of Peroxiredoxins: Gain or Loss of Function? *Antioxidants & redox signaling*, *28*(7), 574-590. https://doi.org/10.1089/ars.2017.7214

Vivancos, A. P., Castillo, E. A., Biteau, B., Nicot, C., Ayte, J., Toledano, M. B., & Hidalgo, E. (2005). A cysteine-sulfinic acid in peroxiredoxin regulates H_2O_2-sensing by the antioxidant Pap1 pathway. *Proceedings of the National Academy of Sciences*, *102*(25), 8875-8880. https://doi.org/10.1073/pnas.0503251102

Vivancos, A. P., Castillo, E. A., Jones, N., Ayté, J., & Hidalgo, E. (2004). Activation of the redox sensor Pap1 by hydrogen peroxide requires modulation of the intracellular oxidant concentration. *Molecular Microbiology*, *52*(5), 1427-1435. https://doi.org/10.1111/j.1365-2958.2004.04065.x

Vivancos, A. P., Jara, M., Zuin, A., Sansó, M., & Hidalgo, E. (2006). Oxidative stress in *Schizosaccharomyces pombe*: different H_2O_2 levels, different response pathways. *Molecular Genetics and Genomics*, *276*(6), 495-502.
Wang, J., Chitsaz, F., Derbyshire, M. K., Gonzales, N. R., Gwadz, M., Lu, S., Marchler, G. H., Song, J. S., Thanki, N., Yamashita, R. A., Yang, M., Zhang, D., Zheng, C., Lanczycki, C. J., & Marchler-Bauer, A. (2023). The conserved domain database in 2023. *Nucleic Acids Research*, *51*(D1), D384-D388. https://doi.org/10.1093/nar/gkac1096
Wang, M., Jiang, Y.-Y., Kim, K. M., Qu, G., Ji, H.-F., Mittenthal, J. E., Zhang, H.-Y., & Caetano-Anollés, G. (2011). A Universal Molecular Clock of Protein Folds and Its Power in Tracing the Early History of Aerobic Metabolism and Planet Oxygenation. *Molecular Biology and Evolution*, *28*(1), 567-582. https://doi.org/10.1093/molbev/msq232
Wang, Y., Branicky, R., Noë, A., & Hekimi, S. (2018). Superoxide dismutases: Dual roles in controlling ROS damage and regulating ROS signaling. *Journal of Cell Biology*, *217*(6), 1915-1928. https://doi.org/10.1083/jcb.201708007
Winterbourn, C. C. (2008). Reconciling the chemistry and biology of reactive oxygen species. *Nature Chemical Biology*, *4*(5), 278-286. https://doi.org/10.1038/nchembio.85
Winterbourn, C. C. (2013). The Biological Chemistry of Hydrogen Peroxide. In E. Cadenas & L. Packer (Eds.), *Methods in Enzymology* (Vol. 528, pp. 3-25). Academic Press. https://doi.org/https://doi.org/10.1016/B978-0-12-405881-1.00001-X
Winterbourn, C. C., & Hampton, M. B. (2008). Thiol chemistry and specificity in redox signaling. *Free Radical Biology and Medicine*, *45*(5), 549-561. https://doi.org/https://doi.org/10.1016/j.freeradbiomed.2008.05.004
Winterbourn, C. C., & Metodiewa, D. (1999). Reactivity of biologically important thiol compounds with superoxide and hydrogen peroxide. *Free Radical Biology and Medicine*, *27*(3), 322-328. https://doi.org/https://doi.org/10.1016/S0891-5849(99)00051-9
Woo, H. A., Won Kang, S., Kim, H. K., Yang, K.-S., Chae, H. Z., & Rhee, S. G. (2003). Reversible Oxidation of the Active Site Cysteine of Peroxiredoxins to Cysteine Sulfinic Acid. *Journal of Biological Chemistry*, *278*(48), 47361-47364. https://doi.org/10.1074/jbc.c300428200
Wood, Z. A., Poole, L. B., & Karplus, P. A. (2003). Peroxiredoxin Evolution and the Regulation of Hydrogen Peroxide Signaling. *Science*, *300*(5619), 650-653. https://doi.org/doi:10.1126/science.1080405
Wood, Z. A., Schröder, E., Harris, J. R., & Poole, L. B. (2003). Structure, mechanism and regulation of peroxiredoxins. *Trends in Biochemical Sciences*, *28*(1), 32-40. https://doi.org/https://doi.org/10.1016/S0968-0004(02)00003-8
Xu, S., Zhang, X., Liu, C., Liu, Q., Chai, H., Luo, Y., & Li, S. (2021). Role of Mitochondria in Neurodegenerative Diseases: From an Epigenetic Perspective. *Frontiers in Cell and Developmental Biology*, *9*. https://doi.org/10.3389/fcell.2021.688789
Yan, C. (1998). Crm1p mediates regulated nuclear export of a yeast AP-1-like transcription factor. *The EMBO journal*, *17*(24), 7416-7429. https://doi.org/10.1093/emboj/17.24.7416
Yang, J., Carroll, K. S., & Liebler, D. C. (2016). The Expanding Landscape of the Thiol Redox Proteome. *Molecular & Cellular Proteomics*, *15*(1), 1-11. https://doi.org/10.1074/mcp.o115.056051
Yang, K.-S., Kang, S. W., Woo, H. A., Hwang, S. C., Chae, H. Z., Kim, K., & Rhee, S. G. (2002). Inactivation of Human Peroxiredoxin I during Catalysis as the Result of the Oxidation of the Catalytic Site Cysteine to Cysteine-sulfinic Acid. *Journal of Biological Chemistry*, *277*(41), 38029-38036. https://doi.org/10.1074/jbc.m206626200

Yang, X.-X., Yang, R., & Zhang, F. (2022). Role of Nrf2 in Parkinson's Disease: Toward New Perspectives. *Frontiers in Pharmacology*, *13*. https://doi.org/10.3389/fphar.2022.919233

Young, D., Pedre, B., Ezeriņa, D., De Smet, B., Lewandowska, A., Tossounian, M.-A., Bodra, N., Huang, J., Rosado, L. A., Van Breusegem, F., & Messens, J. (2019). Protein Promiscuity in H_2O_2 Signaling. *Antioxidants & redox signaling*, *30*(10), 1285-1324. https://doi.org/10.1089/ars.2017.7013

Zhang, D. D., & Hannink, M. (2003). Distinct Cysteine Residues in Keap1 Are Required for Keap1-Dependent Ubiquitination of Nrf2 and for Stabilization of Nrf2 by Chemopreventive Agents and Oxidative Stress. *Molecular and Cellular Biology*, *23*(22), 8137-8151. https://doi.org/10.1128/mcb.23.22.8137-8151.2003

Zheng, M. (1998). Activation of the OxyR Transcription Factor by Reversible Disulfide Bond Formation. *Science*, *279*(5357), 1718-1722. https://doi.org/10.1126/science.279.5357.1718

Chapter 6: APPENDIX

These models were constructed for the double and single oxidation model. They were constructed to be used in PySCeS to simulate the Tpx1-Pap1-Trr1 pathway.

Model S1: The single oxidation Tpx1-Pap1-Trr1 computational model script

```
# A simplified model of the Tpx-Pap pathway.
# The Pap TF is oxidised once in this model and is oxidised once by TpxSH_TpxSOH.
# The parameters are all simplified to 1.
# The Tpx part of the model is simplified.

#####################################################

# Model Reactions

# Reaction 1: Reduction of TrxSS to TrxSH by NADPH catalysed by Trr
R1:     TrxSS + NADPH = TrxSH + NADP
        kcat1 * Trr * (NADPH / k1nadph) * (TrxSS / k1trx1ss) / ((1 + NADPH / k1nadph) * (1 +
        TrxSS / k1trx1ss))

# Reaction 2: Conversion of TpxSH_TpxSH to TpxSH_TpxSOH in the presence of H2O2
R2:     TpxSH_TpxSH + H2O2 = TpxSH_TpxSOH
        k2 * TpxSH_TpxSH * H2O2

# Reaction 3: Conversion of TpxSH_TpxSOH to TpxSH_TpxSS
R3:     TpxSH_TpxSOH = TpxSH_TpxSS
        k3 * TpxSH_TpxSOH

# Reaction 4: Exchange of disulfide bonds between TpxSH_TpxSS and TrxSH
R4:     TpxSH_TpxSS + TrxSH = TpxSH_TpxSH + TrxSS
        k4 * TpxSH_TpxSS * TrxSH

# Reaction 5: Exchange of disulfide bonds between TpxSH_TpxSOH and PapSHSH
R5:     TpxSH_TpxSOH + PapSHSH = TpxSH_TpxSH + PapSSSH
        k5 * TpxSH_TpxSOH * PapSHSH

# Reaction 8: Exchange of disulfide bonds between PapSSSH and TrxSH
R8:     PapSSSH + TrxSH = PapSHSH + TrxSS
        k8 * PapSSSH * TrxSH

#####################################################

# Species Concentrations (µM)

TpxSH_TpxSH = 4
TpxSH_TpxSOH = 0
TpxSH_TpxSS = 0
PapSHSH = 0.0245
PapSSSH = 0
TrxSH = 0.7
TrxSS = 0
```

```
NADPH = 150
NADP = 0
Trr = 0.5
H2O2 = 1
H2O = 0

#####################################################

# Kinetic Parameters (units are s-1; µM; µM.s-1)

kcat1 = 66
k1nadph = 1.3
k1trx1ss = 4.4
k2 = 20
k3 = 1.7
k4 = 0.2
k5 = 0.04
k8 = 0.01
```

Model S2: The double oxidation Tpx1-Pap1-Trr1 computational model script

```
# A simplified model of the Tpx-Pap pathway.
# The Pap TF is oxidised twice in this model and by TpxSH_TpxSOH.
# The parameters are all simplified to 1.
# The Tpx part of the model is simplified.

#####################################################

# Model Reactions

# Reaction 1: Reduction of TrxSS to TrxSH by NADPH catalysed by Trr
R1:     TrxSS + NADPH = TrxSH + NADP
        kcat1 * Trr * (NADPH / k1nadph) * (TrxSS / k1trx1ss) / ((1 + NADPH / k1nadph) * (1 +
        TrxSS / k1trx1ss))

# Reaction 2: Conversion of TpxSH_TpxSH to TpxSH_TpxSOH in the presence of H2O2
R2:     TpxSH_TpxSH + H2O2 = TpxSH_TpxSOH
        k2 * TpxSH_TpxSH * H2O2

# Reaction 3: Conversion of TpxSH_TpxSOH to TpxSH_TpxSS
R3:     TpxSH_TpxSOH = TpxSH_TpxSS
        k3 * TpxSH_TpxSOH

# Reaction 4: Exchange of disulfide bonds between TpxSH_TpxSS and TrxSH
R4:     TpxSH_TpxSS + TrxSH = TpxSH_TpxSH + TrxSS
        k4 * TpxSH_TpxSS * TrxSH

# Reaction 5: Exchange of disulfide bonds between TpxSH_TpxSOH and PapSHSH
R5:     TpxSH_TpxSOH + PapSHSH = TpxSH_TpxSH + PapSSSH
        k5 * TpxSH_TpxSOH * PapSHSH
```

```
# Reaction 6: Additional oxidation of PapSSSH by TpxSH_TpxSOH
R6:     TpxSH_TpxSOH + PapSSSH = TpxSH_TpxSH + PapSSSS
        k6 * TpxSH_TpxSOH * PapSSSH

# Reaction 7: Exchange of disulfide bonds between PapSSSS and TrxSH
R7:     PapSSSS + TrxSH = PapSSSH + TrxSS
        k7 * PapSSSS * TrxSH

# Reaction 8: Exchange of disulfide bonds between PapSSSH and TrxSH
R8:     PapSSSH + TrxSH = PapSHSH + TrxSS
        k8 * PapSSSH * TrxSH

##################################################

# Species Concentrations (µM)

TpxSH_TpxSH = 4
TpxSH_TpxSOH = 0
TpxSH_TpxSS = 0
PapSHSH = 0.0245
PapSSSH = 0
PapSSSS = 0
TrxSH = 0.7
TrxSS = 0
NADPH = 150
NADP = 0
Trr = 0.5
H2O2 = 1
H2O = 0

##################################################

# Kinetic Parameters (units are s-1; µM; µM.s-1)

kcat1 = 66
k1nadph = 1.3
k1trx1ss = 4.4
k2 = 20
k3 = 1.7
k4 = 0.2
k5 = 0.04
k6 = 0.04
k7 = 0.01
k8 = 0.01
```

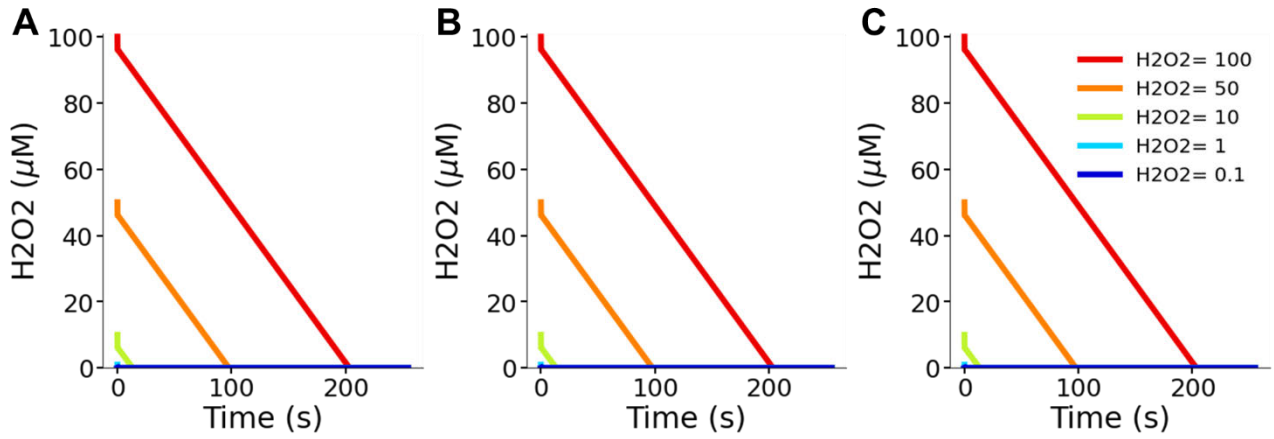

Figure S 1: The hydrogen peroxide concentration time course. (A) The single oxidation model. **(B)** The double oxidation model when k5 = k6. **(C)** The double oxidation model when k5 << k6.

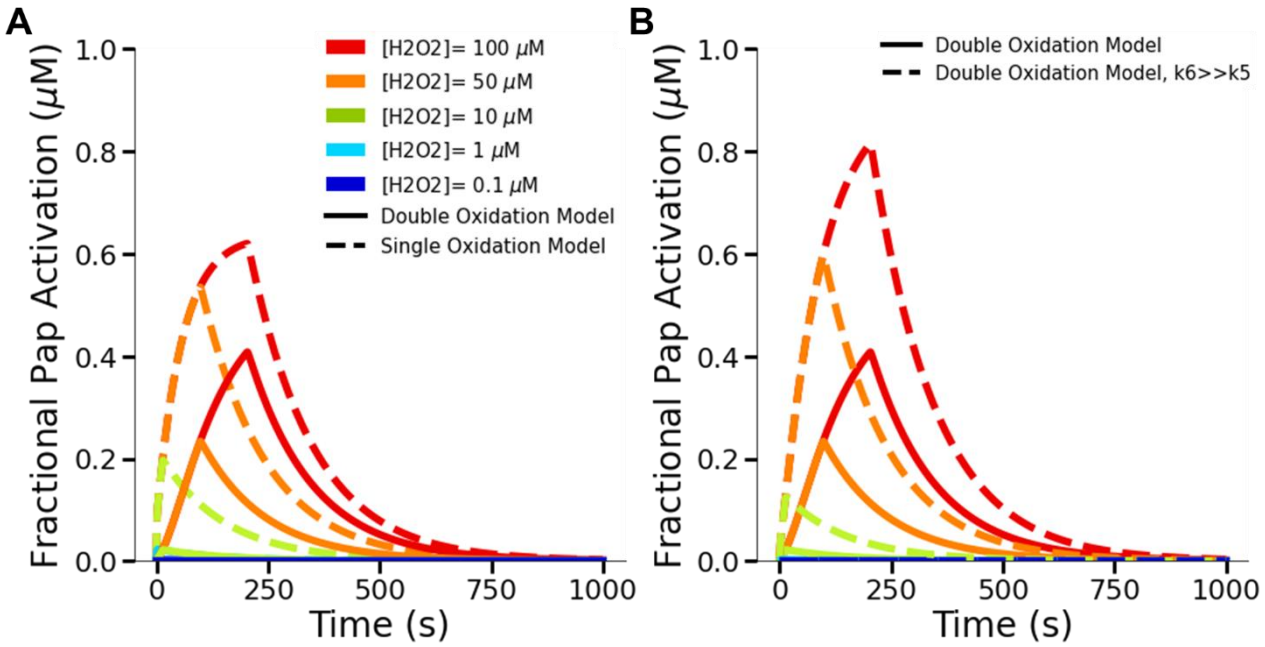

Figure S 2: The fraction of activated Pap1 for three different Tpx1-Pap1-Trr1 pathway for different hydrogen peroxide concentrations. (A) Comparing the double oxidation ($k_5 = k_6$) to the single oxidation model. (B) Comparing the double oxidation model ($k_5 = k_6$) to the double oxidation model ($k_5 << k_6$).

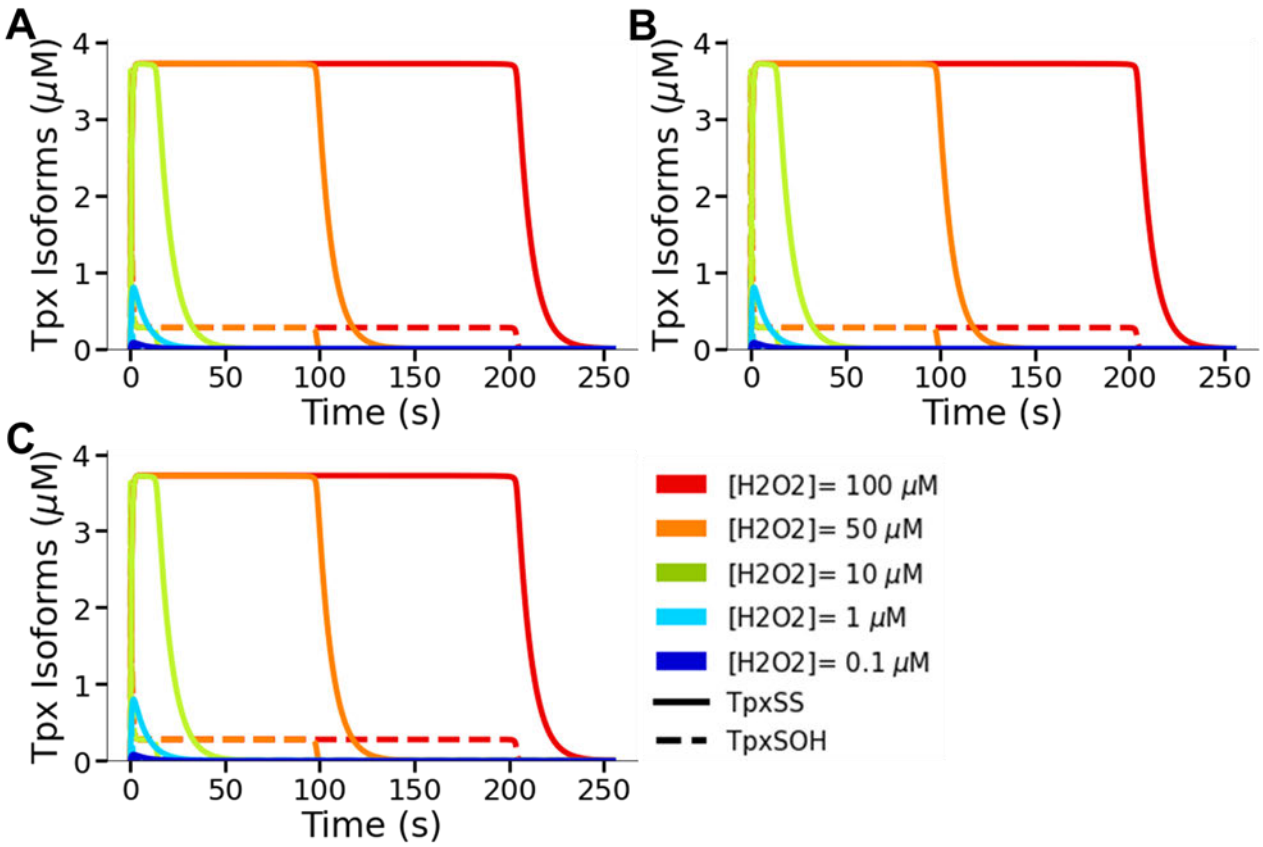

Figure S 3: The Tpx1 isoforms for the three oxidations models. (A) The single oxidation model. **(B)** The double oxidation model ($k_5 = k_6$) and **(C)** the double oxidation model ($k_5 << k_6$).

Table S 1: The densitometry results and analysis of Pap_{ox}/Pap_{tot} from the western blot for 0.4 μM hydrogen peroxide Tpx1-Pap1 experiment. Triplicates of the fractional activated Pap1 from ImageJ analysis, the average of each time point and the standard error.

Time	Exp 1	Exp 2	Exp 3	Mean	SEM
0	0.5155	0.3491	0.507	0.4572	0.0541
1	0.4803	0.4197	0.4572	0.4524	0.0176
5	0.4724	0.4218	0.4654	0.4532	0.0158
15	0.504	0.4267	0.439	0.4566	0.024
30	0.4985	0.4179	0.4752	0.4639	0.024
60	0.5941	0.4596	0.4317	0.4951	0.0501
DTT	0.4724	0.4911	0.4696	0.4777	0.0067

Table S 2: The densitometry results and analysis of Pap_{ox}/Pap_{tot} from the western blot for 4 μM hydrogen peroxide Tpx1-Pap1 experiment. Triplicates of the fractional activated Pap1 from ImageJ analysis, the average of each time point and the standard error.

Time	Exp 1	Exp 2	Exp 3	Mean	SEM
0	0.4394	0.4080	0.5331	0.4602	0.0376
1	0.4906	0.5093	0.5228	0.5076	0.0093
5	0.5040	0.5226	0.4885	0.5050	0.0099
15	0.4580	0.5033	0.5246	0.4953	0.0196
30	0.3532	0.4925	0.5187	0.4548	0.0513
60	0.4380	0.4698	0.4717	0.4598	0.0109

DTT	0.4930	0.5062	0.4920	0.4971	0.0046

Table S 3: The densitometry results and analysis of Pap_{ox}/Pap_{tot} from the western blot for 4 µM hydrogen peroxide Tpx1-Pap1 experiment. Triplicates of the fractional activated Pap1 from ImageJ analysis, the average of each time point and the standard error.

Time	Exp 1	Exp 2	Exp 3	Mean	SEM
0	0.4673	0.3779	0.4902	0.4451	0.0343
1	0.4861	0.4831	0.5120	0.4937	0.0092
5	0.4772	0.4888	0.4580	0.4746	0.0090
15	0.4693	0.4728	0.4829	0.4750	0.0041
30	0.4645	0.4871	0.5047	0.4854	0.0117
60	0.5382	0.4503	0.5176	0.5020	0.0265
DTT	1.0000	0.5138	0.6724	0.7287	0.1432